ENERGY SHAPING OF MECHANICAL SYSTEMS VIA CONTROL LYAPUNOV FUNCTIONS WITH APPLICATIONS TO BIPEDAL LOCOMOTION

A Dissertation

by

RYAN WESLEY SINNET

Submitted to the Office of Graduate and Professional Studies of
Texas A&M University
in partial fulfillment of the requirements for the degree of

DOCTOR OF PHILOSOPHY

Chair of Committee,	Aaron Ames
Committee Members,	Reza Langari
	Richard Malak
	Dylan Shell
Head of Department,	Andreas Polycarpou

May 2015

Major Subject: Mechanical Engineering

ABSTRACT

This dissertation presents a method which attempts to improve the stability properties of periodic orbits in hybrid dynamical systems by shaping the energy. By taking advantage of conservation of energy and the existence of invariant level sets of a conserved quantity of energy corresponding to periodic orbits, energy shaping drives a system to a desired level set. This energy shaping method is similar to existing methods but improves upon them by utilizing control Lyapunov functions, allowing for formal results on stability. The main theoretical result, Theorem 1, states that, given an exponentially-stable limit cycle in a hybrid dynamical system, application of the presented energy shaping controller results in a closed-loop system which is exponentially stable.

The method can be applied to a wide class of problems including bipedal locomotion; because the optimization problem can be formulated as a quadratic program operating on a convex set, existing methods can be used to rapidly obtain the optimal solution. As illustrated through numerical simulations, this method turns out to be useful in practice, taking an existing behavior which corresponds to a periodic orbit of a hybrid system, such as steady state locomotion, and providing an improvement in convergence properties and robustness with respect to perturbations in initial conditions without destabilizing the behavior. The method is even shown to work on complex multi-domain hybrid systems; an example is provided of bipedal locomotion for a robot with non-trivial foot contact which results in a multi-phase gait.

DEDICATION

I dedicate this work to my grandmother Helena Sinnet. She was very excited when I first entered the Ph.D. program but sadly she did not make it through to see me graduate.

ACKNOWLEDGEMENTS

I would like to acknowledge my advisory committee for their thoughtful suggestions while writing this dissertation. I would like to thank my advisor, Aaron Ames, in particular for the tremendous amount of insight he has provided over the years. I would also like to acknowledge Jessy Grizzle and Christine Chevallereau for their insight into hybrid systems and modeling. In addition, the method of energy shaping is based in part on the ideas of Mark Spong whose work laid the foundation for the theory presented herein. Finally, I would like to thank the National Science Foundation for supporting my research through much of my time as a graduate student through the Graduate Research Fellowship Program.

TABLE OF CONTENTS

LIST OF FIGURES

FIGURE Page

LIST OF TABLES

TABLE Page

1. INTRODUCTION

This dissertation discusses energy shaping as a means for improving the stability properties of periodic orbits in mechanical systems. Energy shaping is applicable to a wide range of mechanical systems but this work is chiefly concerned with continuous systems that have intermittent impacts [21] which result in non-smooth solutions. Such a description (not unintentionally) categorizes bipedal walking which is currently an area of widespread interest and is the focal point of the application of energy shaping in this dissertation. By developing energy shaping under the framework of hybrid systems, dealing with robotic locomotion becomes straightforward.

The method presented is similar in concept to the method of total energy shaping as presented in [149], which acts to shape the energy of the system but does so in a way which only guarantees asymptotic stability with respect to an arbitrary energy level and does not guarantee exponential stability of the overall gait and may in fact destabilize gaits. The method of energy shaping presented herein, in contrast, can improve the stability properties of a hybrid periodic orbit while guaranteeing that stability is not lost. This is a valuable extension of existing results which avoided making the unreasoned claim that energy shaping does not destabilize a system. By the results provided in Theorem 1, this claim can now be made with substantiation. It is important to note that this method fits into a class of problems which attempt to study the stability properties of systems which have zero dynamics such as that posed in [4]; the differences between the problem posed in [4] and the problem studied in this dissertation are presented in depth in Section 4.

Numerous methods currently exist for gait design but, aside from specific methods which construct a zero dynamics such as human-inspired control [46], many of these

methods do not have an intrinsic concept of stabilization to a specific gait through gain adjustment; that is to say that that there is a large class of controllers that are used to design periodic orbits (e.g., walking gaits) but, through inherent design limitations, cannot stabilize to these orbits arbitrarily fast. This is especially true of passivity-based methods such as controlled symmetries [148] and other controlled Lagrangian methods [16, 17]. These methods rely on shaping a system through control to reproduce the behavior of a similar system—in the case of controlled symmetries, perhaps shaping a compass-gait biped walking on flat ground to induce the gait of the same model passively walking down a shallow slope, a phenomenon demonstrated by McGeer [97].

Energy shaping owes its development to the observation that the total energy of a system is conserved in the absence of non-conservative forcing. For systems which do exhibit non-conservative forcing, the energy added or removed can be tracked using a storage function and the sum of the total energy of the system and the storage function is conserved; systems which demonstrate this property are called passivity-based systems [149].

When such a conserved energy quantity exists, it is, by definition, constant for periodic orbits of a system. Thus for a hybrid system which exhibits discontinuities, this quantity is constant through the continuous dynamics but experiences jumps due to the discrete dynamics. As a result, it seems reasonable to conclude that stability is largely a result of the discrete dynamics for certain systems. An easily digestible example of this phenomenon can be observed in an uncontrolled compass-gait biped which, as McGeer observed [97], is capable of walking stably down shallow slopes given the appropriate model parameters; this example is presented in Section 6.2 and a historical context is provided in Section 2.3.4.

For hybrid systems—systems which combine continuous dynamics such as leg

swing with discrete dynamics such as foot-strike—the conservation of energy through the continuous dynamics means that the change in energy level occurs from the discrete events in the system—foot-strike for bipeds—which exert non-conservative impulsive forcing as a byproduct of an interaction with the ground. By adding control to the continuous dynamics, overall stability properties of a gait tend to improve as has been observed in, e.g., [147], and as will be demonstrated later in this paper through simulation in Section 6. Formulation of the control objective using a control Lyapunov function makes it possible to achieve these improvements while simultaneously guaranteeing the existence of a control law which does not destabilize the system.

It is important to clarify the specific advantages conferred by energy shaping. One advantage of the method which is presented in this dissertation is a formal guarantee of stability. However, the stability which is proven is local exponential stability and nothing is formally shown about stability at arbitrary distances from the periodic orbit; Section 3.3 discusses stability in more detail and information about historical context can be found in Section 2.1.

In addition to the formal results, the claim is also made (as has been made before [147]) that energy shaping can improve the robustness of gaits. Different notions of robustness exist throughout the literature and one that is rather well known is robustness with respect to model uncertainties (cf. [35]). The theory presented does not treat this form of robustness and assumes perfect knowledge of the model. Another definition which crops up is robustness with respect to perturbations in initial conditions which ties into domain of attraction [25]. This particular definition is the one considered in this dissertation and numerical simulations seem to substantiate the claim that energy shaping improves robustness with respect to initial conditions thereby increasing the domain of attraction. It may be possible for specific systems,

by guessing valid Lyapunov functions, to make formal statements about the domain of attraction, but such investigation is beyond the scope of this work.

In addition to energy shaping, this dissertation contains a section on human-inspired control, which is a framework that was created to achieve human-like walking in bipedal robots. By examining human kinematics data, it becomes apparent that certain kinematics outputs of human walking, termed human outputs, can be encoded with very little loss by fitting the data to canonical walking functions, which have the same form as the solution to a linear spring–mass–damper system. In addition, the methods of hybrid zero dynamics [103] are drawn upon to construct a zero dynamics which can be rendered forward-invariant through feedback linearization, and is, moreover, invariant through impacts (i.e., foot strike), resulting in guaranteed stability properties [3]. Simulations are given to demonstrate human-inspired control in Section 5.

As mentioned, various simulations are given in Section 6. The first example is a simple cart–spring system which help build intuition into energy shaping methods. The next example is the simplest possible biped—the compass-gait biped—that is used to demonstrate energy shaping for the purpose of improving the stability properties of walking gaits. Although this is a comparatively simple model, it is still a hybrid system and is of small enough dimension that meaningful plots can be created to demonstrate the effectiveness of energy shaping. In order to test energy shaping on a more complex model, the results of a simulation of the seven-link biped with feet from [46] are presented. This model is much more complex than the compass-gait biped and has a complex domain structure. Due to high dimensionality, it is difficult to present results with the level of clarity as they are presented for the compass-gait biped, but the results nonetheless show that energy shaping can be applied to more complex models.

2. LITERATURE OVERVIEW

This section describes the literature which pertains to bipedal robotic walking, reviewing work from different fields and perspectives such as biomechanics and dynamical systems. Bipedal robotic walking is inherently interdisciplinary including theoretical and experimental components and drawing inspiration from locomotion found in nature. The exposition is divided by field: research on the stability of dynamical systems is discussed first followed by modeling of hybrid systems. The section ends with a review of bipedal robots and control methods from the literature.

2.1 Stability of Dynamical Systems

Stability of dynamical systems has a long history, appearing in the works of researchers such as Routh [131] and Hurwitz [62]. Contemporary notions of stability in nonlinear systems generally rely on results initially presented in the work of Aleksandr Lyapunov in his doctoral dissertation in 1892 [87]. In said treatise, Lyapunov described two methods for analyzing the stability of equilibrium points of ordinary differential equations.

The *first method*, sometimes called the *indirect method of Lyapunov*, provides a means for understanding the stability properties of an equilibrium point by examining a linearization of the nonlinear system. Due to the nature of linearization, the results of such an analysis only pertain locally and within an unknown region about the equilibrium point. Nonetheless, this method is well-known and sees widespread use due to its simplicity and straightforward nature.

The *second method*, sometimes called the *direct method of Lyapunov* involves the use of scalar-valued functions of the state of a system called *Lyapunov functions* which satisfy specific conditions that are set forth later. Through the use of these

Lyapunov functions, it is possible to prove stability not only locally but in a known region containing an equilibrium point or even globally. These functions are not unique and a major drawback to this method is the lack of an algorithmic procedure for constructing valid Lyapunov functions.

Both methods are used in this work but for different purposes: Lyapunov's indirect method is often used to analyze the stability of hybrid systems by examining the stability of a linearization of the Poincaré map about the equilibrium point; this will be explained in greater detail in Section 3.3. The numerical simulations in this work will rely on this usage of Lyapunov's indirect method. In order to formally demonstrate the stability of energy shaping—the main focus of this work—Lyapunov's direct method will be employed. This method is often used in theoretical constructions and can also be used to understand domain of attraction, although the particular usage will preclude this type of application.

Lyapunov's work on the direct method established sufficient conditions for stability but lacked the notion of *uniform stability* which was required for establishing necessary conditions. The results presented by Lyapunov lay essentially dormant for decades until researchers began to investigate the ideas further. From 1930's onward, researchers established additional results expanding on Lyapunov's ideas. Khalikoff [70] and Malkin [90] proved additional theorems on stability which could be used to show stability in the sense of Lyapunov with relaxed assumptions. As explained in [105], using Lyapunov's direct method, Marachkoff [93] provided a proof of asymptotic stability on systems of the form $\dot{x} = f(t, x)$ using a negative definite Lyapunov function; the negative definiteness requirement was later relaxed to negative semidefinite through the addition of a second Lyapunov function by Matorosov [96].

Masera [94] provided more restrictive definitions, introducing the notion of *equi-*

asymptotic stability. Yet it wasn't until the assumptions of uniformity were provided by Malkin [91] that the necessary framework existed in which to formulate converse theorems. Barbashin and Krasovskiĭ further strengthened Malkin's result in [12].

After these observations were published, converse theorems followed shortly thanks to researchers such as Kurzweil [81] and Massera [95]. Converse theorems have seen substantial development and broad use since these results. Hoppensteadt [58] presented constructions for singularly perturbed systems in which he constructed a C^1 Lyapunov function, extending existing work on singularly perturbed systems to unbounded time intervals. Wilson [172] constructed a C^∞ Lyapunov function for a continuous vector field having an asymptotically stable invariant set. Early results on converse Lyapunov functions for stability of sets are summarized in numerous texts; see, e.g, [8].

In addition to providing necessary and sufficient conditions for stability, researchers have also studied what conditions are necessary for solutions to be integrable for all time. Cesari provides conditions for [23, §1.5] for second-order linear systems. Strauss introduces L^p stability to attempt to provide conditions for more general systems in [153].

As LaSalle points out [83], before the 1960's much of the work done in the USSR was inaccessible to English-speaking audiences, but as the decade progressed, this language barrier gradually dissipated. An early text by LaSalle and Lefschetz (the first such text in English) [84] outlining the methods of Lyapunov stability theory contains proofs which are accessible to those with less extensive mathematical backgrounds. Shortly thereafter, additional texts emerged including those of Krasovskiĭ [75] and of Hahn [49]. Yoshizawa's text from 1975 [178] provides a compilation of results on Lyapunov stability in almost periodic systems.

Additional information on the history of Lyapunov theory can be found through-

out the literature; see, e.g., [100, 159].

2.2 Hybrid Systems

The term hybrid systems derives its name from the mixed nature of the dynamics involved. In general, systems which combine continuous dynamics with discrete dynamics are referred to as such. Contemporary notions of hybrid systems evolved over the past few decades; the term hybrid systems itself is broadly and loosely used in different areas of control. Because of the combination of dynamics, hybrid systems often contain solutions with discontinuities as discussed by Filippov [34].

Many of the developments in hybrid systems have been motivated by applications: Göllü and Varaiya [41] applied hybrid dynamical systems to formulate a control scheme for hard disk drives. In a later work [163], Varaiya also described automated vehicle–highway systems. Similarly, Tomlin, Pappas and Sastry [161] described automated automated air traffic management systems. Brockett [20] described hybrid models for motion control systems, attempting to provide generalizations for a wide class of systems. Such multilayer control schemes as those described earlier by, e.g., Brooks [22], in some sense provided an impetus for more formal descriptions. Simpler examples include thermostat/furnace systems and surge tanks as described by, e.g., Antsaklis, Stiver and Lemmon [9], and the even simpler cat and mouse game mentioned by Manna and Pnueli [92].

Harel [50] presented the idea of statecharts as a visual formalism for modeling of hybrid systems. Other researchers have proposed various languages for hybrid systems such as Hooman [57] and Benveniste, Borgne and Guernic [14].

2.3 Bipedal Robotic Locomotion

Bipedal robotics has been approaches in numerous different ways from the analysis of passive walkers based on simple mechanical design principles to advanced

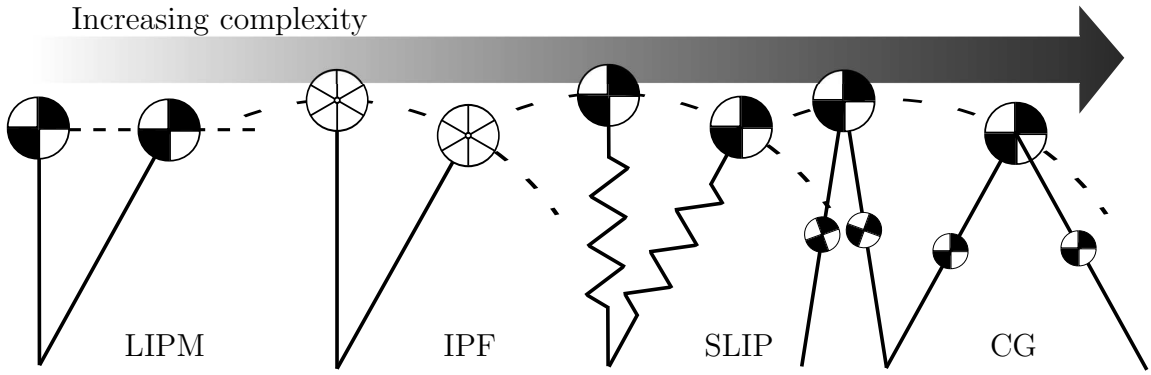

Figure 2.1: Example low-dimensional models. Such models are often used as approximations of walking robots. From left to right: Linear Inverted Pendulum, Inverted Pendulum with Flywheel, Spring-Loaded Inverted Pendulum, Compass-Gait Biped the Linear Inverted Pendulum Model (LIPM) assumes a lumped center-of-mass with constant height and massless legs; the Inverted Pendulum with Flywheel (IPF) adds a flywheel at the CoM to model angular momentum and allows for varying height; the Spring-Loaded Inverted Pendulum (SLIP) considers a spring to model the legs as massless pogo sticks; and the Compass-Gait Biped (CG) is essentially a double pendulum with lumped masses on the stance and swing legs and one at the hip.

multifunctional humanoids. Control designs have been proposed based on models which vary from the low-dimensional representations shown in Figure 2.1 to higher-dimensional dynamic models as developed in Section 3. While simpler models offer the benefits of faster control law computation and easier-to-understand analyses, more complex models can provide tighter control and formal guarantees on stability. In this subsection, some well-known approaches to bipedal gait generation are discussed emphasizing the effect of modeling on control design. Further information is available in [26, 37, 56, 60, 79, 132, 136, 171, 175] and the references therein.

2.3.1 Zero Moment Point and Linear Inverted Pendulum Models

The ZMP control strategy [166, 168] is extremely common in control of bipeds. The ZMP is the point on the ground at which the reaction forces acting between the ground and the foot produce no horizontal moment. Traditionally, ZMP control

strategies achieve walking by planning the motion of a robot's CoM such that the ZMP remains strictly within the convex hull of the stance foot in the case of single support (or convex hull of the stance feet, in the case of double support). Under this condition on the ZMP, the stance foot remains flat on the ground and immobile (not rotating)—much like the base of a traditional manipulator robot—and hence the robot will not topple; see, e.g., [176].

In the special case of the Linear Inverted Pendulum Model (LIPM), the ZMP can be treated with an ordinary differential equation modeling the center-of-mass (CoM) dynamics. This treatment assumes representation of a robot as a point mass with massless telescoping legs. Moreover, the height of the CoM is assumed to be constant. Under these conditions, [66] proved that a model reduces to the LIPM.

The LIPM assumes the height of the center of mass (CoM) and angular momentum about the stance foot are constant through a step. Because they share some key assumptions, the ZMP control method and the LIPM have historically been coupled. While the LIPM originated in the study of human posture and balance (e.g., [39, 173, 114]), it has also been the focus of much research in bipedal locomotion; see, for example, [101, 64, 65].

Early experimental work on bipedal robots came from Japan, where Kato began building the WABOT series of humanoid robots circa 1970. A full-scale anthropomorphic robot, WABOT-1, was described in [69] and it was capable of primitive, statically stable walking while carry objects with its hands. Years later, the ZMP technique was first demonstrated in experiment on the WL10-RD biped in [155]. The study of walking humanoid robots has increased in pace with researchers from designing newer generations of robots like WABIAN-2 [109], ASIMO [133], HRP-4 [68], KHR-3 [111], and Johnnie [116].n

Though ZMP methods have been vastly successful, a number of drawbacks still

presents challenges. By the nature of the models, ZMP gaits usually do not consider impacts and so the swing foot trajectory must be specified such that ground impact is minimal. Moreover, ZMP condition alone is not sufficient for asymptotic stability of periodic walking [27]. Despite this, researchers have pursued numerous methods of gait generation using ZMP: Nagasaka et al [107] used the optimal gradient method; Kajita et al [67] examined potential energy conserving orbits; Lim et al [86] computed ZMP-consistent trajectories off-line and stabilized them using trunk motion; Nishiwaki et al [108] generated ZMP-consistent trajectories in real-time while walking; and Kurazume et al [80] used analytical solutions to the ZMP dynamics; Additional information on ZMP-based methods and related ground reference points is given in [43, 166, 167, 117].

2.3.2 Nonlinear Inverted Pendulum Models

In order to overcome limitations resulting from the simplicity of the LIPM model, researchers have considered more complex models. Park et al [112] explored the Gravity Compensated LIPM which adds an additional point mass at the location of the swing foot to achieve higher modeling accuracy. In [122], Pratt and Drakunov relaxed the requirement of constant CoM height on the LIPM leading to a nonlinear inverted pendulum model. In another common model, a flywheel is added to the inverted pendulum; examples can be found throughout the literature: Stephens [151] used it for posture control, Takenaka et al [157] used it to with on-line error compensation to mitigate the effect of modeling errors on gait generation, and Komura et al [72] used it to simulate pathological gaits. The various pendulum models have been widely used in analysis of push recovery and balance [156, 53, 63, 150].

Pratt et al [119] considered a flywheel model in order to present the idea of the *capture point*—a point on the ground on which a biped can step and come to

a complete (upright) stop without falling over; additional information on capture points can be found in [73, 121]. The capture point [124] has gained recognition as a convenient method for stabilizing a biped. Intuitively, a capture point is a point on the ground where a biped can place its swing foot to be able to avoid falling over—the set of all capture points is called the *capture region*. This method, which considers a robot as an inverted pendulum with a flywheel, has been used not only for standing but for robust walking as well. Because the model makes many simplifying assumptions, the capture regions can have a large error and this has motivated the combining of capture point with learning in, e.g., [130].

2.3.3 Spring-Loaded Inverted Pendulum Models

In the 1980's, a large amount of pioneering work was done at MIT by Marc Raibert. Raibert constructed a spring-loaded leg and tested new ideas using low-dimensional models for hopping and running His two-dimensional hopper could "run" at a speed of 1 m/s [125, 126, 128]. A three-dimensional version of the origin hopper was also successful [126, Chap. 3] followed up by multi-legged robots [52, 127, 129]. This work led the way for researchers studying the Spring-Loaded Inverted Pendulum (SLIP) model, which has been shown to approximate the center-of-mass dynamics of *steady-state running gaits* on a numerous animals from insects all the way to humans [15, 99, 32, 36, 30, 135]. Using Raibert's principles, other simple robots have achieved running such as the ARL-Monopod II [2] and the CMU Bowleg Hopper [179].

More complex robots were later build with knees and compliance including the Spring Flamingo and Spring Turkey [55, 123, 118, 120]. These robots used a type of series elastic actuator (SEA) designed for force control as opposed to energy storage. The recent COMAN robot discussed in [85] includes passive compliance to reduce energy consumption during walking.

2.3.4 Passive Walkers and the Compass-Gait Biped

In contrast to the minimalist models just discussed, some researchers create robots with dynamics designed to realize a simplified model and thus, in such cases, mechanical design plays an important role in dynamic stability. Even these complex designs, however, often achieve walking through controllers designed for low-dimensional models such as the ZMP strategy. Low-dimensional models are generally easier to model and it is more straightforward to take into account impact dynamics. As impacts play an important role in dynamic stability, this confers a valuable advantage over gaits designed with simpler methods such as LIPM methods.

In 1980, Mochon and McMahon [102] pointed out that human walking is similar to a double pendulum thereby hinting at the passive nature of human walking and the importance of mechanical design. In the late 80's, McGeer built planar, passive bipedal walkers which helped to validate the claims of Mochon and McMahon. His bipeds which included a compass-gait walker [97] and kneed version [98] could walk stably down shallow slopes with no actuation. This began a trend of studying *passive dynamic walking*. Based on McGeer's original ideas, researchers have constructed minimalist bipeds which achieve walking by injecting and removing small amounts of energy as described in [28] The result is "human-looking" walking, but the remarkable elegance and economy of these walkers comes at the cost of poor ability in achieving tasks other than walking at a fixed speed; they cannot climb stairs, pause, turn or run.

More in-depth work was later done to analyze the properties of passive walkers, for instance, in [31, 38, 18]. Spong [146] looked at passive dynamic walking with energy-based methods to design passivity-based control strategies such as controlled symmetries, introduced in [148], which was later used to obtain anthropomorphic foot

action in [138, 139] and recently extended to underactuated bipeds in [59]. Spong's work on energy shaping methods such as controlled symmetries provides a starting point for the methods provided in this dissertation. Other important contributions to passive dynamic walking are given in [7, 77, 78, 175].

2.3.5 Quadratic Programs and Lyapunov Funnels

Early implementations of ZMP methods would generally rely on center-of-mass trajectories generated offline using the LIPM. In addition, these implementations usually ignored impact dynamics. Contemporary methods have achieved better results by structuring the control problem as a *quadratic program* (QP), thereby allowing on-line updating of gaits for improved robustness and stability properties [76, 152, 51].

In a similar fashion, sums of squares methods, also consider trajectory generation using convex optimization [158]. As an added benefit, these methods can produce formal guarantees on stability as in [89]. The idea is to investigate controllability by composing sequential funnels (verified with sum of squares Lyapunov inequalities), each leading to predefined goals. This can result in the creation of a trajectory with guaranteed stability properties: at any given time, the state of the system is within one of the known domains (regions of attraction) and can thus be funneled into the desired state. The sum of squares formulation renders the trajectory optimization more tractable, easing the verification of stability for low-dimensional models.

3. MODELING

Though the methods presented in this dissertation may be useful on a variety of control systems, the primary application described herein is to mechanical systems. In particular, this work attempts to demonstrate the application of energy shaping in bipedal robotic locomotion. Walking is characterized by phases of continuous motion with periodic discrete impacts. The combination of continuous and discrete dynamics motivates the use of hybrid systems methods for modeling and controlling bipeds. This section presents a development of modeling for hybrid systems which is sufficient to understand the theory and examples presented.

3.1 Hybrid Dynamical Systems

Hybrid dynamical systems are systems which combine continuous and discrete dynamics. By their nature, they provide a useful framework for modeling mechanical systems with impacts. The combination of dynamics motivates the use of hybrid systems in modeling numerous physical phenomena including bipedal walking, which is the motivating example most pertinent to this dissertation.

Hybrid dynamical systems have seen widespread use and comprehensive formal development over the years; see, e.g., [19, 40, 46, 162, 171]. Other frameworks exist for modeling the same physical phenomena such as differential inclusions as discussed in [34] but hybrid systems methods are becoming increasingly popular.

With the goal of modeling a mechanical system exhibiting both continuous and discrete dynamics, consider a hybrid dynamical system with total energy $E(q, \dot{q})$ where the coordinates $q \in \mathcal{Q}$ take values in the *configuration space* $\mathcal{Q}$ and the velocities are in the tangent bundle, $T\mathcal{Q}$. For ease of exposition, let the generalized coordinates of the system be represented by $(q, \dot{q}) = x \in \mathcal{X}$ where $\mathcal{X}$ is the state

space. The evolution of the system depends on a *unilateral constraint*, $h : \mathcal{Q} \to \mathbb{R}_{\geq 0}$, which can be used to define the *guard* or *switching surface*. In the case of a bipedal robot with simple foot behavior, a common selection for the unilateral constraint is the height of the swing foot, i.e., $h(x) = h_{\text{nsf}}(q)$. Through definition of an appropriate unilateral constraint on a hybrid system whose zero crossings correspond to discrete transitions, certain properties of the system follow. Defining a unilateral constraint to be non-negative leads a definition of the *domain of admissibility* as

$$D = \{q \in \mathcal{Q} : h(q) \geq 0\}, \tag{3.1}$$

which describes the admissible states of the system. This is the simplest definition and can be expanded to include additional considerations such as friction; this is shown later for more complex models. The boundary at the zero level set of $h(q)$ naturally gives rise to the switching surface,

$$S = \left\{(q, \dot{q}) \in D : h(q) = 0 \text{ and } \dot{h}(q, \dot{q}) < 0\right\}. \tag{3.2}$$

Using these spaces, an uncontrolled hybrid system can be expressed as

$$\Sigma = \begin{cases} \dot{x} &= f(x), \quad x^- \in D \setminus S, \\ x^+ &= \Delta(x^-), \quad x^- \in S, \end{cases} \tag{3.3}$$

where $f(x)$ is a smooth vector field and $\Delta : S \to D \setminus S$ is a smooth map called the reset map (see, e.g., [103]). In addition, $x^-(t) = \lim_{\tau \nearrow t} x(\tau)$ and $x^+(t) = \lim_{\tau \searrow t} x(\tau)$ are the left and right limits of the solution $x(t)$, respectively. For compactness of

notation, a hybrid system is sometimes written as

$$\Sigma = (D,\, S,\, \Delta,\, f).$$

as in [138]. Under the action of control effort u, the corresponding hybrid control system has the form

$$\Sigma^c = \begin{cases} \dot{x} \;\; = f(x) + g(x)\, u, & x^- \in D \setminus S, \\ x^+ = \Delta(x^-), & x^- \in S, \end{cases} \tag{3.4}$$

for control values in a set of *admissible controls*, $\mathcal{U} \subseteq \mathbb{R}^m$. Here, $g(x)$ is a smooth vector field. As with hybrid systems, hybrid control systems are sometimes written more compactly:

$$\Sigma^c = (D,\, S,\, \mathcal{U},\, \Delta,\, f,\, g).$$

Using these basic formalisms of hybrid systems, the next three subsections describe how to construct hybrid systems for mechanical systems.

3.2 Solutions to Hybrid Systems

Consider the hybrid system Σ given in (3.3). The solution involves the *dynamical system*

$$\dot{x} = f(x). \tag{3.5}$$

This differential equation defines the continuous dynamics of (3.3) as well as the reset map

$$\dot{x}^+ = \Delta(x^-) \tag{3.6}$$

which defines the discrete dynamics. Solutions to the differential equation governing the dynamics are valid on an open subset of $\mathbb{R}^n$, namely the domain, $D \subset \mathbb{R}^n$. The vector field is assumed to be continuously differentiable viz. $f \in C^1(D)$. For an initial condition $x_0 \in D$, the solution $x(t)$ will evolve according to (3.5) until it reaches the edge of D, intersecting the guard S by assumption (transversality).

Define the *flow* of the differential equation as

$$\phi_t(t_0, x_0) = x_0 + \int_{t_0}^{t} f(x(\tau))\ d\tau.$$

This function represents a trajectory of the differential equation (3.5) which starts at time t_0 with initial value x_0 and flows until time t with final state $x(t)$. From this expression, it is clear also that there is a *time-to-impact* function $T_I : D \to \mathbb{R}_{\geq 0}$ guaranteed by the implicit function theorem around an invariant orbit $\mathscr{O}$ as follows: using the unilateral constraint h associated with the hybrid system, define the function

$$N(t, x) = h(\phi_t(\Delta(x^*))).$$

This function is continuous in x as it involves a smooth vector field. By the assumption of transversality solutions do not travel along the guard and thus it follows

that

$$\frac{\partial N(T, x^*)}{\partial t} = \dot{h}(\phi_t(\Delta(x^*))) \neq 0.$$

By the implicit function theorem, there exists a $\delta > 0$ and a unique function $T_I(x)$ defined and locally continuous for all $x \in B_\delta(x^*)$ such that $T_I(x^*) = T$ where T is the period of the invariant orbit, which will be defined shortly. This function maps a given state x to the time until that solution crosses the guard.

Stability analysis of hybrid systems often involves a method attributable to Poincaré. This method is widely used in various types of systems including continuous systems, discrete systems, and hybrid systems; for some examples, see [46, 47, 113, 115]. The method of Poincaré sections allows one to select a transverse hypersurface, called a Poincaré section, at which the system is sampled. The Poincaré section can be chosen such that a discrete system is created by sampling with either a time-based or an event-based rule. For mechanical systems with impacts, an event-based rule is constructed by choosing the Poincaré section to correspond to impact events. More specifics about the Poincaré method are introduced in Section 4. Note that the methods discussed ignore Zeno phenomena; see [82, 110] for more information.

Using the time-to-impact function, one can define the *Poincaré first return* map, $P : S \to S$, as the following partial map:

$$P(x) = \Delta(\phi_{T_I(x)}(x)), \ \forall x \in S. \tag{3.7}$$

One can see that the Poincaré map is also continuous. Stability of the hybrid system can then be analyzed by examining stability of the discrete system [104] defined by

the Poincaré map (3.7). A solution $\phi_t(t_0, x_0)$ is *periodic* if there exists a $T > 0$ such that

$$x(0) = \phi_T(x(0)),$$

A set $\mathscr{O} \subset D$ is a *periodic orbit* if

$$\mathscr{O} = \{\Delta(\phi_t(x)) : 0 < t < T_I(x(0))\}$$

for some periodic solution $\phi_t(t_0, x_0)$.

For hybrid systems, a discrete event may occur periodically throughout the flow leading to discontinuities. The periodic orbit in such a case is not closed. Beginning at time t_0, a solution to (3.3) evolves according to (3.5) until the trajectory reaches the hypersurface S at time t_1. At this point, the reset map instantaneously alters the state according to (3.6) which causes a discontinuity in the solution $x(t)$ resulting in a discrete state update law which yields a new initial condition,

$$x^+(t_1) = \Delta(x^-(t_1)).$$

From this new initial condition, the solution then continues to evolve based on (3.5).

Because the discrete dynamics is considered to operate on the solution instantaneously, it is important to distinguish between the pre-impact state,

$$x(t^-) = x^- = \lim_{\tau \nearrow t} x(\tau),$$

which occurs at time t^-, and the post-impact state,

$$x(t^+) = x^+ = \lim_{\tau \searrow t} x(\tau),$$

which occurs at time t^+. The discrepancy in left- and right-hand limits is due to the discontinuities in solutions introduced by the reset map.

A solution can be created by piecing together these solutions which each describes the evolution of coordinates as the state flows from a point on S through the domain D until it intersects S again. Such solutions are often called *hybrid flows* or *hybrid executions*. Formally, a hybrid flow of (3.3) is a tuple

$$\Upsilon^\Sigma = (\mathscr{K}, \mathscr{I}, \mathscr{C})$$

where $\mathscr{K} = \{0, 1, 2, \ldots\} \subseteq \mathbb{N}$ is a finite or countably infinite *indexing set*, $\mathscr{I} = \{I_k\}_{k \in \mathscr{K}}$ is a *hybrid interval* with $I_k = [t_k, t_{k+1}]$, and $\mathscr{C} = \{c_k\}_{k \in \mathscr{K}}$ is a collection of continuous solutions of $f(x)$, i.e., $\dot{c}_k(t) = f(c_k(t)) \, \forall k \in \mathscr{K}$. In order to maintain consistency, the following conditions must be met:

1. $c_k(t_{k+1}) \in S$
2. $\Delta(c_k(t_{k+1})) = c_{k+1}(t_{i+1})$

Further details about solutions of hybrid systems also appear in Section 4. For additional notions of solutions in hybrid systems, see [34, 40, 48, 88, 177].

3.3 Stability Definitions

Because of the unique nature of hybrid systems, analysis of stability requires special treatment which is distinct from continuous-time systems and more closely parallels that used for discrete-time systems. In order to understand the theory

presented in this work, it is necessary to understand not only the stability of hybrid systems but also the stability of continuous systems and discrete systems which partly comprise hybrid systems. This subsection presents formal definitions of stability (based on those found in [71, Ch. 4]) which are key to understanding the results presented in this work. For more on stability, see, e.g., [71, 160, 165]. For comments on the literature, see Section 2.1.

3.3.1 Continuous Systems

This work is chiefly concerned with autonomous systems of the form

$$\dot{x} = f(x) \tag{3.8}$$

where $f : D \to \mathbb{R}^n$ is a locally Lipschitz vector field valid on some domain $D \subset \mathbb{R}^n$. Without loss of generality, suppose that the system (3.8) has an equilibrium point at the origin; in other words, $f(\mathbf{0}) = \mathbf{0}$.

Definition 1. *The equilibrium point $x = \mathbf{0}$ is stable if, for each $\epsilon > 0$, $\exists\ \delta > 0$ such that*

$$\|x(0)\| < \delta \Rightarrow \|x(t)\| < \epsilon\ \forall\ t \geq 0.$$

The equilibrium point is unstable if it is not stable.

In addition to the above definition, a stricter forms of stability is defined as follows:

Definition 2. *The equilibrium point $x = \mathbf{0}$ is* **asymptotically stable** *if it is stable*

and δ can be chosen such that

$$\|x(0)\| < \delta \Rightarrow \lim_{t\to\infty} x(t) = \mathbf{0}.$$

Further, an even stronger form of stability is of interest in this work:

Definition 3. *The equilibrium point $x = \mathbf{0}$ is* **exponentially stable** *if there exist real constants $c, k, \lambda > 0$ such that*

$$\|x(t)\| \leq k\|x(t_0)\|e^{-\lambda(t-t_0)} \ \forall \ \|x(t_0)\| < c.$$

3.3.2 Discrete Systems

In analogy to continuous systems, consider the autonomous system which satisfies the difference equation

$$x_{k+1} = f(x_k). \tag{3.9}$$

where $f : D \to D$ is a locally Lipschitz vector field valid on some domain $D \subset \mathbb{R}^n$. Without loss of generality, suppose that the system (3.9) has an equilibrium point at the origin; in other words, $f(\mathbf{0}) = \mathbf{0}$.

Definition 4. *The equilibrium point $x = \mathbf{0}$ of* (3.9) *is stable if, for each $\epsilon > 0$, $\exists\ \delta > 0$ such that*

$$\|x_0\| < \delta \Rightarrow \|x_k\| < \epsilon \ \forall \ k \geq 0.$$

The equilibrium point is unstable if it is not stable.

Similar to continuous systems, asymptotic stability is defined as follows:

Definition 5. *The equilibrium point* $x = \mathbf{0}$ *of* (3.9) *is* **asymptotically stable** *if it is stable and* δ *can be chosen such that*

$$\|x_0\| < \delta \Rightarrow \lim_{k\to\infty} x_k = \mathbf{0}.$$

Exponential stability for discrete systems is formally defined as follows:

Definition 6. *The equilibrium point* $x = \mathbf{0}$ *of* (3.9) *is* **exponentially stable** *if there exist real constants* $\alpha, \beta, c > 0$ *such that, for all* $\|x_{k_0}\| < c$ *and* $k \geq k_0$*,*

$$\|x_k\| \leq \beta \|x_{k_0}\|^{\alpha}.$$

These definitions will tie into the work later in Section 4.

3.4 Rigid Body Kinematics

At its core, the modeling of complex mechanical systems involves a straightforward, if often complicated, application of Newton's Second Law (see [33]), namely,

$$F = m\,a,$$

which expresses the basic property of physics that applying a force to a massive object induces a particular acceleration. Through the property of superposition, this relationship eventually leads to the standard dynamic model of a robot given later in (3.10). But despite the development of complex models, all physics-based models fundamentally demonstrate Newton's Second Law.

Consider a three-dimensional rigid body with no contact assumptions; i.e., the body is free to move in space. With the dynamics of the system being dominated by Newton's laws of motion [33], the state of the system can be expressed by asso-

ciating a reference frame to a fix pointed on the body and using coordinates which express the position and orientation of this point with respect to a global frame or the world frame. In three-dimensional space, this transformation between world frame and robot frame can be parameterized with six coordinates: three representing the Euclidean position and three respresenting, for example, an Euler angle–based derivation, namely, the product of three rotation matrices [13, Ch. 7]. The set of all admissible configurations for such a body represents a specific topological space referred to as the *special Euclidean group*, $\mathbf{SE}(3)$. This group can be thought of as the Cartesian product of the position and orientation of a body, i.e., $\mathbf{SE}(3) = \mathbb{R}^3 \times \mathbf{SO}(3)$, where $\mathbf{SO}(3)$ is the *special orthogonal group* which can be understood as

$$\mathbf{SO}(n) = \left\{ R \in \mathbb{R}^{n \times n} : RR^T = I, \det R = 1 \right\}.$$

For more information on these topological spaces, consult [106, Ch. 2].

Newton's laws eventually lead to the understanding that the motion of such a system can be captured by the following dynamic model:

$$\begin{aligned} I_x \dot{\omega}_x + (I_z - I_y)\omega_y \omega_z &= M_x \\ I_y \dot{\omega}_y + (I_x - I_z)\omega_z \omega_x &= M_y \\ I_z \dot{\omega}_z + (I_y - I_x)\omega_x \omega_y &= M_z \\ m\dot{v}_x &= F_x, \\ m\dot{v}_y &= F_y, \\ m\dot{v}_z &= F_z, \end{aligned}$$

where linear and angular velocity are represented by v and ω, respectively, and the corresponding accelerations are shown as time derivatives. The applied forces and

moments are shown as F and M, respectively, and the I_x, I_y, and I_z terms are the principal moments of inertia about the appropriate axes. As one might guess, this requires that the fixed frame be located at the center of mass and oriented along the principal axes of inertia; it is straightforward to redefine the base coordinates but this form—the simplest form —is given for clarity of presentation. For the full development of the above, see, for example, [13, Ch. 8].

Typical robots consist of kinematic chains of rigid bodies attached with prismatic or revolute joints, and for simplicity, the resulting dynamics generally has the appropriate contact assumptions baked in to simplify computation (as in (3.10)), but it is possible to consider each rigid body separately and solve for the appropriate reaction forces which can be applied through F and M to maintain the proper contact (this is typically called the Newton–Euler method [54]). For robotic motion, non-holonomic constraints act to reduce the allowable motion and, as a consequence, there exists a minimal set of coordinates which can be used to describe a robot's dynamics. This minimal set is referred to as the *generalized coordinates*.

3.5 Langrangian Formulation

With the basic understanding provided in the previous subsection, some additional details will now be provided. Begin with a bipedal robot in either two or three dimensions—the discussions herein are applicable to either case. Then construct a Lagrangian for the biped in a general position—specifically, no assumptions are made on ground contact—and use non-holonomic constraints to enforce ground contact conditions.

Let R_0 be a fixed inertial or world frame and let R_b be a reference frame attached to the body of the biped with position $p_b \in \mathbb{R}^3$ and orientation $\phi_b \in \mathbf{SO}(3)$ where $\mathbf{SO}(n)$ represents the special orthogonal group in n dimensions (see [29]). Let $q_s \in \mathcal{Q}_s$

represent a choice of *body* or *shape coordinates* for the robot with $\mathcal{Q}_s$ the configuration space. Herein, q_s represents the relative angles between adjacent links of the robot. The *generalized coordinates* are then found by combining the shape coordinates with the position and orientation of the body-fixed frame, R_b, viz.

$$q = (p_b, \phi_b, q_s) \in \mathcal{Q} = \mathbb{R}^3 \times \mathbf{SO}(3) \times \mathcal{Q}_s,$$

where $\mathcal{Q}$ is the generalized configuration space.

The Lagrangian of a bipedal robot, $L : T\mathcal{Q} \to \mathbb{R}$, can be stated in terms of the kinetic energy, $K : T\mathcal{Q} \to \mathbb{R}$, and the potential energy, $U : \mathcal{Q} \to \mathbb{R}$, as:

$$L(q, \dot{q}) = K(q, \dot{q}) - U(q).$$

For robots, the kinetic energy has the form

$$K(q, \dot{q}) = \dot{q}^T M(q)\, \dot{q}.$$

where $M(q)$ is a manipulator inertia matrix which has the property of being symmetric and positive definite. The Euler–Lagrange equation can be used to find the dynamics, which, for robotic systems [106, pp. 171], is written:

$$M(q)\, \ddot{q} + H(q, \dot{q}) = B(q)\, u \tag{3.10}$$

where, here, $M(q)$, the manipulator inertia matrix, and $B(q)$, the torque distribution matrix, only depend on q, u is a vector of applied torques, and

$$H(q, \dot{q}) = C(q, \dot{q})\, \dot{q} + G(q)$$

contains terms resulting from the Coriolis effect, centrifugal forces, and gravity grouped into a single vector. The contribution from gravity is related to the potential energy:

$$G(q) = \frac{\partial U(q)}{\partial q}.$$

The elements of $C(q, \dot{q})$ can be found by computing the Christoffel symbols of $M(q)$:

$$C_{ij}(q, \dot{q}) = \frac{1}{2} \sum_{k=1}^{n} \left(\frac{\partial M_{ij}}{\partial q_k} + \frac{\partial M_{ik}}{\partial q_j} - \frac{\partial M_{kj}}{\partial q_i} \right) \dot{q}_k.$$

See [106, pp. 170] for more information. The dynamics of (3.10) can be expressed as the control system (f, g) where

$$f(q, \dot{q}) = \begin{pmatrix} \dot{q} \\ -M^{-1}(q)\, H(q, \dot{q}) \end{pmatrix}, \quad g(q) = \begin{pmatrix} \mathbf{0} \\ -M^{-1}(q)\, B(q) \end{pmatrix} \tag{3.11}$$

Equation (3.10) is the simplest dynamic model of robotic motion and does not include any contact constraints. This is not necessarily a problem if one reduces the coordinates q by locating the body-fixed reference frame R_b at a stationary point fixing certain degrees of freedom, thereby factoring in ground contact constraints. To understand this, consider the following example:

Example 1. *The dynamics of a 2D model with point feet that walks in the x–z plane along the x-axis as that shown in Figure 3.1 can be modeled with the coordinates $q = (\phi_b^y, q_1)$ using* (3.10).

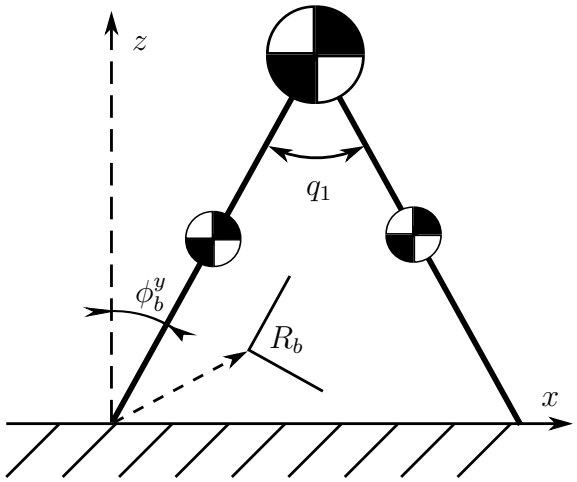

Figure 3.1: Example robot coordinates for a compass-gait biped. The body-fixed frame R_b is located at the interface between the stance foot and the ground. The coordinate ϕ_b^y tracks the orientation of R_b relative to a fixed world frame. The only body or shape coordinate for this simple model is q_1.

3.6 Constraining Forces

As mentioned, the motion of a rigid-body robot is governed by (3.10). The formulation of the equation, however, does not allow for analysis of reaction forces. This models takes into account reaction forces but they do not appear in the equations as they must be included in the form of kinematic constraints which alter the form of the dynamics by fixing coordinates as in Example 1.

In some cases, one may wish, for a variety of reasons, to compute the reaction forces themselves. For those who study materials and mechanism design of bipedal robots, it may be important to understand the forces present at the joints or at the feet to aid in design. Control theorists may wish to understand the moment at the stance foot in order to design gaits in which the foot does not rotate inadvertently. In addition, researchers may wish to study foot-strike which requires the use of impulsive constraining forces. For these reasons and others, it is important to consider a more

generalized model that, at the very least, includes reaction forces at the feet.

This subsection will show how constraints can be added to the standard robotic model. There are two different types of constraints which should be distinguished; see [106, Ch. 6] for further details. Holonomic constraints act to restrict the motion of a system to a smooth hypersurface of the configuration space $\mathcal{Q}$. Similarly, non-holonomic constraints act to restrict the motion of a system through a restriction on velocity. The modeling of constraints necessary for robots can generally be handled by considering only non-holonomic constraints, which have the form

$$J(q)\,\dot{q} = constant, \tag{3.12}$$

where $J(q)$ can be thought of as a Jacobian matrix. It is assumed that the constraints are linearly independent and thus $J(q)$ has full row rank. Intuitively, the rows of $J(q)$ represent maps to velocities of the system—i.e., for $J_i(q)$ which is the i^{th} row of $J(q)$, the quantity $J_i(q)\,\dot{q}$ represents an output velocity—which are to be restricted to a constant. Generally and all throughout this dissertation, the constant is zero; that is, the constraints are designed to prevent any motion rather than enforce constant, non-zero velocity.

Revisiting the standard robot model, consider augmenting the model to allow additional forces for imposing non-holonomic constraints:

$$M(q)\,\ddot{q} + H(q,\dot{q}) + J^T(q)\,\lambda = B(q)\,u. \tag{3.13}$$

In the literature, λ is often referred to as a Lagrange multiplier [13, §4.10] and $J^T(q)$ is a map from the space in which the output velocity constraints are represented (output space) to joint space and thus the constraining forces in joint space are

given by

$$F_c = J^T(q)\,\lambda.$$

The idea is to solve (3.13) for λ in terms of q, $\dot{q}$, and u such that (3.12) is satisfied. Differentiating (3.12) results in

$$\dot{J}(q,\dot{q})\,\dot{q} + J(q,\dot{q})\,\ddot{q} = 0.$$

Then solving (3.13) for $\ddot{q}$ and substituting into the above results in

$$\dot{J}(q,\dot{q})\,\dot{q} + J(q,\dot{q})\,M^{-1}(q)\left(B(q)\,u - H(q,\dot{q}) - J^T(q)\,\lambda\right) = 0.$$

Finally, solving for λ gives

$$\lambda = \left(J(q,\dot{q})\,M^{-1}(q)\,J^T(q)\right)^{-1}\left(\dot{J}(q,\dot{q})\,\dot{q} + J(q,\dot{q})\,M^{-1}(q)\,(B(q)\,u - H(q,\dot{q}))\right). \tag{3.14}$$

This formulation can be used to treat robots in a generalized configuration with non-holonomic constraints such as ground contact. The dynamic model (3.13) corresponds to the control system (f, g) where

$$f(q,\dot{q}) = \begin{pmatrix} \dot{q} \\ \left(J(q,\dot{q})\,M^{-1}(q)\,J^T(q)\right)^{-1}\left(\dot{J}(q,\dot{q})\,\dot{q} - J(q,\dot{q})\,M^{-1}(q)\,H(q,\dot{q})\right) \end{pmatrix},$$

$$g(q) = \begin{pmatrix} \mathbf{0} \\ \left(J(q,\dot{q})\,M^{-1}(q)\,J^T(q)\right)^{-1} J(q,\dot{q})\,M^{-1}(q)\,B(q)\,u. \end{pmatrix}. \tag{3.15}$$

Using the developments in this subsection, the next subsection will show how to

treat impacts which require constraining forces.

3.7 Discrete Impacts

When studying bipedal walking, it is important for the sake of thoroughness, to consider impacts and their effect on the motion of a system. Simple models like the linear inverted pendulum model ignore foot strike which results in a greater gap between simulation and experiment. For more on the different models and how impacts are treated, see Section 2.3. Non-smooth mechanics is a complicated topic; more detail can be found in, for example, [21, 74]. The mechanics of non-smooth impacts has been addressed for tool use in [42, 137]. In addition to the rigid models considered in this dissertation (as those treated by Hurmuzlu and Marghitu [61]), elastic impacts and model deformation have also been considered [24, 169].

For the purposes of this work, an impact is considered to occur when a rigid body (the foot) comes into contact with the ground. For simplicity, impacts are assumed to be rigid and plastic. Consider the extended robot dynamics equation (3.13). The Lagrange multiplier λ can be used with impacts by considering it to be representative of impulsive forcing. Denote by $\dot{q}^- = \lim_{\tau \nearrow t} \dot{q}(\tau)$ and $\dot{q}^+ = \lim_{\tau \searrow t} \dot{q}(\tau)$ the left and right limits to the solution $\dot{q}_e(t)$, respectively. Thus $\dot{q}^-$ and $\dot{q}^+$ respectively represent pre- and post-impact velocities. In addition, by assumption the configuration coordinates are continuous in time so $q^- = q^+ = q$. Assuming actuators do not produce impulsive forces and integrating the model (3.13) results in

$$M(q)(\dot{q}^+ - \dot{q}^-) = J^T(q)\, F_{imp} \tag{3.16}$$

where the impulsive force F_{imp} is given by

$$F_{imp} = \int_{t^-}^{t^+} \lambda(q(\tau), \dot{q}(\tau))\, d\tau.$$

Based on the desired constraints, one can construct a Jacobian matrix, $J(q)$, whose rows contain individual constraints. Combining (3.13) with (3.16) results in the impact model:

$$\begin{pmatrix} M(q) & -J^T(q) \\ J(q) & \mathbf{0} \end{pmatrix} \begin{pmatrix} \dot{q}^+ \\ F_{imp} \end{pmatrix} = \begin{pmatrix} M(q)\,\dot{q}^- \\ \mathbf{0} \end{pmatrix}. \tag{3.17}$$

This model is used throughout this dissertation wherever impacts arise. Using the Schur complement [180], the post-impact velocity can be written as

$$\dot{q}^+ = P(q, \dot{q}^-) = \left(I - M^{-1}(q)\, J^T(q)\, (J(q)\, M^{-1}(q)\, J(q))^{-1}\, J(q)\right)\, \dot{q}^- \tag{3.18}$$

with I the identity matrix of the appropriate dimension. The above equation can be used for any discrete transition. The forces in F_{imp} are reactionary impulsive forces and must satisfy realistic conditions, e.g., the floor must not pull on the robot. More on this for robot with feet is given in the next section.

In an attempt to simplify the model and obtain bi-periodic behavior in the walking, the "left" and "right" leg must be "swapped"; this "trick" is common throughout the literature [44]. This is done with a coordinate transformation, switching the role of the left and right leg, i.e., a state relabeling procedure, which is included in the calculation of the reset map. For the shape coordinates, this will be a linear map, but for reference frame coordinates, one may need to solve an inverse kinematics problem if the reference frame is relocated as part of the reset map. This problem

can be avoided by locating the reference frame on the torso as opposed to on the stance foot.

The information provided thus far is sufficient to handle simple bipeds with point feet but for more complex models, the definitions for hybrid systems must be expanded. This will be done in the next section.

3.8 Complex Domain Structure

A large portion of the research on bipedal robotic walking focuses on models of robots with point feet or flat-foot walking. This results in a simple hybrid model with a single domain which can be treated using the methods described earlier in this section. This idealization leads to walking gaits which lack some of the distinguishing characteristics of human locomotion. In particular, the foot behavior of human walking is highly recognizable and sets human walking apart from the flat-footed gaits seen on many of the early bipedal robots.

Under a more general view, a human walking gait can be seen to consist of multiple *phases* or *domains*—in each domain, the system evolves in a continuous fashion according to a dynamic model derived from a Lagrangian modeling the mechanical system on that domain. The dynamic model will vary depending on which points on the robot are in contact with the ground—having these fixed points introduces non-holonomic constraints on the system. At a certain point in each domain, i.e., when the contact points change, the model will discretely change to another phase of walking with a different dynamic model and different control. In the case of an end-effector on the robot coming into contact with the environment, impulsive forces act on the contact point which instantaneously alter the velocity of the system.

In this subsection, a formalism for multi-domain hybrid systems is introduced and a discussion is given explaining how the equations of motion of a robot together

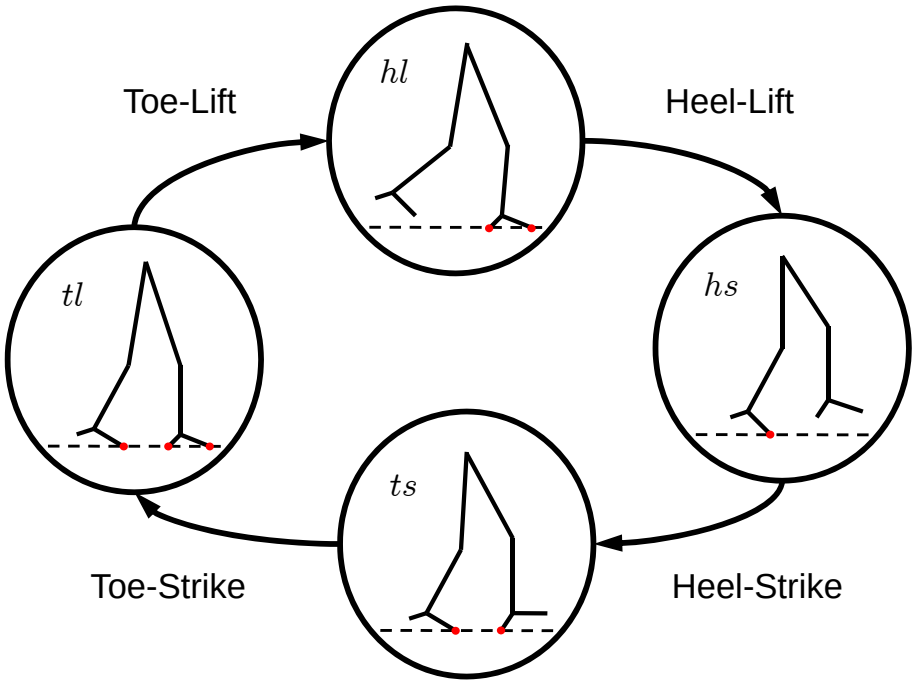

Figure 3.2: An example of a *domain breakdown*. That is, a combination of discrete phases of a walking gait with a specific temporal ordering. The red dots indicate which constraints are enforced in each discrete phase (or domain). The domain labels are selected based on which event causes a given domain to transition to the next.

with a temporal ordering of discrete events, i.e., change in contact points, completely determine the hybrid model of a system. More specifically, to model bipedal robots, one need only consider the domain breakdown and the Lagrangian on each domain. Details are provided to show how the breakdown can be derived by considering the kinematic constraints imposed on the system throughout the course of a step.

3.8.1 Formal Definitions

Steady state bipedal walking is naturally periodic with discrete impacts leading to different walking phases. Therefore, when studying walking, one should consider multi-domain hybrid systems with a temporal ordering of events, i.e., systems in which the domain graph is a *directed cycle*:

Definition 7. *A* **directed cycle** *is a graph* $\Gamma = (V, E)$*, with* V *a set of* **vertices** *and* E *a set of* **edges***—for an edge* $e \in E$*, denote the* **source** *by* $\mathrm{sor}(e)$ *and the* **target** *by* $\mathrm{tar}(e)$*—in which the vertices and edges can be written*

$$\begin{aligned} V &= \{v_1, v_2, \ldots, v_p\}, \\ E &= \{e_1 = \{v_1, v_2\}, e_2 = \{v_2, v_3\}, \ldots, e_p = \{v_p, v_1\}\}, \end{aligned} \tag{3.19}$$

where p *is the number of discrete domains in the corresponding hybrid model.*

This concept is illustrated in the following example, which will be used later in Section 5:

Example 2. *The domain breakdown pictured in Figure 3.2 has an underlying graph that is a directed cycle; the graph is given by* $\Gamma = (V, E)$*. In particular, there are four vertices and four edges with*

$$\begin{aligned} V &= \{ts, tl, hl, hs\}, \\ E &= \{\{ts, tl\}, \{tl, hl\}, \{hl, hs\}, \{hs, ts\}\}. \end{aligned}$$

The concept of a directed cycle is a fundamental component in the formulation of multi-domain hybrid systems:

Definition 8. *A* **hybrid control system in a cycle** *is a tuple,*

$$\Sigma^c = (\Gamma, D, \mathcal{U}, S, \Delta, \mathcal{FG}),$$

where

- $\Gamma = (V, E)$ *is a* **directed cycle**,

- $D = \{D_v\}_{v \in V}$ *is a set of* **domains** *with* $D_v \subseteq \mathcal{X}_v \times \mathcal{U}_v$ *a smooth submanifold, where* $\mathcal{X}_v$ *represents the state space,*
- $\mathcal{U} = \{\mathcal{U}_v\}_{v \in V}$ *with* $\mathcal{U}_v \subseteq \mathbb{R}^{m_v}$ *a set of* **admissible controls**,
- $S = \{S_e\}_{e \in E}$ *is a set of* **guards** *or* **switching surfaces**, *with* $S_e \subseteq D_{\mathrm{sor}(e)}$,
- $\Delta = \{\Delta_e\}_{e \in E}$ *is a set of* **reset maps**, *with* $\Delta_e : S_e \to \mathcal{X}_{\mathrm{tar}(e)}$ *a smooth map,*
- $\mathcal{FG} = \{(f_v,\, g_v)\}_{v \in V}$ *with* $(f_v,\, g_v)$ *a* **control system** *on* D_v, *i.e.,* $\dot{x} = f_v(x) + g_v(x)\, u \;\forall\; (x, u) \in D_v$,

for $v \in V$ *with edge* $e \in E$ *satisfying* $v = \mathrm{sor}(e)$. *This can also be described as an indexed system with impulse effects:*

$$\Sigma_v^c = \begin{cases} \dot{x} = f_v(x) + g_v(x)\, u, & (x^-, u^-) \in D_v \setminus S_e, \\ x^+ = \Delta_e(x^-), & (x^-, u^-) \in S_e, \end{cases} \tag{3.20}$$

The set of hybrid control systems for all domains in V *can be written* $\Sigma^c = \{\Sigma_v^c\}_{v \in V}$.

Definition 9. *A* **hybrid system** *is a hybrid control system with* $\mathcal{U}_v = \emptyset \;\forall\; v \in V$, *e.g., any relevant feedback controllers have been applied, making the system closed-loop:*

$$\Sigma = (\Gamma,\, D,\, S,\, \Delta,\, \mathcal{F}),$$

where $\mathcal{F} = \{f_v\}_{v \in V}$, *with* f_v *a (possibly non-autonomous)* **dynamical system** *on* $\mathcal{X} \subseteq D_v$, *i.e.,* $\dot{x} = f_v(x, t)$ *for* $v \in V$ *with edge* $e \in E$ *satisfying* $v = \mathrm{sor}(e)$. *The other elements are the same as those defined for hybrid control systems. This corresponds*

to the following system with impulse effects:

$$\Sigma_v = \begin{cases} \dot{x} = f_v(x) & x^- \in D_v \setminus S_e, \\ x^+ = \Delta_e(x^-), & x^- \in S_e. \end{cases} \tag{3.21}$$

The set of hybrid systems for all domains in V can be written $\Sigma = \{\Sigma_v\}_{v \in V}$.

Comparing the above definitions and (3.20) and (3.21), it is clear that the domain of admissibility and the guard are dependent on control. This dependence is a result of considering the dynamic moment of the system in formulating these particular spaces and will be clarified further in Section 3.8.3.2.

3.8.2 Obtaining Hybrid Systems from Constraints

The remainder of this subsection is devoted to discussing how the Lagrangian for a biped, together with a domain breakdown (which determines the constraints at each vertex of the associated cycle), allows one to explicitly construct a hybrid model of the system. Examples can be found throughout the literature; see, for example, [45, 46, 138].

3.8.2.1 Constraints

The continuous dynamics of a system depends on which constraints are enforced at any given time while the discrete dynamics depends on the change in constraints. Constraints and their enforcement are dictated by the configuration of contact points between the system and the ground. Specifically, one can define a *contact set* $\mathcal{C} = \{c_1, c_2, \ldots, c_k\}$, with each c_i a specific type of foot/ground contact possible in the biped. Assuming that foot contact is restricted to edges parallel to the y-axis (i.e., the toe edge or the heel edge)—and this is the case in 2D as in this work—there are

four contact points of interest:

$$\mathcal{C} = \{c_{\text{sth}},\, c_{\text{stt}},\, c_{\text{nsh}},\, c_{\text{nst}}\},$$

where these constraints physically represent the stance heel, stance toe, non-stance heel, and non-stance toe, respectively. The reason for choosing this set of contact points will become clear after data analysis.

Remark 1. *In some of the literature, the term non-stance is referred to as swing. This is an artifact of point-foot bipedal models which have only single support and instantaneous double support (at impact). This dissertation instead uses the term non-stance due to the existence of noninstantaneous double support phases where there are periods with no free swinging behavior. In this case the naming of the stance/non-stance legs is arbitrary; in this dissertation, the stance leg is defined as the leg holding most of the weight of the robot.*

Contact points introduce *non-holonomic constraints*, η_c for $c \in \mathcal{C}$, on the system; this vector must be held constant for contact to be maintained. To construct these constraints, consider a reference frame R_c at the contact point c such that the axis of rotation about this point (either the heel or toe) is along the y-axis. Let $R_0^c(q)$ be a rotation matrix between reference frames from R_0 and R_c. Let $p_c : \mathcal{Q} \to \mathbb{R}^3$ represent the position of the frame and let $v_c(q, \dot{q}) = \dot{p}_c(q, \dot{q})$ represent the velocity.

The body-fixed angular velocity of the frame can then be found:

$$\Omega_c(q,\dot{q}) = (R_0^c(q))^T \frac{\partial R_0^c(q)}{\partial q}\,\dot{q} \tag{3.22}$$
$$= \begin{bmatrix} 0 & -\omega_c^z(q,\dot{q}) & \omega_c^y(q,\dot{q}) \\ \omega_c^z(q,\dot{q}) & 0 & -\omega_c^x(q,\dot{q}) \\ -\omega_c^y(q,\dot{q}) & \omega_c^x(q,\dot{q}) & 0 \end{bmatrix}.$$

The angular velocity vector

$$\omega_c(q,\dot{q}) = (\omega_c^x(q,\dot{q}),\, \omega_c^y(q,\dot{q}),\, \omega_c^z(q,\dot{q}))$$

is dual to the skew-symmetric matrix $\Omega(q,\dot{q})$. Furthermore,

$$v_c(q,\dot{q}) = \frac{\partial p_c(q)}{\partial q}\,\dot{q} \tag{3.23}$$

with $p_c(q)$ the Cartesian position of the contact point c. It is apparent from (3.22) and (3.23) that $v_c(q,\dot{q})$ and $\omega_c(q,\dot{q})$ are linearly dependent on $\dot{q}$. Thus, the non-holonomic constraint can be written

$$\eta_c(q,\dot{q}) = \begin{bmatrix} v_c(q,\dot{q}) \\ \omega_c^x(q,\dot{q}) \\ \omega_c^z(q,\dot{q}) \end{bmatrix} = J_c(q)\,\dot{q}.$$

Therefore, it is possible to find the associated Jacobian matrix through differentiation:

$$J_c(q) = \frac{\partial \eta_c(q,\dot{q})}{\partial \dot{q}}.$$

In the case of a 2D biped, the treatment is exactly the same but

$$\eta_c(q, \dot{q}) = (v_c^x(q, \dot{q}),\, v_c^z(q, \dot{q})).$$

The end result of this choice of coordinates is a non-holonomic constraint which enforces the condition $\eta_c(q, \dot{q}) = \text{constant}$—this fixes the contact point to the ground but allows rotation about the heel or toe depending on the specific type of contact. It is useful to express the collection of all non-holonomic constraints in a single matrix $\eta(q, \dot{q}) \in \mathbb{R}^{20\times 4}$ as:

$$\eta(q, \dot{q}) = \text{blk diag}(\eta_{\text{sth}}(q, \dot{q}),\, \eta_{\text{stt}}(q, \dot{q}),\, \eta_{\text{nsh}}(q, \dot{q}),\, \eta_{\text{nst}}(q, \dot{q}))$$

Another class of constraints that is important is the class of *unilateral constraints*, $h_c(q)$ for $c \in \mathcal{C}$, since they dictate the set of admissible configurations of the system. Assuming that the knees do not lock, these constraints represent the height of a contact point above the ground, $h_c(q) = p_c^z(q)$, and can be put in the form of a matrix $h(q) \in \mathbb{R}^{4\times 4}$ in the same manner as non-holonomic constraints; that is,

$$h(q) = \text{diag}(h_{\text{sth}}(q),\, h_{\text{stt}}(q),\, h_{\text{nsh}}(q),\, h_{\text{nst}}(q)).$$

3.8.2.2 Domain Breakdowns

A domain breakdown is a directed cycle together with a specific choice of contact points for each vertex of the graph. To define this formally, assign to each vertex a binary vector describing which contact points are enforced on each domain.

Definition 10. *Let $\mathcal{C} = \{c_1, c_2, \ldots, c_k\}$ be a set of contact points and Γ be a directed cycle. A* **domain breakdown** *is a binary map $\mathcal{B} : V \to \mathbb{Z}_2^k$ such that $\mathcal{B}_i(v) = 1$ if*

c_i is in contact on v and $\mathcal{B}_i(v) = 0$ otherwise.

Example 3. *In the case of the graph Γ_u given in Example 2 and the set of contact points $\mathcal{C} = \{c_{\text{sth}}, c_{\text{stt}}, c_{\text{nsh}}, c_{\text{nst}}\}$, for the graph shown in Figure 3.2, the domain breakdown is formally given by $B_u : V_u \to \mathbb{Z}_2^4$ where*

$$\begin{aligned} \mathcal{B}_u(ts) &= (1,0,0,1)^T, \\ \mathcal{B}_u(tl) &= (1,1,0,1)^T, \\ \mathcal{B}_u(hl) &= (1,1,0,0)^T, \\ \mathcal{B}_u(hs) &= (0,1,0,0)^T. \end{aligned} \tag{3.24}$$

3.8.3 Hybrid System Construction

It will now be shown that, given a Lagrangian, a directed cycle, and a domain breakdown, a hybrid system can be explicitly constructed. Since the Lagrangian is intrinsic to the robot being considered, a domain breakdown alone dictates the mathematical model of the biped.

3.8.3.1 Continuous Dynamics

The control system

$$\dot{x} = f_v(x) + g_v(x)\, u$$

can be explicity constructed through the constraints imposed on each domain by the domain breakdown. For the domain $v \in V$, the imposed non-holonomic constraints are given by:

$$\eta_v(q, \dot{q}) = \eta(q, \dot{q})\, \mathcal{B}(v),$$

where the domain breakdown dictates which constraints are enforced. One can calculate the Jacobian matrix used to enforce the constraints by differentiating the non-holonomic constraint and removing redundancies as follows:

$$J_v(q) = \text{Basis}\left(\text{Row Sp}\left(\frac{\partial \eta_v(q,\dot{q})}{\partial \dot{q}}\right)\right).$$

By taking a basis for the row space of the Jacobian, redundant constraints are removed so that $J_v(q)$ has full row rank. Using this Jacobian, the constrained dynamic model is given by (3.13). where the wrench contains forces and moments expressed in the reference frame R_c. Because the robot is modeled in a generalized position with ground contact enforced through constraints, the matrices $M(q)$, $H(q,\dot{q})$, and $B(q)$ are identical in every domain.

3.8.3.2 Discrete Dynamics

The discrete dynamics consist of the domains, guards and reset maps for a hybrid system and are related to the domain breakdown.

Given a vertex $v \in V$, the domain D_v is the set of admissible configurations of the system factoring in both friction and a unilateral constraint. Specifically, from the wrench $W_v(q,\dot{q},u)$, one can ensure that the foot does not slip by considering inequalities on the friction which can be stated in the form:

$$\mu_v(q)\, W_v(q,\dot{q},u) \geq 0, \tag{3.25}$$

with $\mu_v(q)$ a matrix of friction parameters and constants defining the geometry of the foot [45]. Additionally, it has been shown in [26, 168] that the moment produced

by the ground is limited; this limitation can be written in the form:

$$\nu_v(q)\, W_v(q, \dot{q}, u) \geq 0, \tag{3.26}$$

where $\nu_v(q)$ depends on the physical parameters and state of the system. Equations (3.25) and (3.26) for a given domain can be coupled with the unilateral constraint on the domain, $h_v(q) = h(q)\, B(v)$, if present, to yield the set of admissible configurations:

$$A_v(q, \dot{q}, u) = \begin{bmatrix} \mu_v(q)\, W_v(q, \dot{q}, u) \\ \nu_v(q)\, W_v(q, \dot{q}, u) \\ h_v(q) \end{bmatrix} \geq 0. \tag{3.27}$$

Thus, the domain is given by

$$D_v = \{(q, \dot{q}, u) \in T\mathcal{Q} \times \mathcal{U}_v : A_v(q, \dot{q}, u) \geq 0\}. \tag{3.28}$$

The guard is just the boundary of this domain with the additional assumption that the set of admissible configurations is decreasing, i.e., the vector field is pointed outside of the domain, or, for an edge $e = (v,\, v') \in E$,

$$S_e = \Big\{(q, \dot{q}, u) \in T\mathcal{Q} \times \mathbb{R}^{m_v} :\ A_v(q, \dot{q}, u) = 0 \text{ and } \dot{A}_v(q, \dot{q}, u) \leq 0\Big\}.$$

The impact equations are obtained by considering the constraints enforced on the subsequent domain; denote the Jacobian associated to these constraints by $J_{v'}$. For an edge $e = \{v,\, v'\} \in E$, the post-impact velocity $\dot{q}^+$ is given in terms of the pre-impact velocity $\dot{q}^-$ using the impact model given in (3.17). For transitions where a contact point strikes the ground, there will be a discrete change in velocities given

by (3.18). For transitions where a contact point lifts from the ground, there will not be a discrete change; thus the impact map will be the identity map. The reset map is then constructed using the impact map and factoring in coordinate relabeling if necessary. For multi-domain walking, one selects an edge at which relabeling occurs each step.

The reset map then takes a point on the guard of a domain and maps it into the next domain specified by the domain breakdown. For the sake of clarification, consider the following example:

Example 4. *In the case of domain ts, the impact event is toe-strike. A plastic impact occurs with the stance toe, resulting in zero post-impact velocity of the stance toe. The stance heel and non-stance toe both remains on the ground. In order to properly achieve this transition, non-holonomic constraints on the velocities of stance toe, stance heel, and non-stance toe must be; these constraints lead to the Jacobian matrix* J_{hl} *which is used in* (3.18)*; and, in fact, these are the same constraints present in the domain breakdown in* (3.24)*.*

The end result is that, given a domain breakdown and a bipedal robot, the hybrid model for the biped is completely determined.

4. ENERGY SHAPING

This section focuses on the primary contribution of this dissertation: stabilization of periodic behaviors in hybrid dynamical systems through *energy shaping*. This method provides a manner for understanding the dynamics of both conservative and non-conservative systems in terms of energy exchange and employs Lyapunov methods to alter the stability properties of controllers for such systems. The formal theoretical contribution appears in Theorem 1 which states that the energy shaping controller presented does not destabilize the system to which it is applied for small enough control gains. Although nothing is formally shown regarding the robustness of the shaped system to perturbations in initial conditions, myriad numerical simulations later show that, the method can result in a larger domain of attraction and shorter stabilization times for limit cycles of certain systems.

It should be mentioned that this problem falls under a class of problems involving stability of systems with zero dynamics. In [4], a similar problem was considered in which a stabilizing control law was constructed using control Lyapunov functions to stabilize to a zero dynamics which exhibited hybrid invariance; that is, for initial conditions on the intersection of the switching surface and the hybrid zero dynamics manifold, application of the reset map will result in a state which is still on the hybrid zero dynamics. This was a key assumption underlying the [4] but this assumption does not hold for energy shaping as energy is generally not invariant through impact, though there may be pathological examples which demonstrate this property. In fact, for certain conservative systems like the compass gait biped shown in Figure 4.1, which exhibits local exponential stability, energy change can only occur through discrete transitions and so impacts actually act as a stabilizing influence.

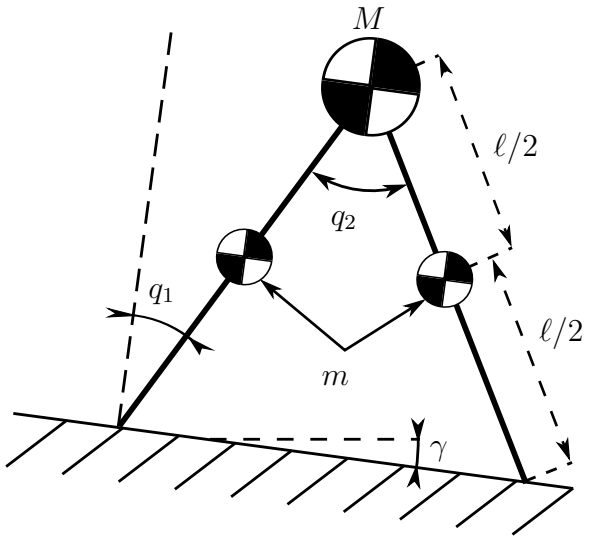

Figure 4.1: Compass-gait biped falling down a slope.

Energy shaping has been considered for conservative systems [147] and for non-conservative systems [149]. There is, however, a dearth of formal results and this dissertation aims to fill in some of the gaps in the literature. In [147], Spong and Bhatia presented the idea of designing a controller to shape the total energy of the system for the compass-gait biped and showed that the controller would guarantee asymptotic stability to the desired energy level through the continuous dynamics. Later in [149], the results were extended to non-conservative systems by considering storage functions of the form shown in (4.2). The exposition was generally based around numerical simulations and had limited formal results.

Another key difference is the assumption of stability which is necessary for the application of energy shaping. Whereas [4] requires stability of the system for states restricted to the hybrid zero dynamics, this work requires stability of the nominal system and does not require hybrid invariance of the zero dynamics. Thus, while the problems are somewhat similar, they also have their differences and are applicable to different types of systems and problems.

4.1 Overview

Periodic behaviors in mechanical systems have specific energy signatures that evolve over time. The energy dynamics of a conservative system can be understood as an interplay between kinetic and potential energy, with energy transfer occurring between these two quantities. Indeed for conservative systems, the energy is constant, i.e.,

$$E_0 \equiv E(q, \dot{q}) = T(q, \dot{q}) + U(q),$$

where $T : T\mathcal{Q} \to \mathbb{R}_{\geq 0}$ represents the kinetic energy and $U : \mathcal{Q} \to \mathbb{R}$ represents the potential energy. In a non-conservative system, this relationship does not hold, but the dynamics of energy can still be understood as

$$E_0 \equiv E_c(t) = T(q(t), \dot{q}(t)) + U(q(t)) - W(t). \tag{4.1}$$

with the storage function $W : \mathbb{R}_{\geq 0} \to \mathbb{R}$ defined by

$$W(t) = \int_0^t F_{\text{nc}}(\tau) \cdot \frac{dq(\tau)}{d\tau} \, d\tau \tag{4.2}$$

where $F_{\text{nc}} : \mathbb{R}_{\geq 0} \to \mathbb{R}^n$ represents non-conservative forcing. From the above definition it is clear that the storage function is dependent on initial conditions. This work will consider forcing that takes the form of an autonomous feedback control law, i.e.,

$$F_{\text{nc}}(t) = F_{\text{nc}}^{\text{a}}(q(t), \dot{q}(t))$$

for autonomous forcing

$$F^{\mathrm{a}}_{\mathrm{nc}}(q, \dot{q}) := B(q)\, v(q, \dot{q}).$$

While the state variables q and $\dot{q}$ vary with time, the forcing is autonomous in the normal sense of the term in that the forcing does not depend on the value of an independent variable time variable directly but rather only on the values of q and $\dot{q}$ at any given point in time. Time can be shifted arbitrarily and the resulting evolution of coordinates will not changed. For more on the difference between autonomous and non-autonomous (time-based) systems, see, for example, [115, pp. 63].

Under such an assumption, (4.2) becomes

$$W(t) = \int_0^t B(q(\tau))\, v(q(\tau), \dot{q}(\tau)) \cdot \frac{dq(\tau)}{d\tau}\, d\tau. \tag{4.3}$$

From the relationship stated in (4.1) and (4.2), it is clear that the total energy present in the system plus the energy removed by non-conservative forcing is constant. In other words, the integral term represents the flow of energy into and out of the system. This phenomenon is well understood and it holds for all motion in mechanical systems, not just for periodic behaviors. This storage function is central to passivity-based control, a topic which has appeared previously in the literature; e.g., [149].

Understanding the energy dynamics of a system is key to the method of energy shaping. By taking advantage of the presence of energy level sets in periodic behaviors, energy shaping seeks to augment certain types of controllers which do not necessarily have an intrinsic notion of stabilizing to a zero dynamics as in [4]. In doing so, the goal is to alter the properties of robustness with respect to perturba-

tions in initial conditions for existing controllers. The design of such a controller will therefore seek to satisfy the above goals and formal proof will be given that the designed controller does not destabilize the existing behavior (induced by an existing control law).

4.2 Setup

The main idea behind energy shaping is to impose exponential convergence to a conserved energy function through the continuous dynamics of a hybrid system of the form (3.4) with the goal of not destabilizing the overall hybrid system. As mentioned in Section 3.3, there are multiple types of stability depending upon the type convergence exhibited by a system. Energy shaping shaping seeks to achieve exponential convergence to a desired energy level; formally, given a conserved energy function E_c as in (4.1), the following condition is desired:

$$E_c(t) \leq E_c(0)\, e^{-\alpha t}$$

for some positive real constant α and for $t \geq 0$.

For non-conservative systems, as mentioned above, a storage function is necessary to track energy flow into and out of the system due to non-conservative forcing as doing so allows energy shaping to take advantage of conservation of energy. The storage function that is of interest was described in (4.3) but the evolution of the function must be expressed as a differential equation for the dynamics to be properly understood. By the fundamental theorem of calculus, it is clear that the desired storage function must satisfy

$$dW = R(q, \dot{q})\, dt$$

where R is given by

$$R(q, \dot{q}) := \left(B(q)\, v(q, \dot{q})\right)^T \frac{dq}{dt}.$$

Using the storage function W, augment the state space viz.

$$x := (q, \dot{q}, W).$$

In addition, the vector fields must be augmented to take the W dynamics into account as follows:

$$\bar{f}(q, \dot{q}) := \begin{pmatrix} f(q, \dot{q}) + g(q, \dot{q})\, v(q, \dot{q}) \\ R(q, \dot{q}) \end{pmatrix}, \qquad \bar{g}(q) := \begin{pmatrix} g(q) \\ \mathbf{0} \end{pmatrix}.$$

Using the augmented state leads to the following hybrid control system:

$$\overline{\Sigma}_c = \left\{ \begin{array}{rcll} \dot{x} & = & \bar{f}(q, \dot{q}) + \bar{g}(q)\, u & \\ q^+ & = & \Delta_q(q^-) & \text{if } (q^-, \dot{q}^-) \in D \setminus S, \\ \dot{q}^+ & = & \Delta_{\dot{q}}(q^-, \dot{q}^-) & \\ W^+ & = & \Delta_W = 0 & \text{if } (q^-, \dot{q}^-) \in S. \end{array} \right. \tag{4.4}$$

where Δ_q, $\Delta_{\dot{q}}$, and Δ_W, respectively, represent the q, $\dot{q}$, and W components of the reset map, Δ. Under this formulation, the conserved energy can be expressed as

$$E_c(q, \dot{q}, W) = T(q, \dot{q}) + U(q) - W.$$

In this form, it is clear that the system of interest is an autonomous one. This formulation will be used to state and prove the energy shaping theorem (Theorem 1).

However, before stating the theorem, it is important to first introduce and discuss a tool which will play a crucial part in achieving energy stabilization: the control Lyapunov function.

4.3 Control Lyapunov Functions

The energy shaping controller relies on the use of the *control Lyapunov function* [10, 35], which is a natural extension of Lyapunov's direct method. Recall that a system of the form

$$\dot{x} = f(x) \tag{4.5}$$

is stable about the origin if there exists a function $V : \mathcal{X} \to \mathbb{R}_{\geq 0}$ that is positive definite and zero at the origin. Stability can be achieved about any given equilibrium point but a coordinate transformation can be constructed to shift any point to the origin without loss of generality. For a system with no control (or a closed-loop system) of the form (4.5), Lyapunov stability can formally be defined:

Definition 11. *For a system of the form* (4.5)*, a continuously differentiable function* $V : D \to \mathbb{R}_{\geq 0}$ *is said to be a* ***Lyapunov function*** *if there exist constants* $c_1, c_2, c_3 \in \mathbb{R}_{>0}$ *such that for all* $x \in D$*,*

$$c_1\|x\| \leq V(x) \leq c_2\|x\|,$$
$$\dot{V}(x) + c_3 V(x) \leq 0.$$

From the above definition, it is easy to see that

$$\frac{dV(x)}{dt} + c_3 V(x) \leq 0 \Rightarrow V(t) \leq V_0\, e^{c_3 t},$$

where $V_0 = V(x(\mathbf{0}))$.

A natural extension of Lyapunov functions is the notion of control Lyapunov functions which generalize the time derivative to include a control term. For a system with no control, the time derivative of a function $V : \mathbb{R}_{\geq 0} \to \mathbb{R}$ can be expressed as

$$L_f V(x) = \frac{dV(x)}{dt}$$

where $L_f V(x)$ represents the Lie derivative (see, e.g., [134]) of the function $V(x)$ along the vector field f, i.e.,

$$L_f V(x) = \frac{\partial V(x)}{\partial x} \cdot \frac{dx}{dt}.$$

If control acts on the system as in

$$\dot{x} = f(x) + g(x)\, u, \tag{4.6}$$

the time derivative becomes

$$\dot{x} = L_f V(x) + L_g V(x)\, u.$$

This understanding of differentiation along vectors fields motivates the introduction of control Lyapunov functions:

Definition 12. *For a system of the form* (4.6)*, a continuously differentiable function* $V : D \to \mathbb{R}_{\geq 0}$ *is said to be a* ***control Lyapunov function (CLF)*** *if there exist*

constants $c_1, c_2, c_3 z \in \mathbb{R}_{>0}$ *such that for all* $x \in D$,

$$c_1\|x\| \leq V(x) \leq c_2\|x\|,$$
$$\inf_{u\in\mathcal{U}} \left[L_f V(x) + L_g V(x)\, u + c_3 V(x)\right] \leq 0.$$

In order to guarantee a stricter form of convergence, a modified notion of these functions is used (c.f. [4]):

Definition 13. *For the continuous dynamics of a system of the form* (3.3)*, a continuously differentiable function* $V_\varepsilon : D \to \mathbb{R}_{\geq 0}$ *is said to be a* ***rapidly exponentially stablizing control Lyapunov function (RES–CLF)*** *(see [4]) if there exist constants* $c_1, c_2, c_3 \in \mathbb{R}_{>0}$ *such that for all* $\varepsilon > 0$ *and for all* $x \in D$,

$$c_1\|x\| \leq V_\varepsilon(x) \leq \tfrac{c_2}{\varepsilon^2}\|x\|,$$
$$\inf_{u\in\mathcal{U}} \left[L_\Phi V_\varepsilon(x) + L_\Gamma V_\varepsilon(x)\, u + \tfrac{c_3}{\varepsilon} V_\varepsilon(x)\right] \leq 0.$$

For the continuous dynamics, define a candidate Lyapunov function, $V : D \to \mathbb{R}_{\geq 0}$, of the form

$$V_\varepsilon(x) = \frac{1}{2}(E_c(x) - E_{\text{ref}})^2, \tag{4.7}$$

with E_{ref} the energy associated with the periodic orbit, and use it as a control Lyapunov function to construct the energy shaping controller

$$\mu_\varepsilon(x) = \underset{u(x)\in\mathbb{R}^m}{\arg\min}\ u(x)^T u(x) \tag{4.8}$$
$$\text{s.t. } L_f V_\varepsilon(x) + L_g V_\varepsilon(x)\, u(x) + \frac{c_3}{\varepsilon} V_\varepsilon(x) \leq 0.$$

Applying this to the system (3.4) results in

$$\Sigma = \begin{cases} \dot{x} = f(x) + g(x)\,\mu_\varepsilon(x), & x^- \in D \setminus S, \\ x^+ = \Delta(x^-), & x^- \in S. \end{cases} \tag{4.9}$$

As a result of the control law construction in (4.8), the closed-loop dynamics of (4.9) is stabilized with respect to the zero level set of the Lyapunov function (4.7) thus satisfying the convergence specified in Definition 13.

As an added remark, it bears mentioning that a closed-form, continuously differentiable solution to the QP (4.8) is given by the min-norm controller (see, e.g., [35]),

$$\mu_\varepsilon(x) = -\frac{\psi_0^\varepsilon(x)\psi_1^\varepsilon(x)}{(\psi_1^\varepsilon(x))^T\psi_1^\varepsilon(x)}, \tag{4.10}$$

where

$$\psi_0^\varepsilon(x) := L_f V_\varepsilon(x) + \frac{c_3}{\varepsilon}, \qquad \psi_1^\varepsilon(x) := \left(L_g V_\varepsilon(x)\right)^T.$$

This solution is practically useful for several reasons. Most importantly, it provides a closed-form solution which is important for proving Theorem 1 (which is stated subsequently in Section 4.4). In addition, it can be used in numerical simulations in place of a quadratic program to reduce the computational overhead (in most cases). In the simulations described in Section 6, the min-norm solution (4.10) is used to reduce computation time.

4.4 Stability of the Shaped System

With the preceding setup in mind, the main formal idea behind energy shaping can now be stated:

Theorem 1. *Given an exponentially-stable limit cycle in a hybrid system of the form* (3.3)*, application of the energy shaping controller* (4.8) *to the control system* (3.4) *results in the closed-loop hybrid system* (4.9)*, which is exponentially stable.*

The proof is given later after some discussion.

In order to achieve the stated goal, it is necessary to show that, given a system with a limit cycle representing the desired behavior, energy shaping can be applied and the resulting system will have an invariant orbit which is equivalent to the nominal system. Simply put, the control contribution from the energy shaping controller must be identically zero on the orbit. Consider the following lemma:

Lemma 1. *Applying the energy shaping controller* (4.8) *to a hybrid control system* (3.4) *results in a closed-loop hybrid system* (4.9) *that demonstrates a periodic orbit which is identical to the unshaped system* (3.3)*.*

Proof. For states on the periodic orbit, i.e., $x^{\mathscr{O}} \in \mathscr{O}$, the conserved energy is a known constant, $E_c(x^{\mathscr{O}}) = E_{\text{ref}}$. Therefore, the limit cycle represents an invariant level set of the energy. By construction of the Lyapunov function (4.7) used in the controller (4.8), it is clear that $V(x^{\mathscr{O}}) = 0$ and, moreover, that

$$\inf_{x \in D} V(x) = 0.$$

The solution to the optimization problem (4.8) has cost $u(x)^T u(x) = 0$ (which implies that all elements of $u(x)$ are zero when $V(x) = 0$) and this satisfies the stability condition of the control Lyapunov function; indeed $\dot{V}(x^*) = 0$ since the conserved energy does not change if $u(x) = \mathbf{0}$. Thus, the periodic orbits are equivalent. □

4.5 Zero Dynamics Formulation

In order to understand the nature of energy shaping, consider breaking up the system into two sets of coordinates,

$$\begin{aligned} \dot{\xi} &= p(\xi, \zeta) + r(\xi, \zeta)\, u, \\ \dot{\zeta} &= s(\xi, \zeta) + w(\xi, \zeta)\, u, \end{aligned} \tag{4.11}$$

with states $\xi \in \Xi$ and $\zeta \in Z$ and control inputs $u \in \mathcal{U}$. The vector fields p, r, s, and w are assumed to be locally Lipschitz continuous. To simplify notation, define

$$\Phi(\xi, \zeta) = \begin{pmatrix} p(\xi, \zeta) \\ s(\xi, \zeta) \end{pmatrix}, \qquad \Gamma(\xi, \zeta) = \begin{pmatrix} r(\xi, \zeta) \\ w(\xi, \zeta) \end{pmatrix}.$$

The natural choice of transformation to convert the continuous dynamics of (3.4) to (4.11) is through energy. Thus, for mechanical systems where $x = (q, \dot{q}, W) \in T\mathcal{Q}$, consider the coordinate transformation

$$\begin{aligned} \xi &= E_c(x) - E_{\text{ref}}, \\ \zeta &= (q_1,\ \ldots,\ q_n,\ \dot{q}_1,\ \ldots,\ \dot{q}_{n-1},\ W), \end{aligned}$$

where n is the size of the configuration space, $\mathcal{Q}$. By construction, the fixed point of the hybrid system can be chosen to occur at $(\xi, \zeta) = (0, \zeta^*)$ such that $\Delta(0, \zeta^*) = (0, \mathbf{0})$. Moreover, because conserved energy does not change by the natural dynamics, $f(\xi, \zeta) = 0$.

The coordinate transformation is valid if it is locally diffeomorphic. For mechan-

ical systems, which are of interest to this paper, energy takes the form

$$E_c(x) = \frac{1}{2}\dot{q}^T M(q)\,\dot{q} + U(q) - W, \tag{4.12}$$

where the first and second terms represent the kinetic and mechanical energy, respectively. Because $M(q)$ is invertible for mechanical systems, it never has determinant zero. In addition, for the specific ordering of coordinates

$$\begin{aligned}\Psi :=&(\zeta_1,\ \ldots,\ \zeta_{2n-1},\ \xi,\ \zeta_{2n})\\ =&(q_1,\ \ldots,\ q_n,\ \dot{q}_1,\ \ldots,\ \dot{q}_{n-1},\ E_c(x) - E_{\text{ref}},\ W),\end{aligned}$$

the Jacobian matrix associated with the transformation is

$$\frac{\partial \Psi(q,\dot{q},W)}{\partial(q,\dot{q},W)} = \begin{pmatrix} I & \mathbf{0}_{2n-1\times 1} & \mathbf{0}_{2n-1\times 1} \\ \frac{\partial E_c(q,\dot{q},W)}{\partial(q_1,\ \ldots,\ q_n,\ \dot{q}_1,\ \ldots,\ \dot{q}_{n-1})} & \frac{\partial E_c(q,\dot{q},W)}{\partial \dot{q}_n} & 0 \\ \mathbf{0}_{1\times 2n-1} & 0 & -1 \end{pmatrix}. \tag{4.13}$$

This matrix is invertible when

$$\det \Psi(\xi,\zeta) = -\frac{\partial E_c(q,\dot{q},W)}{\partial \dot{q}_n} \neq 0.$$

This condition guarantees that the transformation (4.13) is a valid diffeomorphism. It may not necessarily hold through the entire operating space, $T\mathcal{Q}$, of the system but it need only hold locally around the orbit. Some analysis of this criterion is given for specific examples in Section 6.

Applying the control law (4.8), the dynamics (4.11) becomes

$$\begin{aligned}\dot{\xi} &= p(\xi,\zeta) + r(\xi,\zeta)\,\mu_\varepsilon(\xi,\zeta),\\ \dot{\zeta} &= s(\xi,\zeta) + w(\xi,\zeta)\,\mu_\varepsilon(\xi,\zeta).\end{aligned} \tag{4.14}$$

By the construction of the control law (4.8), it is clear that $\mu_\varepsilon(0,\zeta) = 0$ and thus it follows that $p(0,\zeta) = 0$. In other words, the zero dynamics manifold $\mathcal{Z}$ is the restricted subset of $\mathcal{X}$ such that $\xi = 0$. Rewrite the candidate Lyapunov function (4.7) in the zero dynamics coordinates,

$$V(\xi) = \frac{1}{2}\xi^2$$

and consider the following:

Proposition 1. *Exponential stability of the continuous ξ dynamics is guaranteed if a RES–CLF exists satisfying*

$$\begin{gathered}c_1\,|\xi|^2 \le V(\xi) \le \tfrac{c_2}{\varepsilon^2}\,|\xi|^2,\\ \inf_{u\in\mathcal{U}}\left[L_\Phi V(\xi,\zeta) + L_\Gamma V(\xi,\zeta)\,u + \tfrac{c_3}{\varepsilon}V(\xi)\right] \le 0,\end{gathered} \tag{4.15}$$

for all $(\xi,\zeta) \in \Xi \times Z$.

Proof. It is easy to see that the first inequality is satisfied for $c_1 \le \frac{1}{2}$ and $c_2 \ge \frac{\varepsilon^2}{2}$. Define the set

$$K_\varepsilon = \left\{u \in \mathcal{U} : L_\Phi V(\xi,\zeta) + L_\Gamma V(\xi,\zeta)\,u + \frac{c_3}{\varepsilon}V(\xi) \le 0\right\}. \tag{4.16}$$

In order to see that the set K_ε is not empty, consider the control Lypaunov function system in the original coordinates as given in (4.7). The time derivative is

$$\begin{aligned}\dot{V}_\varepsilon(x) &= E(x)\frac{\partial E(x)}{\partial x}(p(x) + r(x)\,u) \\ &\geq E(q,\dot{q}) \begin{pmatrix} \frac{\partial E(q,\dot{q})}{\partial q} & \frac{\partial E(q,\dot{q})}{\partial \dot{q}} \end{pmatrix} \cdot \left[\begin{pmatrix} \dot{q} \\ -M^{-1}(q)H(q,\dot{q}) \end{pmatrix} + \begin{pmatrix} \mathbf{0}_{n\times m} \\ -M^{-1}(q)B(q) \end{pmatrix} u \right].\end{aligned}$$

For a fully-actuated system, $m = n$ so $B : \mathcal{Q} \to \mathbb{R}^{n\times m}$ is full rank. Since $M(q)$ is invertible for physical bodies, $M(q)\,B(q)$ is invertible. Thus there exists at least one $u(q,\dot{q})$ satisfying

$$M^{-1}(q)B(q)\,u(q,\dot{q}) = \frac{c_3}{\varepsilon}\frac{1}{2}E^2(q,\dot{q}) + \frac{\partial E(q,\dot{q})}{\partial q}\dot{q} - \frac{\partial E(q,\dot{q})}{\partial \dot{q}}M^{-1}(q)H(q,\dot{q}).$$

and, for the CLF (4.15) with any such locally Lipschitz continuous feedback control law $u : \Xi \times Z \to K$, it follows that solutions satisfy

$$\|\xi(t)\| \leq \frac{1}{\varepsilon}\sqrt{\frac{c_2}{c_1}}e^{-\frac{c_3}{2\varepsilon}t}\|\xi(0)\| \tag{4.17}$$

for all $t \geq 0$. □

A hybrid system can be constructed to describe the system under the zero dynamics coordinates by combining the continuous dynamics (4.11) with the reset map

(expressed in the zero dynamics coordinates) viz.

$$\overline{\Sigma}_c = \left\{ \begin{array}{rcl} \dot{\xi} &=& p(\xi,\zeta) + r(\xi,\zeta)\,u \\ \dot{\zeta} &=& s(\xi,\zeta) + w(\xi,\zeta)\,u \\ \xi^+ &=& \Delta_\Xi(\xi^-,\zeta^-) \\ \zeta^+ &=& \Delta_Z(\xi^-,\zeta^-) \end{array} \right\} \begin{array}{l} \text{if } (\xi^-,\zeta^-) \in D \setminus S, \\ \\ \\ \text{if } (\xi^-,\zeta^-) \in S. \end{array} \tag{4.18}$$

Applying a valid Lipschitz continuous control law (which takes values in (4.16)) to the hybrid control system (4.18) results in the closed-loop hybrid system

$$\overline{\Sigma}_\varepsilon = \left\{ \begin{array}{rcl} \dot{\xi} &=& p(\xi,\zeta) + r(\xi,\zeta)\,\mu_\varepsilon(\xi,\zeta) \\ \dot{\zeta} &=& s(\xi,\zeta) + w(\xi,\zeta)\,\mu_\varepsilon(\xi,\zeta) \\ \xi^+ &=& \Delta_\Xi(\xi^-,\zeta^-) \\ \zeta^+ &=& \Delta_Z(\xi^-,\zeta^-) \end{array} \right\} \begin{array}{l} \text{if } (\xi^-,\zeta^-) \in D \setminus S, \\ \\ \\ \text{if } (\xi^-,\zeta^-) \in S. \end{array} \tag{4.19}$$

4.7 Proof of Main Result

Let the Poincaré map of (4.9) be denoted $P_\varepsilon : S \to S$ and let $\phi_t(\xi,\zeta)$ represent a flow of the vector field for time t starting from state (ξ,ζ). The Poincaré map takes the form

$$P_\varepsilon(\xi,\zeta) = \phi^\varepsilon_{T^\varepsilon_I(\xi,\zeta)}(\Delta(\xi,\zeta)), \tag{4.20}$$

where $T^\varepsilon_I(\xi,\zeta)$ is the time to impact. Before proving the main theorem, some bounds related to the Poincaré map must be established using arguments similar to those presented in [4, 103].

First, however, note that since the reset map is locally Lipschitz continuous about

the fixed point $(\xi, \zeta) = (0, \zeta^*)$ and because $\Delta_\Xi(0, \zeta^*) = 0$, it follows that

$$\begin{aligned} \|\Delta_\Xi(\xi, \zeta) - \Delta_\Xi(0, \zeta^*)\| &\leq \|\Delta(\xi, \zeta) - \Delta(0, \zeta^*)\| \\ &\leq L_\Delta \|(\xi, \zeta - \zeta^*)\| \end{aligned} \tag{4.21}$$

for some $(\xi, \zeta) \in B_\gamma(0, \zeta^*)$ with $\gamma > 0$ where L_Δ is the Lipschitz constant of $\Delta(\xi, \zeta)$.

Now, consider the following bounds on the time-to-impact functions and Poincaré maps:

Lemma 2. *For the control system* (4.19)*,*

$$\begin{aligned} |T_I^\varepsilon(\Delta(\xi, \zeta)) - T_I(\Delta(\xi, \zeta))| &\leq A_{T_I}(\varepsilon) \|(\xi, \zeta - \zeta^*)\|, \\ \|P_\varepsilon(\xi, \zeta) - P(\xi, \zeta)\| &\leq A_P(\varepsilon) \|(\xi, \zeta - \zeta^*)\|, \end{aligned}$$

where $\lim_{\varepsilon \nearrow +\infty} A_{T_I}(\varepsilon) = 0$ *and* $\lim_{\varepsilon \nearrow +\infty} A_P(\varepsilon) = 0$.

Proof. Consider the Poincaré section $\mathcal{P}$ which is the guard from (3.2). Using the change of coordinates $\rho(\varepsilon) := \frac{1}{\varepsilon}$, define the function

$$N(t, \rho, \xi, \zeta) = h(\phi_t^\rho(\Delta(\xi, \zeta))),$$

which is locally Lipschitz continuous in ξ, ζ, and ρ by construction as a composition of Lipschitz continuous functions. By the transversality assumption, it follows that

$$\frac{\partial N(T, 0, 0, \zeta^*)}{\partial t} = \dot{h}(\phi_t^0(\Delta(0, \zeta^*)) \neq 0.$$

Thus, by the implicit function theorem ([154]), there exists a $\delta > 0$ and a unique function $\tau^\rho(\rho, \xi, \zeta)$ defined and locally Lipschitz for all $(\rho, \xi, \zeta) \in B_\delta(0, 0, \zeta^*)$ such

that $\tau^0(0,\zeta^*) = T_I(0,\zeta^*) = T^*$ where T^* is the period of the invariant orbit $\mathscr{O}$ and

$$N(\tau^\rho(\xi,\zeta),\rho,\xi,\zeta) = 0.$$

In addition, selecting a fixed $\varepsilon > 0$ and a Lipschitz continuous feedback control law $\mu_\varepsilon \in K_\varepsilon(\xi,\zeta)$ such as the min-norm controller [35], it follows that for some (possibly smaller) $\delta > 0$ and $(\xi,\zeta) \in B_\delta(0,\zeta^*) \cap S$, the time-to-impact function $T_I^\varepsilon(\xi,\zeta)$ satisfies

$$0.9T^* \leq T_I^\varepsilon(\xi,\zeta) \leq 1.1T^*. \tag{4.22}$$

The rest of the proof involves constructing an auxiliary time-to-impact function, T_B, which is locally Lipshitz continuous and independent of ε, and then relating it to T_I^ε.

Let $\eta \in \mathbb{R}^n$ be a constant vector and, using the guard $h(\xi,\zeta)$, define

$$T_B(\eta,\xi,\zeta) = \inf\{t \geq 0 : h(\eta + \phi_t(\Delta(0,\zeta^*))) = 0\}.$$

From this, it directly follows that $T_B(0,\xi,\zeta) = T_I(\xi,\zeta)$. Just as with T_I^ε, T_B is locally Lipschitz continuous. Thus,

$$|T_B(\eta,\xi,\zeta) - T_I(\xi,\zeta)| \leq L_B\|\eta\|$$

where L_B is the local Lipschitz constant.

Let $(\xi_1(t),\zeta_1(t))$ and $(\xi_2(t),\zeta_2(t))$ satisfy

$$(\dot{\xi}_1(t),\dot{\zeta}_1(t)) = \phi^\varepsilon(\xi_1(t),\zeta_1(t)),$$
$$(\dot{\xi}_2(t),\dot{\zeta}_2(t)) = \phi(\xi_2(t),\zeta_2(t)),$$

respectively, with initial conditions

$$(\xi_1(0), \zeta_1(\mathbf{0})) = (\xi_2(0), \zeta_2(\mathbf{0})) = \Delta(0, \zeta^*).$$

Define

$$\eta_\varepsilon = (\xi_1(t), \zeta_1(t))|_{t=T_I^\varepsilon(\xi,\zeta)} - (\xi_2(t), \zeta_2(t))|_{t=T_I^\varepsilon(\xi,\zeta)} \tag{4.23}$$

and as a result,

$$T_I^\varepsilon(\xi, \zeta) = T_B(\eta_\varepsilon, \xi, \zeta).$$

Now μ must be bounded.

The explicit solution to the QP (4.8) is given by the min-norm control law [35]:

$$\mu_\varepsilon(\xi, \zeta) = -\frac{\psi_0^\varepsilon(\xi, \zeta)\psi_1^\varepsilon(\xi, \zeta)}{(\psi_1^\varepsilon)^T(\xi, \zeta)\psi_1^\varepsilon(\xi, \zeta)},$$

with

$$\psi_1^\varepsilon(\xi, \zeta) := L_\Phi V_\varepsilon(\xi, \zeta) + \frac{c_3}{\varepsilon}, \qquad \psi_2^\varepsilon(\xi, \zeta) := \left(L_\Gamma V_\varepsilon(\xi, \zeta)\right)^T,$$

where $L_\Phi V_\varepsilon(\xi, \zeta) \equiv 0$ by the choice of $V_\varepsilon(\xi, \zeta)$ as energy. Since energy does not change by the natural dynamics,

$$\mu_\varepsilon(\xi, \zeta) = -\frac{\frac{c_3}{\varepsilon} V_\varepsilon(\xi, \zeta)\Gamma^T(\xi, \zeta)\left(\frac{\partial V_e(\xi,\zeta)}{\partial(\xi,\zeta)}\right)^T}{\frac{\partial V_e(\xi,\zeta)}{\partial(\xi,\zeta)}\Gamma(\xi, \zeta)\Gamma^T(\xi, \zeta)\left(\frac{\partial V_e(\xi,\zeta)}{\partial(\xi,\zeta)}\right)^T}.$$

If, in addition, Γ is full rank and takes values in a compact set for states near the

orbit, i.e., $\Gamma(\xi,\zeta) \in \Omega$ and $d_1 \leq \|\Gamma(\xi,\zeta)\| \leq d_2$, then

$$\begin{aligned}
\|\mu_\varepsilon(\xi,\zeta)\| &\leq \frac{\frac{c_2 c_3}{\varepsilon^3}|\xi|^2 \left\| \Gamma^T(\xi,\zeta) \begin{pmatrix} \xi \\ \mathbf{0} \end{pmatrix} \right\|}{\left\| \begin{pmatrix} \xi & \mathbf{0} \end{pmatrix} \Gamma(\xi,\zeta)\Gamma^T(\xi,\zeta) \begin{pmatrix} \xi \\ \mathbf{0} \end{pmatrix} \right\|} \\
&\leq \frac{\frac{c_2 c_3}{\varepsilon^3}|\xi|^2 \|\Gamma(\xi,\zeta)\,\xi\|}{\left\|\sum_i \Gamma_{i,i}^2(\xi,\zeta)\right\| |\xi|^2} \\
&\leq \frac{c_2 c_3}{\varepsilon^3}\frac{\lambda_{\max}}{\lambda_{\min}}|\xi|\,, \qquad (4.24)
\end{aligned}$$

with

$$\begin{aligned}
\lambda_{\max} &:= \sup\left\{\lambda_{\max}\Gamma(\xi,\zeta) : (\xi,\zeta) \in \Omega\right\}, \\
\lambda_{\min} &:= \inf\left\{\lambda_{\min}\Gamma(\xi,\zeta) : (\xi,\zeta) \in \Omega\right\},
\end{aligned}$$

where $\Omega \subset D$ is a stable tube around the periodic orbit $\mathscr{O}$. In addition, by the Lipschitz assumption Φ is bounded around $\mathscr{O}$, hence

$$\Upsilon := \sup\left\{\|\Phi(\xi,\zeta)\| : (\xi,\zeta) \in \Omega\right\}.$$

The expression η_ε in (4.23) is bounded using (4.24) and (4.17):

$$\begin{aligned}
\|\eta_\varepsilon\| &\leq \int_0^{T_I^\varepsilon(\xi,\zeta)} \|\Gamma(\xi(\tau),\zeta(\tau))\,\mu_\varepsilon(\xi(\tau),\zeta(\tau))\,\|\,d\tau \\
&\leq \frac{c_2 c_3}{\varepsilon^3}\frac{\lambda_{\max}^2}{\lambda_{\min}^2}\int_0^{T_I^\varepsilon(\Delta(\xi,\zeta))} |\xi(t)| d\tau \\
&\leq \frac{c_2^{\frac{3}{2}} c_3}{c_1^{\frac{1}{2}}\varepsilon^4}\frac{\lambda_{\max}^2}{\lambda_{\min}^2}|\xi(0)| \int_0^{T_I^\varepsilon(\Delta(\xi,\zeta))} \left| e^{-\frac{c_3}{2\varepsilon}\tau} \right| d\tau \\
&\leq \frac{c_2^{\frac{3}{2}} c_3^2}{2c_1^{\frac{1}{2}}\varepsilon^5}\frac{\lambda_{\max}^2}{\lambda_{\min}^2}|\xi(0)|\ e^{-\frac{c_3}{2\varepsilon}\tau}\Big|_{\tau=T_I^\varepsilon(\Delta(\xi,\zeta))}^{0}. \\
&\leq \frac{c_2^{\frac{3}{2}} c_3^2}{2c_1^{\frac{1}{2}}\varepsilon^5}\frac{\lambda_{\max}^2}{\lambda_{\min}^2}\left(1 - e^{-\frac{c_3}{2\varepsilon}1.1T^*}\right)\|\Delta_\Xi(\xi,\zeta) - \Delta_\Xi(0,\zeta^*)\| \\
&\leq L_\Delta \frac{c_2^{\frac{3}{2}} c_3^2}{2c_1^{\frac{1}{2}}\varepsilon^5}\frac{\lambda_{\max}^2}{\lambda_{\min}^2}\left(1 - e^{-\frac{c_3}{2\varepsilon}1.1T^*}\right)\|(\xi,\zeta-\zeta^*)\|. \qquad (4.25)
\end{aligned}$$

Using this bound with T_B leads to

$$\begin{aligned}
&|T_I^\varepsilon(\xi,\zeta) - T_I(\xi,\zeta)| \\
&\qquad = |T_B(\eta_\varepsilon,\xi,\zeta) - T_B(0,\xi,\zeta)| \\
&\qquad \leq L_B\|\eta_\varepsilon\| \\
&\qquad \leq L_B L_\Delta \frac{c_2^{\frac{3}{2}} c_3^2}{2c_1^{\frac{1}{2}}\varepsilon^5}\frac{\lambda_{\max}^2}{\lambda_{\min}^2}\left(1 - e^{-\frac{c_3}{2\varepsilon}1.1T^*}\right)\|(\xi,\zeta-\zeta^*)\|.
\end{aligned}$$

Defining $A_{T_I}(\varepsilon)$ as the coefficient of $\|(\xi,\zeta-\zeta^*)\|$ in the preceding equation establishes the first part of the lemma.

To complete the proof, consider the bound

$$\begin{aligned}
&\|P_\varepsilon(\xi,\zeta) - P(\xi,\zeta)\| \leq \qquad (4.26) \\
&\int_{T_I(\Delta(\xi,\zeta))}^{T_I^\varepsilon(\Delta(\xi,\zeta))} \|\Phi(\xi(\tau),\zeta(\tau))\|\ d\tau + \int_0^{T_I^\varepsilon(\Delta(\xi,\zeta))} \|\Gamma(\xi(\tau),\zeta(\tau))\,\mu_\varepsilon(\xi(\tau),\zeta(\tau))\,\|\,d\tau.
\end{aligned}$$

For simplicity, consider the two terms separately. The first term can be bounded as follows:

$$\begin{aligned}\int_{T_I(\Delta(\xi,\zeta))}^{T_I^\varepsilon(\Delta(\xi,\zeta)))} \|\Phi(\xi(\tau),\zeta(\tau))\|\, d\tau &\le \Upsilon \int_{T_I(\Delta(\xi,\zeta))}^{T_I^\varepsilon(\Delta(\xi,\zeta))} d\tau \\ &\le \Upsilon \tau|_{\tau=T_I(\Delta(\xi,\zeta))}^{T_I^\varepsilon(\Delta(\xi,\zeta))} \\ &\le \Upsilon \left\|T_I^\varepsilon(\Delta(\xi,\zeta)) - T_I(\Delta(\xi,\zeta))\right\| \\ &\le \Upsilon A_{T_I}(\varepsilon) \left\|(\xi,\zeta-\zeta^*)\right\|. \end{aligned} \tag{4.27}$$

The second term has already been bounded in (4.25). Finally, combining (4.25), (4.26), and (4.27) results in

$$\|P_\varepsilon(\xi,\zeta) - P(\xi,\zeta)\| \le A_P(\varepsilon)\|(\xi,\zeta-\zeta^*)\|,$$

where

$$A_P(\varepsilon) := L_\Delta \frac{c_2^{\frac{3}{2}} c_3^2}{2c_1^{\frac{1}{2}}\varepsilon^5} \frac{\lambda_{\max}^2}{\lambda_{\min}^2} \left(1 - e^{-\frac{c_3}{2\varepsilon}1.1T^*}\right) + A_{T_I}(\varepsilon)\left\|(\xi,\zeta-\zeta^*)\right\|.$$

From this expression, it is clear that the limiting behavior is $\lim_{\varepsilon\nearrow+\infty} A_P(\varepsilon) = 0$. □

Now Theorem 1 can be proven:

Proof. [Theorem 1] By the discrete converse Lyapunov theorem, exponential stability of $\mathscr{O}$ implies the existence of a discrete Lyapunov function $V_n : B_\delta(0,\zeta^*) \cap S \to \mathbb{R}_{\ge 0}$

satisfying

$$
\begin{aligned}
&r_1 \left\|(\xi,\zeta)\right\|^2 \leq V_n(\xi,\zeta) \leq r_2 \left\|(\xi,\zeta-\zeta^*)\right\|^2, \\
&V_n(P(\xi,\zeta)) - V_n(\xi,\zeta) \leq -r_3 \left\|(\xi,\zeta-\zeta^*)\right\|^2, \\
&|V_n(\xi,\zeta) - V_n(\xi',\zeta')| \leq r_4 \|(\xi,\zeta-\zeta^*) - (\xi',\zeta'-\zeta^*)\| \cdot \\
&\qquad\qquad (\|(\xi,\zeta-\zeta^*)\| + \|(\xi',\zeta'-\zeta^*)\|)
\end{aligned}
\tag{4.28}
$$

for some $r_1, r_2, r_3, r_4 \in \mathbb{R}_{>0}$. In addition, consider the CLF associated with (4.8) which is $V_\varepsilon : \Xi \to \mathbb{R}_{\geq 0}$. Denote by $V_{\varepsilon,\Xi} = V_\varepsilon|_{\S}$ the restriction of the CLF V_ε to the switching surface S. Using these Lyapunov functions, define the candidate Lyapunov function

$$V_{P_\varepsilon}(\xi,\zeta) = V_n(\xi,\zeta) + \sigma V_{\varepsilon,\Xi}(\xi).$$

From (4.15) and (4.28), it is apparent that $V_{P_\varepsilon}(\xi,\zeta)$ is bounded as follows:

$$\sigma c_1 \left|\xi\right|^2 + r_1 \left\|(\xi,\zeta-\zeta^*)\right\|^2 \leq V_{P_\varepsilon}(\xi,\zeta) \leq \sigma \frac{c_2}{\varepsilon^2} \left|\xi\right|^2 + r_2 \left\|(\xi,\zeta-\zeta^*)\right\|^2.$$

Next, note that

$$
\begin{aligned}
&V_{P_\varepsilon}(P_\varepsilon(\xi,\zeta)) - V_{P_\varepsilon}(\xi,\zeta) = \\
&\qquad V_n(P_\varepsilon(\xi,\zeta)) - V_n(\xi,\zeta) + \sigma(V_{\varepsilon,\Xi}(P_\varepsilon(\xi,\zeta)) - V_{\varepsilon,\Xi}(\xi)).
\end{aligned}
\tag{4.29}
$$

By construction of the control law (4.8), it is true that

$$V_{\varepsilon,\Xi}(\xi) \leq \frac{c_2}{\varepsilon^2} \|\xi\|^2, \tag{4.30}$$
$$V_{\varepsilon,\Xi}(P_\varepsilon^\xi(\xi,\zeta)) \leq \frac{c_2}{\varepsilon^2} e^{-\frac{c_3}{\varepsilon}T_I^\varepsilon(\xi,\zeta)} \|\Delta_\Xi(\xi,\zeta)\|^2.$$

Combining (4.21) and (4.30) yields

$$\begin{aligned} V_{\varepsilon,\Xi}(P_\varepsilon^\xi(\xi,\zeta)) &\leq \frac{c_2}{\varepsilon^2} e^{-\frac{c_3}{\varepsilon}T_I^\varepsilon(\xi,\zeta)} \|\Delta_\Xi(\xi,\zeta) - \Delta_\Xi(0,\zeta^*)\|^2 \\ &\leq \frac{c_2}{\varepsilon^2} e^{-\frac{c_3}{\varepsilon}T_I^\varepsilon(\xi,\zeta)} L_\Delta^2 \|(\xi,\zeta-\zeta^*)\|^2. \end{aligned}$$

Using Lemma 2 and defining $\beta_1(\varepsilon) := \frac{c_2}{\varepsilon^2} L_\Delta^2 e^{-\frac{c_3}{\varepsilon}.9T^*}$ yields

$$V_{\varepsilon,\Xi}(P_\varepsilon^\xi(\xi,\zeta)) - V_{\varepsilon,\Xi}(\xi) \leq \beta_1(\varepsilon) \|(\xi,\zeta-\zeta^*)\|^2 - \frac{c_2}{\varepsilon^2} |\xi|^2. \tag{4.31}$$

Now the Lyapunov function from the converse theorem must be bounded. As a result of Lemma 2 and the assumption of exponential stability about the origin, it follows that

$$\|P_\varepsilon(\xi,\zeta) - P(\xi,\zeta)\| \leq A_P(\varepsilon) \|(\xi,\zeta-\zeta^*)\|, \tag{4.32}$$
$$\begin{aligned} \|P_\varepsilon(\xi,\zeta)\| &= \|P_\varepsilon^\zeta(\xi,\zeta) - P(\xi,\zeta) + P(\xi,\zeta) - P(0,\zeta^*)\| \\ &\leq A_P(\varepsilon) \|(\xi,\zeta-\zeta^*)\| + L_P \|(\xi,\zeta-\zeta^*)\|, \end{aligned}$$
$$\|P(\xi,\zeta)\| \leq N\alpha \|(\xi,\zeta-\zeta^*)\|,$$

where L_P is the Lipschitz constant for P. Then, using (4.28),

$$|V_n(P_\varepsilon(\xi,\zeta)) - V_n(P(\xi,\zeta))| \leq \\ r_4\|P_\varepsilon(\xi,\zeta) - P(\xi,\zeta)\| \left(\|P_\varepsilon(\xi,\zeta)\| + \|P(\xi,\zeta)\|\right).$$

Applying (4.32) to the above results in

$$|V_n(P_\varepsilon(\xi,\zeta)) - V_n(P(\xi,\zeta))| \leq \beta_2(\varepsilon)\left\|(\xi,\zeta-\zeta^*)\right\|^2 \tag{4.33}$$

where, for simplicity, $\beta_2(\varepsilon) := r_4 A_P(\varepsilon)(N\alpha + A_P(\varepsilon) + L_P)$. Application of (4.33) to the nominal part of (4.29) gives the following bounds:

$$\begin{aligned} &V_n(P_\varepsilon(\xi,\zeta)) - V_n(\xi,\zeta) \\ &= V_n(P_\varepsilon(\xi,\zeta)) - V_n(P(\xi,\zeta)) + V_n(P(\xi,\zeta)) - V_n(\xi,\zeta) \\ &\leq \beta_2(\varepsilon)\left\|(\xi,\zeta-\zeta^*)\right\|^2 - r_3\left\|(\xi,\zeta-\zeta^*)\right\|^2. \end{aligned} \tag{4.34}$$

Combining (4.29), (4.31), and (4.34) yields

$$V_{P_\varepsilon}(P_\varepsilon(\xi,\zeta)) - V_{P_\varepsilon}(\xi,\zeta) \leq -\begin{pmatrix} |\xi| & \|\zeta-\zeta^*\| \end{pmatrix} \Lambda(\varepsilon) \begin{pmatrix} |\xi| \\ \|\zeta-\zeta^*\| \end{pmatrix}$$

with

$$\Lambda(\varepsilon) = \begin{pmatrix} r_3 - \beta_2(\varepsilon) - \sigma(\beta_1(\varepsilon) - \frac{c_2}{\varepsilon^2}) & r_3 - \beta_2(\varepsilon) - \sigma\beta_1(\varepsilon) \\ r_3 - \beta_2(\varepsilon) - \sigma\beta_1(\varepsilon) & r_3 - \beta_2(\varepsilon) - \sigma\beta_1(\varepsilon) \end{pmatrix}.$$

The matrix $\Lambda(\varepsilon)$ is positive definite if

$$\det \Lambda(\varepsilon) = \sigma \frac{c_2}{\varepsilon^2}(r_3 - \beta_2(\varepsilon) - \sigma\beta_1(\varepsilon)) > 0,$$

and thus stability is achieved when

$$\beta_2(\varepsilon) + \sigma\beta_1(\varepsilon) < r_3.$$

Examining the limits, it becomes apparent that

$$\lim_{\varepsilon \nearrow +\infty} \beta_1(\varepsilon) = 0, \qquad \lim_{\varepsilon \nearrow +\infty} \beta_2(\varepsilon) = 0,$$

and thus for small enough values of $\sigma > 0$ and large enough values of ε, stability is maintained. □

5. HUMAN-INSPIRED CONTROL

The human-inspired control framework is based on the idea of designing robotic behaviors based on kinematic analysis of human motion. Originally applied to a four-domain hybrid model of a robot with feet and knees [144] in two dimensions, the method was later found to apply to a wide range of models including the compass-gait biped [143] and hybrid human–robot simulations of a human with a transfemoral prosthesis [145]. By combining human-inspired control with functional Routhian reduction, three-dimensional walking was also achieved [140, 141]. This section discusses the basics of human-inspired control method.

5.1 Domain Breakdown from Human Data

This subsection shows how to determine the domain breakdown for human walking. The procedure provided is a data-driven approach based on a prior experiment involving human test subjects documented in [5]. First, a discussion is given on the human experiment and how the data were handled. Then a method is presented for determining the domain breakdown by finding the times when the constraint for a given contact point is enforced through a method that fits the "simplest" function to the motion of the contact point when the constraint is not enforced (or, in other words, when the contact point is not in contact with the ground); the time intervals during a step when the constraints are enforced are simply the times when this function is not being followed. The end result of this procedure is a temporal ordering of events which creates a discrete structure termed the domain breakdown.

Application of the presented method to each of the tests subjects results in an identical domain breakdown for each subject, purporting that there is indeed a *universal* domain breakdown for healthy human walking. This result is a significant step

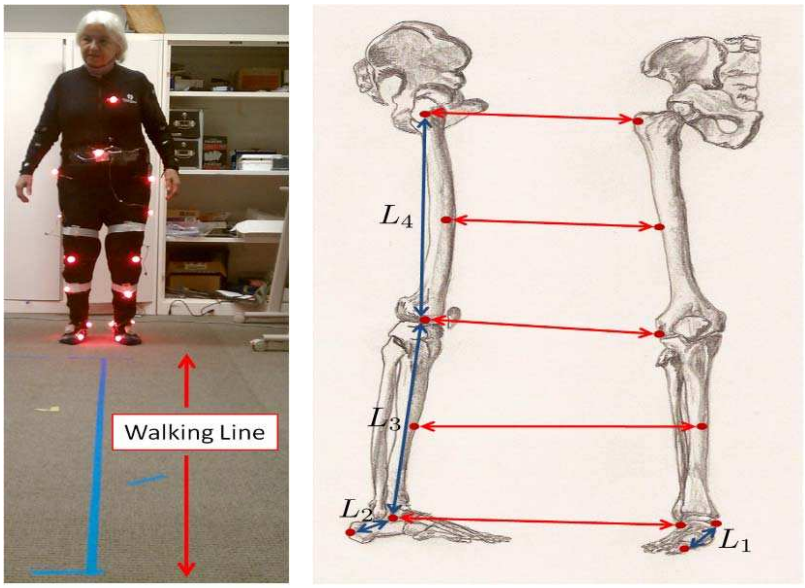

Figure 5.1: Illustrations of the experimental setup (left) and sensor placement (right). Each subject in the experiment was required to wear a suit where the LED sensors are fastened in place. The sensors were placed at the joints as illustrated with the red dots on the right lateral and anterior aspects of the right leg. Sensors were placed identically on the left leg. The same sensors drawn from different views are connected with red arrows. The blue arrows illustrate the leg segment lengths of interest, i.e. L_1, L_2, L_3, L_4. The diversity of the subjects with respect to these lengths can be seen in Table 5.1.

toward understanding human walking. Accordingly, this universal domain breakdown will be considered when constructing the hybrid model of the biped of interest. This domain breakdown has been used to formulate a metric on the human-like nature of robotic walking gaits [6, 164].

5.1.1 Walking Experiment

The data used in this work are taken from an experiment described in [5]. A summary of the collection procedure is provided for reference: data were collected on nine subjects using the Phase Space System[1] which computes the 3D position

[1] `http://www.phasespace.com/`

Table 5.1: Measurements describing each of the subjects. The subject number is in the left column and the L_1, L_2, L_3, L_4 measurements correspond to the lengths described in Figure 5.1. The anthropometric measurements in column 4 are in kilograms and the measurements in columns 5–9 are in centimeters.

	Sex	Age	Weight	Height	L_1	L_2	L_3	L_4
1	M	30	90.7	184	14.5	8.5	43.0	44.0
2	F	19	53.5	164	15.0	8.0	41.0	44.0
3	M	17	83.9	189	16.5	8.0	45.5	55.5
4	M	22	90.7	170	14.5	9.0	43.0	39.0
5	M	30	68.9	170	15.0	8.0	43.0	43.0
6	M	29	59.8	161	14.0	8.5	37.0	40.0
7	M	26	58.9	164	14.0	9.0	39.0	41.0
8	F	77	63.5	163	14.0	8.0	40.0	42.0
9	F	23	47.6	165	15.0	8.0	45.0	43.0

of 19 LED sensors at 480 frames per second using 12 cameras. The cameras were calibrated prior to the experiment and were placed to achieve a one millimeter level of accuracy for a space of size five by five by five meters cubed. Eight LED sensors were placed on each leg at the joints and on the heel and toe as shown in Figure 5.1, one LED sensor was placed on the sternum, one LED sensor was placed on the back behind the sternum, and one LED sensor was placed on the umbilicus.

Each trial of the experiment required the subject to walk three meters along a straight line drawn on the floor. Each subject performed 12 trials which constituted a single experiment. Three female and six male subjects were tested with ages ranging between 17 and 77 years, heights ranging between 161 and 189 centimeters, and masses ranging between 47.6 and 90.7 kilograms. Table 5.1 describes the measurements of each of the subjects and a visual representation is given in Figure 5.2. The data for each individual were rotated so the walking occurs in the x-direction and, for each subject, the 12 walking trials were averaged (after appropriately shifting the data in time) which resulted in a single trajectory for each constraint for each

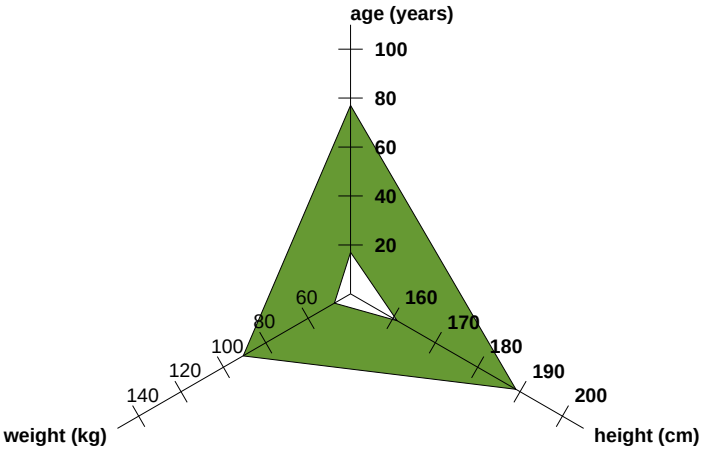

Figure 5.2: The ranges of age, height, and mass of the test subjects.

subject for at least two steps (one step per leg); the resulting data can be seen in Figure 5.3.

5.1.2 Function Fitting

In order to determine the domain breakdowns for the subjects in the walking experiment, it is necessary to determine the times when the human–ground contact points change, i.e., the *event times*. Rather than looking for when the contact point is constrained (through thresholds), one can look for the "simplest" function that the contact point follows when not enforced. Then, for the domains in which the constraint *is not* enforced, use the simple function; in the other domains, those in which the constraint *is* enforced, fit a flat line to the constraint as it should be essentially constant. This is an optimization problem which can be stated as follows:

1. Select a simple function which is qualitatively similar to the trajectory of the constraint in the domains in which it is not enforced and choose an initial guess

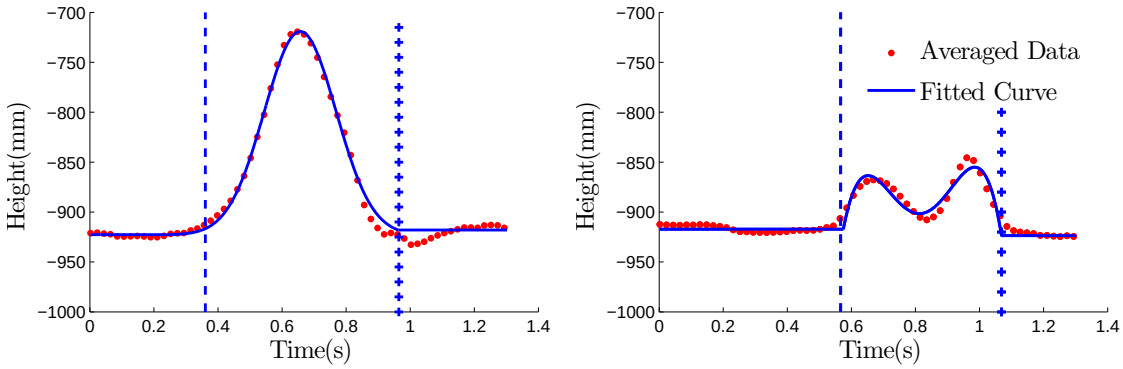

(a) Heel height (b) Toe height

Figure 5.3: The data for the heights of the heel and toe. Also shown are the fittings of a constant→Gaussian→constant for the heel and a constant→fourth-order polynomial→constant for the toe. The vertical lines on the left and right indicate the lift and strike times, respectively.

for the event times.

2. Create the fitted function as a piecewise combination of the chosen function fitted to the data in the domains in which the constraint *is not* enforced and a flat line fitted to the data in the domains in which the constraint *is* enforced.

3. Compute the cost function as the sum of squares of the difference between the data and value of the fitted trajectory at each datum for one full step (one step with each leg).

4. Minimize the cost function by choosing a new guess for the event times and then repeating steps 2–4.

To formalize the idea of function fitting to determine event times, given a set of contact points $\mathcal{C}$, let $s_c(t, a_c)$ be the "simplest" function that a given contact point $c \in \mathcal{C}$ follows when not in contact with the ground; here $a_c \in R^{n_c}$ is a collection of parameters for the function $s_c(t, a_c)$ corresponding to contact point c. Denote the

indexed human data for contact point c by $y_c[k]$, with $\tau[k]$ the time corresponding to datum $y_c[k]$ for discrete index variable $k \in \{1, \ldots, T\}$. When the contact point is constrained, it is constant, and when it is unconstrained, it follows $s_c(t, a_c)$. For each contact point $c \in \mathcal{C}$, consider the function:

$$f_c(t, k_c^\ell, k_c^s, a_c) = \begin{cases} s_c(\tau[k_c^\ell], a_c), & t \leq \tau[k_c^\ell], \\ s_c(t, a_c), & \tau[k_c^\ell] < t < \tau[k_c^s], \\ s_c(\tau[k_c^s], a_c), & \tau[k_c^s] \leq t, \end{cases}$$

where $\tau[k_c^\ell], \tau[k_c^s] \in \{\tau[k]\}_{k=1}^T$ are the event times indicating when contact point c becomes unconstrained (lift) and constrained (strike), respectively. It is assumed that $k_c^\ell < k_c^s$. If this is not the case, then f_c would consist of the "simplest" function, followed by a constant, followed by the "simplest" function. After the construction of the f_c functions in this section, the optimization parameters are supressed—i.e., $f_c(t) = f_c(t, k_c^\ell, k_c^s, a_c)$—but it is assumed they have been determined. To calculate the event times as they best fit the data, one must solve the following optimization problem

$$\min_{k_c^\ell, k_c^s \in \{1, \ldots, T\}} \min_{a_c \in \mathbb{R}^{n_c}} \sum_{k=1}^{T} \left(f_c(t, k_c^\ell, k_c^s, a_c) - y_c(t) \right)^2$$

for each $c \in \mathcal{C}$. In the case of humans with flat feet, there are four constraints of interest: one at the heel and one at the toe for both the left and right feet. Since each constraint has a lift and strike time, there is a total of eight domains in one whole step. However, when referring to a step in robotics, researchers typically use stance and non-stance legs; without the distinction of left and right, the system is reduced to a four-domain model. Doing this allows one to exploit the symmetry inherent in bipedal walking to simplfy controller design.

To illustrate this procedure, consider the averaged data for the heel and toe shown in Figure 5.3. Looking at these data, the trajectory of the heel appears to follow a constant, followed by a Gaussian, followed by a constant. In a similar fashion, the averaged data for the toe appear to follow a constant, followed by a fourth-order polynomial, followed by a constant. With these observations in hand, fit the averaged heel and toe data to these functions using the described procedure. The results of the fitting procedure are shown in the topmost graph of Figure 5.3; the transition points $\tau[k_c^\ell]$ and $\tau[k_c^s]$ are indicated by vertical lines. The fits quite accurately represent the data given the simplicity of the functions chosen; to quantify this, the coefficients of correlatation are 0.9968 for the heel and 0.9699 for the toe.

5.1.3 Determining the Domain Breakdown

Given the data for a contact point $c \in \mathcal{C}$, the lift and strike times are determined for each contact point, $\tau[k_c^\ell]$ and $\tau[k_c^s]$ for $c \in \mathcal{C} = \{c_1, c_2, c_3, c_4\} = \{c_{lh}, c_{lt}, c_{rh}, c_{rt}\}$, over the time interval of the averaged data, $\big[\tau[1], \tau[T]\big]$, using the aforementioned techniques. Since the data comprise at least two steps (one step with each leg), there are multiple lift and strike times over the period of the data. Denote by $\mathcal{J}_c \subset \big[\tau[1], \tau[T]\big]$ the period where the constraints associated with a contact point are enforced, i.e., $t \in \mathcal{J}_c$ if $f_c(t) =$ constant with f_c the fitting function for the contact point $c \in \mathcal{C}$; these intervals are shown in blue in Figure 5.4 over the course of one step (not the entire data period) in the case of $\mathcal{C} = \{c_{lh}, c_{lt}, c_{rh}, c_{rt}\}$. Analogous to the definition of a domain breakdown (Definition 10), one can define a binary vector, $b(t) \in \mathbb{Z}_2^{|\mathcal{C}|}$ with $|\mathcal{C}|$ representing the cardinality of $\mathcal{C}$, encoding which contact points are constrained at any given time by letting $b_i(t) = 1$ if $t \in \mathcal{J}_{c_i}$ for $i \in \{1, \dots, |\mathcal{C}|\}$.

To determine the domain breakdown associated with walking, begin by defining the directed cycle Γ (if it exists, which is not guaranteed). The function $b(t)$ takes

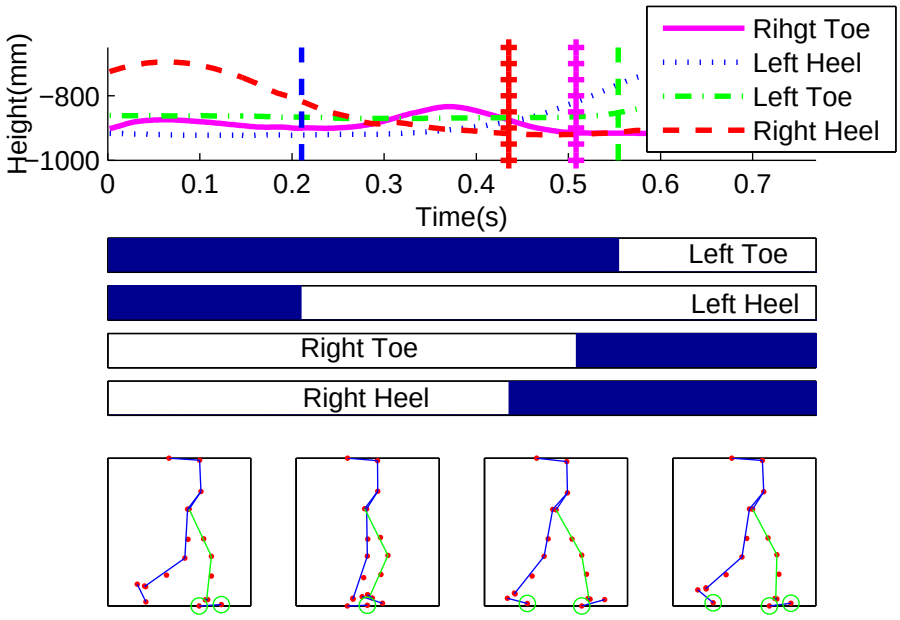

Figure 5.4: An overview of how the domain breakdown is achieved. The top row illustrates the height of the toe and heel of each leg over one step along with the lifting and strike time for each constraint (illustrated with vertical lines). The middle row illustrates which constraints are active based upon the fitting. The bottom row is the resulting domain breakdown where enforced constraints are drawn in green circles.

on only a finite number of values, say, N values; let these values be represented by $d[n]$ for $i \in \{1, \ldots, N\}$. For the walking to be periodic, there must exist a positive value of $p \in \mathbb{Z}$ satisfying

$$d[n+p] = \begin{bmatrix} \mathbf{0} & I \\ I & \mathbf{0} \end{bmatrix} d[n] \tag{5.1}$$

for $n \in \{1, \ldots, N-p\}$ with I the identity matrix and $\mathbf{0}, I \in \mathbb{R}^{\frac{|\mathcal{C}|}{2} \times \frac{|\mathcal{C}|}{2}}$. Note: if the data constitute multiple steps, there will be more than one possible value for p; in this case, the proper value of p is the smallest of these values as this represents one

step. The matrix that is premultiplied by $d[n]$ serves the purpose of reordering the right leg and left leg. If this p can be found, periodic walking over the course of two steps has been discovered in the data with the behavior of the left leg mirroring the behavior of the right leg. In this case, one constructs a directed cycle with p domains (as in (3.19)) and this is the graph Γ. The corresponding domain breakdown B is given by $B(v_n) = d[n]$ for $n \in \{1, \ldots, p\}$. The application of this procedure to a single subject can be seen in Figure 5.4.

5.1.4 Results

The outlined process is performed on the set of contact points $\mathcal{C} = \{c_{lh}, c_{lt}, c_{rh}, c_{rt}\}$ for the nine test subjects that performed the walking experiment. The end result showed that each subject had the same, *universal*, domain breakdown; this can be seen in Figure 3.2. In the context of this work, a single subject was chosen for study based upon the completeness of the sensor data, which, in this case, was Subject 4; the domain breakdown and the time spent in each domain for the subject can be seen in Figure 5.5. It is important to note that the results are consistent with those found in the biomechanics literature. Specifically, performing the breakdown process on data from the literature [174] resulted in the same domain breakdown. Additionally, the amount of time spent having single and double support are similar to previous studies [1].

5.2 Human-Inspired Controller Design

The goal of this subsection is to find functions that are "canonical" to human walking, i.e., outputs on the configuration of the human, such as the angle of the knee, that seem to be intrinsic to walking. These functions will be used in the design of control laws, for a bipedal robot with anthropomorphic measurements, using the standard method of input/output linearization [134]. This control design strategy

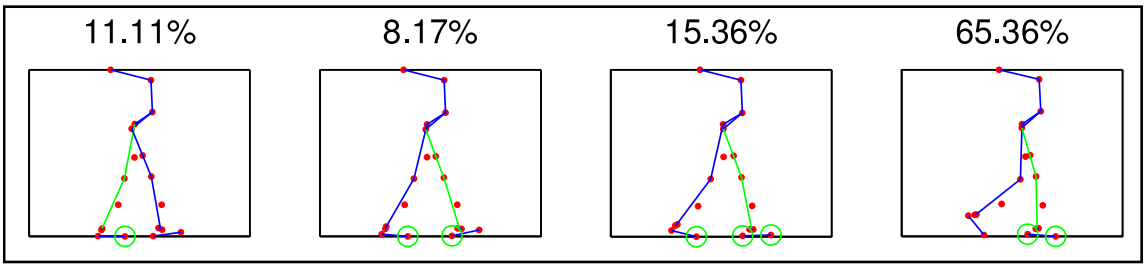

Figure 5.5: The domain breakdown for Subject 4. Also shown is the amount of time spent in each domain. Each illustration is a snapshot of the subject's configuration at the beginning of the domain together with the contact points enforced.

results in anthropomorphic walking behavior.

5.2.1 "Canonical" Walking Functions

Rather than just using trajectories from the human data, functions are sought which have both "simple" representations (much like in the case of heel and toe height discussed in Section 5.1) and appear to be intrinsic to human walking. From the perspective of control, these functions must not conflict with the constraints of the system on each domain resulting from the enforced contact points as dictated by the domain breakdown. That is, the system must not be overconstrained.

Data are considered from Subject 4 as they contain the least noise; these data are obtained through the process outlined in Section 5.1. A variety of functions are inspected—these represent different fundamental behaviors of human walking, e.g., the movement of the torso or of the legs. Examination of the human data, reveals that functions describing the behavior of the torso, the hip, the non-stance leg slope (the slope of the line connecting the non-stance ankle to the hip), the knee angles, and the heel and toe heights seem to encode the most fundamental behaviors related to walking, as dictated by the correlation between the data and the fitted functions. The human behavior of these different functions throughout the course of the walking

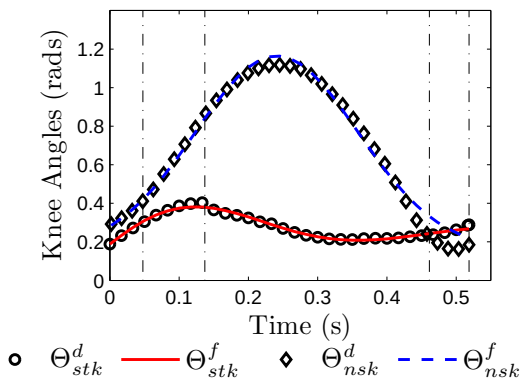

(a) Angular constraints

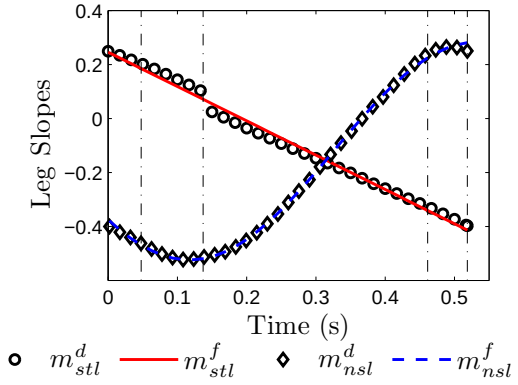

(b) Slope constraints

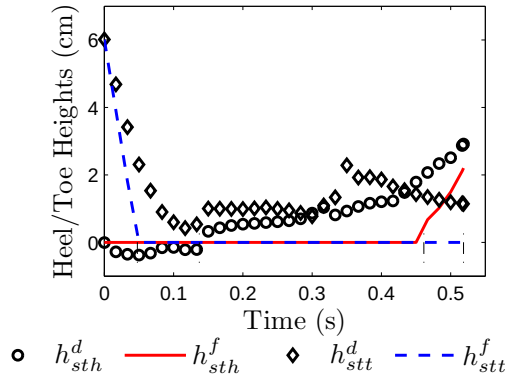

(c) Height constraints

Figure 5.6: Human data over the course of one step for one leg. Also shown are "canonical" functions that are fitted to these data. d superscripts represent the data and f superscripts represent the fits. The plots start at the beginning of the domain ts, with vertical lines indicating when transitions between domains occur.

gait can be seen in Figure 5.6, with the data beginning at the start of domain ts. The specific constraints that are plotted can be seen in Figure 5.7.

Before further detail is given, a remark on the choice of constraints is in order:

Remark 2. *When choosing which functions to track, it is important to consider which joints will have actuation and which actuators will do most of the work nec-*

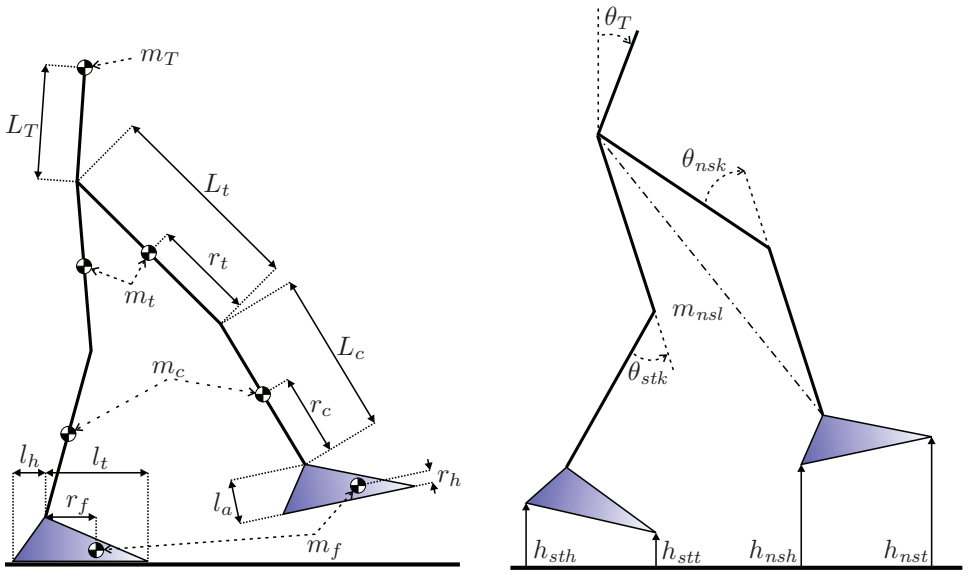

(a) Robot configuration (b) Tracking outputs

Figure 5.7: Kinematic and dynamic model of the 2D bipedal robot: (a) The general configuration of the 2D bipedal robot with knees and feet; (b) The different configuration-based outputs considered in the fitting of the "canonical" functions.

essary to track a given constraint. An example of a poor choice of constraints would be the stance knee, the stance leg slope, and the stance hip position. The reason this is a poor choice is as follows: to track these three constraints, only two degrees of actuation will do most of the work—the stance ankle and the stance knee. Thus, the dynamics of the system will be ill-behaved. Indeed, if one tries to track three constraints on a two-link pendulum, the result will be an overconstrained system unless *two of the constraints match up perfectly—in other words, two* independent *constraints are being tracked. This same argument extends to the specified robot, which is a multi-link kinematic chain. Examples of reasonable output choices can be found in [142].*

5.2.1.1 Knee

Inspecting the behavior of the human knee over the course of the gait (see Figure 5.6(a)) reveals that the angle of the human knee appears to follow a Gaussian when it is swinging (the non-stance leg) and a second order system response (i.e., the step response of a spring damper system) when the weight of the person is on the leg (i.e., when the leg is the stance leg). With this in mind, the following functions are fit to the human data for the knee angles of the stance and non-stance legs:

$$y_{d,nsk\angle}(t) = A_{5,1}\ \exp\left(\frac{-(t - A_{5,2})^2}{2(A_{5,3})^2}\right) + A_{5,4},$$
$$y_{d,stk\angle}(t) = -A_{2,1}\ \frac{\cos(A_{2,2}\,t) - A_{2,3}\sin(A_{2,2}\,t)}{\exp(A_{2,4}\,t)} + A_{2,5}.$$

An intuitive explanation of this is as follows: when the leg is in "stance" mode, the human knee acts like a spring-damper system responding to the impulse of the human as he or she puts his or her body weight on the stance leg—that is, the human tries to prevent the leg from collapsing by stiffening it, resulting in a spring-damper effect. When the human leg is in "non-stance" mode, the weight of the human is primarily not on it, so the knee is free to swing—there is no reason to keep the leg stiff.

5.2.1.2 Leg

In the data for the slope of the non-stance leg as seen in Figure 5.6(b)—here, leg is defined as the straight line connecting the ankle to the hip—the slope appears to follow a sinusoid; thus the following function is fit:

$$y_{d,nslm}(t) = A_{6,1}\ \sin(A_{6,2}\,t + A_{6,3}) + A_{6,4}.$$

Intuitively, this just means that the non-stance leg swings freely much like the non-stance knee. Note that while it is possible to choose the slope of the stance leg as a constraint to track—indeed, a simple function can be fitted to the slope of the stance leg—the forward velocity of the hip is instead chosen. In terms of time-control this will not make much of a difference, but the reader will see that, when the control is migrated to pure feedback, tracking the hip velocity will allow for direct control over walking speed.

5.2.1.3 Hip

The behavior of the hip is quite simple. Examination of the data reveals that the hip moves forward monotically in time at an approximately constant rate. However, instead of tracking the position of the hip, the velocity of the hip is instead tracked, thus motivating the following function:

$$y_{d,hv} = A_{3,1}.$$

The reason for tracking the velocity instead of the position is related to the method used to impose feedback control on the system and requires some explanation; however, due to the level of detail, this discussion will be deferred until later. It is of interest, however, to note that, as mentioned previously, tracking hip velocity allows for direct control over the walking speed of the robot.

5.2.1.4 Torso

The data show that a human tends to keep his or her torso upright throughout his or her walking gait. Specifically, the data indicates that the absolute angle of the torso with respect to the world frame closely follows a sine wave, but the amplitude

is small, so it is approximated with a constant:

$$y_{d,T\angle} = A_{4,1}.$$

Note that, the choice of tracking a constant results in a poor correlation between the function and data; however, one can argue that the tiny amount of motion from the torso has very little effect on the overall gait.

5.2.1.5 Ankle

When the non-stance leg is swinging, to prevent the non-stance ankle from rotating freely, the behavior of the ankle angle is approximated by a constant:

$$y_{d,nsa\angle} = A_{8,1}.$$

One can justify this choice by claiming that the motion of the ankle has only a marginal effect on the overall gait provided that ground clearance is not an issue. As in the case of the torso, the correlation between this fit and the data will not be good but, again, this does not have a large effect on the gait.

5.2.1.6 Foot

Finally, the behaviors of the heel and toe are found to be significantly more complicated than the previously discussed behaviors, as can be seen in Figure 5.6(c). Although the actual functions describing these heights are quite simple (see Figure 5.3), it is generally not effective to follow these functions—see Remark 3. Since the foot is constrained during certain phases of the gait, it would not make sense to track the constrained points during these phases. Therefore, the behavior of the feet is segmented based on the domain breakdown of the human gait. In particular, the

transition from domain *ts* to domain *tl* occurs when the stance toe strikes the ground, and, in fact, it is found that the height of the toe approximately follows a constant as it approaches the ground in domain *ts*. In order to satisfy this local objective, an attempt is made to track the height of the toe using the following function:

$$y_{d,stth}(t) = A_{7,1}\, t + A_{7,2}.$$

After domain *ts*, the toe is fixed to the ground and thus, is no longer tracked. In a similar light, when domain *hl* is reached, the goal is to effect heel lift. As such, analysis of the data reveals that non-stance heel begins to lift approximately according to a Gaussian, thus motivating the following function:

$$y_{d,sthh}(t) = A_{1,1}\, \exp\left(\frac{-(t - A_{1,2})^2}{2(A_{1,3})^2}\right) + A_{1,4}.$$

Remark 3. *Certain constraint functions represent dimensionalized constraints, e.g., heel height, whereas other functions discussed, e.g., angles and slopes, represent nondimensionalized constraints. In general it is not effective to follow dimensionalized constraints as they represent constraints on specific points of the system and thus have the potential to introduce extreme restrictions on the configuration space of the entire system. This should be thought of in terms of the inverse kinematics problem: consider an end-effector and solve for the range of possible configurations on the angles leading up to that point. Thus, dimensionalized constraints are not robust with respect to length parameters. Additionally, these dimensionalized constraints can conflict with other holonomic constraints being tracked. Recall that the intent is to track the height of the stance toe; in this case, the issue of configuration restriction is minimal: only the heel is pinned to the ground so tracking the toe's*

Table 5.2: Correlations of fitted functions and usage on each domain. Note that many fits have extremely high correlations. For the four right columns, a • indicates the constraint for that row is tracked on the corresponding domain.

Eq.	**Constraint**	r	ts	tl	hl	hs
$y_{d,sthh}$	Stance heel height	0.73671				•
$y_{d,stk\angle}$	Stance knee angle	0.99213	•	•	•	•
$y_{d,hv}$	Hip forward velocity	*	•	•	•	•
$y_{d,T\angle}$	Torso absolute angle	*	•	•	•	•
$y_{d,nsk\angle}$	Non-stance knee angle	0.99301	•	•	•	•
$y_{d,nslm}$	Non-stance leg slope	0.99971			•	
$y_{d,stth}$	Stance toe height	0.99971	•			
$y_{d,nsa\angle}$	Non-stance ankle angle	*			•	•

height is equivalent to tracking the angle or slope of the foot.

5.2.1.7 Fitting

The paramaters of the "canonical" functions can be found by minimizing the error between the human data and the corresponding functions. Formally, given a function choice $y_d(t, A)$, with $A \in \mathbb{R}^{n_d}$ the n_d parameters, and the corresponding data function $x_d[k]$ with indexed time $\tau_d[k]$ for data index $k \in \{1, \ldots, K\}$ (for K data points), a solution is sought for the optimization problem:

$$\min_{A \in \mathbb{R}^{n_d}} \sum_{k=1}^{K} (y_d(\tau_d[k], A) - x_d[k])^2. \tag{5.2}$$

The fits that result from solving (5.2) are shown in Figure 5.6. The correlation coefficient for the fits of each of the respective functions can be found in Table 5.2. In all cases (with the exception of the torso and ankle), the fits are very good. One final note of import: in order to achieve walking in simulation, some parameters had to be tweaked by hand; the parameters generated as well as the tweaked parameters can be found in Table 5.3.

Table 5.3: Human function parameters. Asterisks (*) denote no additional parameters.

$$A = \begin{bmatrix} 0.2039 & 0.7540 & 0.1109 & 0.0000 & * \\ 0.0710 & 13.3920 & 2.6671 & 3.7440 & 0.1881 \\ 1.1771 & * & * & * & * \\ 0.0595 & * & * & * & * \\ 1.1500 & 0.2480 & 0.1170 & 0.1669 & * \\ 0.4035 & 7.5204 & -2.4442 & -0.1202 & * \\ -0.1638 & 0.0078 & * & * & * \\ -0.0800 & * & * & * & * \end{bmatrix}$$

5.2.2 Robotic Hybrid Model & Controllers

Consider the robotic walker shown in Figure 5.7. The goal is to use the human-inspired domain breakdown and "canonical" walking functions to design controllers for this robot.

5.2.2.1 Robotic Model

It was shown in Section 3.8 that, given a collection of contact points and a domain breakdown (defined on a cycle graph), one can explicitly construct a hybrid control system. In particular, using the procedure discussed, a domain breakdown B is obtained, which is associated to human walking (see Example 3) defined on the cycle $\Gamma_u = (V, E)$ (given in Example 2). As a result of the construction in Section 3.8, one obtains a hybrid control system describing this robot:

$$\Sigma^c = (\Gamma, D, \mathcal{U}, S, \Delta, \mathcal{FG}). \tag{5.3}$$

As discussed previously, attach a reference frame R_b to the hip. Let ϕ_b be the orientation of R_b (with respect to the y-axis for a two-dimensional model) and let

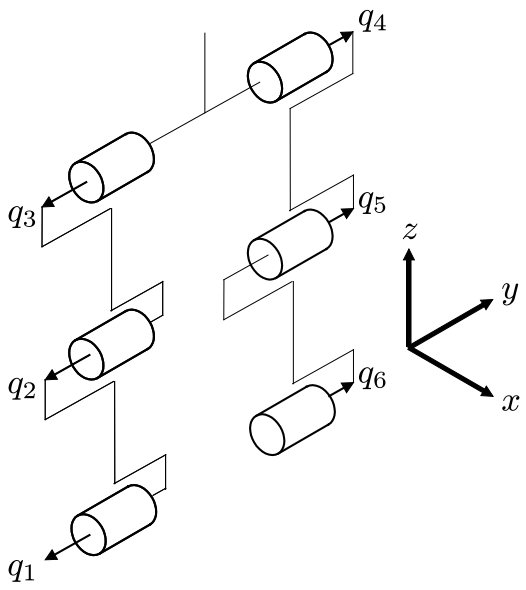

Figure 5.8: The shape coordinates for the biped labeled q_i. The corresponding arrows represent twists. The x-axis is coming out of the page. The hip width is zero and is shown for illustration purposes only. The axes shown represents the body-fixed frame which has orientation about the y-axis given by ϕ_b.

p_b^x, p_b^z be the Cartesian position of R_b. The shape coordinates q_s for the biped are chosen to be the relative angles between any two successive links starting at the stance foot as shown in Figure 5.8. Combining ϕ_b, p_b^x, p_b^z, and q_s gives the configuration space for the biped. The only unknowns for the model are the physical parameters of the system; these are obtained from the anthropometric data for Subject 4, given in Table 5.1. In particular, the lengths are given and the mass of each point mass in the robot (as seen in Figure 5.7) is estimated from the overall mass of the person using a standard mass distribution of a human from the literature [174].

5.2.2.2 Controller Design

The goal now is to design a controller to track the desired functions given in Section 5.2.1. Before discussing which of these functions are tracked on each domain, a description technique used to track the desired functions, input/output linearization

[134, Ch. 9], is given.

Consider a control system of the form (f_v, g_v), $v \in V$ as given in Definition 8 for an arbitrary domain in the domain breakdown. Let $y_v^a(q)$ represent the vector of "actual" outputs on the system (e.g., the height of the stance heel)—these can be found by computation of forward kinematics [106]. Let $y_v^d(t)$ represent the vector of "desired" output functions to be tracked, which consists of combinations of the human-based "canonical" constraint functions. Let $n = \dim(Q)$ and let m be the number of constraint functions being tracked on a given domain. Motivated by the desire to drive $y_v^a(q(t)) \to y_v^d(t)$ as $t \to \infty$, a definition is given for the following virtual output vector:

$$y_v(q,t) = y_v^a(q) - y_v^d(t). \tag{5.4}$$

As the functions tracked consists of both positions and velocities, the system has mixed relative degree. That is, the output corresponding to velocity will have relative degree one whereas the outputs corresponding to positions will each have relative degree two. Reorder the outputs as follows:

$$y_v(q,\dot{q},t) = (y_{v,1}(q,\dot{q},t), y_{v,2}(q,t)) \tag{5.5}$$

with $y_{v,1}$ a vector containing the relative-degree-one outputs and $y_{v,2}$ a vector containing the relative-degree-two outputs. (In this dissertation, $y_{v,1}$ is a scalar.) A

control law which drives (5.5) to zero is

$$u(q,\dot{q},t) = \\ -\mathcal{A}_v^{-1}(q,\dot{q},t)\left(\begin{bmatrix} 0 \\ L_{f_v}L_{f_v}y_{v,2}(q,t)\end{bmatrix} + \begin{bmatrix} L_{f_v}y_{v,1}(q,\dot{q},t) \\ 2\varepsilon L_{f_v}y_{v,2}(q,t)\end{bmatrix} + \begin{bmatrix} \varepsilon y_{v,1}(q,\dot{q},t) \\ \varepsilon^2 y_{v,2}(q,t)\end{bmatrix}\right),$$

with $\mathcal{A}_v(q,\dot{q},t)$ the decoupling matrix given by

$$\mathcal{A}_v(q,\dot{q},t) = \begin{bmatrix} L_{g_v}y_{v,1}(q,\dot{q},t) \\ L_{g_v}L_{f_v}y_{v,2}(q,t)\end{bmatrix},$$

where, again, $(f_v,\, g_v)$ is given in Definition 8. In the above,

$$L_{f_v}y(q,\dot{q},t) = \frac{\partial y(q,\dot{q},t)}{\partial(q,\dot{q},t)}\cdot f_v(q,\dot{q},t)$$

represents the Lie derivative with $q, \dot{q}, t$ representing independent variables. Applying the given control law yields the non-autonomous closed-loop dynamical system

$$f_{cl,v}(q,\dot{q},t) = f_v(q,\dot{q}) + g_v(q)\, u(q,\dot{q},t). \tag{5.6}$$

Completion of the controller construction requires the specification of the vectors y_v^a and y_v^d for $v \in V$ which are specific to each of the four domains in Figure 3.2. As mentioned previously, the vector y_v^a consists of the robotic constraints pictured in Figure 5.7, which are computed directly from the kinematics of the robot. Therefore, the only decision remaining is which of the "canonical" human functions to track on each domain. The specific choice of functions is shown in Table 5.2 where black dots indicate which functions are tracked on which domains. The choice of functions is

based on the discussion in Section 5.2.1 coupled with choosing collections of functions that do not conflict with the holonomic constraints imposed on the system as a result of ground contact (see Remarks 2 and 3). Applying these collections of controllers to the hybrid control system (5.3) yields the non-autonomous hybrid system:

$$\Sigma_t = (\Gamma,\, D,\, S,\, \Delta,\, \mathcal{F}). \tag{5.7}$$

Remark 4. *One final point worthy of mention is transitioning from domains with no impact, i.e., contact point becomes unconstrained. Looking at equations,* (3.15) *and* (3.14)*, it is apparent that one can achieve lift by simply solving for a value of u which will cause the heel to lift. Such a value would be outside the domain as defined in* (3.28)*; specifically, this value of u will violate* (3.26)*. Provided that* (3.26) *is satisfied during the a given phase, it becomes a control decision when to lift the heel or toe. A criterion is chosen and then appropriate control is applied to instantaneously achieve heel or toe lift. In the domain that follows, the control laws implicit in* (5.6) *will be responsible for causing the toe or heel to continue to lift.*

5.2.3 Simulation of Time-Based Feedback Controller

This subsection presents the results of a simulation of the bipedal robot modeled by (5.7). The parameters used for the human functions are given in Table 5.3. It is important to note that, in order to achieve walking, it was necessary to tweak the parameters; specifically, this amounted to the multiplication of the row corresponding to the non-stance leg slope (row six) by 1.25. Videos of the walking can be found online.[2] It is found through simulation that the biped has stable walking. This is checked by finding a fixed point on the orbit and verifying its stability using the Poincaré map technique [113]. Using the model parameters found online[2] and the

[2] `http://www.rwsinnet.com/phdthesis/`

input/output linearization control gain $\varepsilon = 15$, the system is simulated and the following fixed point is found:

$$q^*_{s,t} = \begin{pmatrix} -.460 & .246 & .272 & -.441 & .323 & .162 \end{pmatrix} \tag{5.8}$$

$$\dot{q}^*_{s,t} = \begin{pmatrix} -.951 & .452 & .518 & -.309 & -2.660 & -.509 \end{pmatrix} \tag{5.9}$$

which is on the guard of domain hl. This verifies that there exists a walking gait. Note that only the shape coordinates are given for the fixed point as the other coordinates will be completely determined by the condition that the biped is on the guard; that is, the constraints that exist on the system, e.g., the stance toe is on the ground, are enough to uniquely determine the rest of the variables, ϕ_b, p_x, and p_z.

In the context of bipedal walking, a stable limit cycle or an exponentially stable periodic orbit implies stable walking. It is, therefore, desirable to show that the system has a stable limit cycle. This is achieved by examining the Jacobian of the Poincaré map linearized about the fixed point $(q^*, \dot{q}^*)$ [113]. This Poincaré map will be stable if all the eigenvalues of the Jacobian have magnitude below unity. Then, stability of the Poincaré map implies stability of the system. The Jacobian matrix can be approximated by perturbing along the guard about the fixed point with respect to the coordinates q and $\dot{q}$. A numerical approximation yields eigenvalues of the following magnitudes:

$$|\lambda_t| \in \{0.2640,\, 0.2492,\, 0.0337,\, 0.0337,\, 0.0011,\, \ldots\}, \tag{5.10}$$

where, for the sake of space, only the five eigenvalues with the largest magnitudes are included. At this point in the discussion, a remark about zero eigenvalues is appropriate:

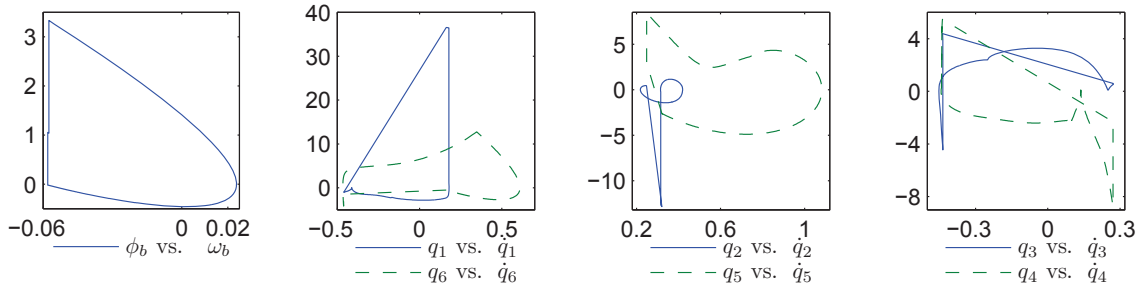

(a) Body frame angle (b) Ankle angles (c) Knee angles (d) Hip angles

Figure 5.9: Phase portraits of simulation of time-based system Σ_t.

Remark 5. *When considering a Poincaré section S which is a guard of a hybrid system with constraints, some of the eigenvalues will be zero. This is a result of the difference in the dimension of the Jacobian and the dimension of the guard which is a transverse hyperplane of the continuous trajectory. Specifically, consider the guard used here as S. In this case, the guard restricts the previously nine-dimensional position space such that the state of the system, throwing out cyclic variables such as x-position, can be determined completely using only six position variables. This results in a number of zero eigenvalues, in this case, three relating to position and three for the corresponding velocities. More on this topic can be found in the literature [170].*

The eigenvalues in (5.10) have magnitude below unity, and thus, the system has a locally exponentially stable periodic orbit. The phase portraits are shown in Figure 5.9. These phase portraits are closed—in other words, they contain a closed periodic orbit. Snapshots of the walking gait are shown in Figure 5.10. These simulation results imply that, through a choice of functions intrinsic to human walking, humanlike walking was indeed obtained for on an anthropomorphic biped. The humanlike nature of the simulated gait can best be seen in a video of the walking

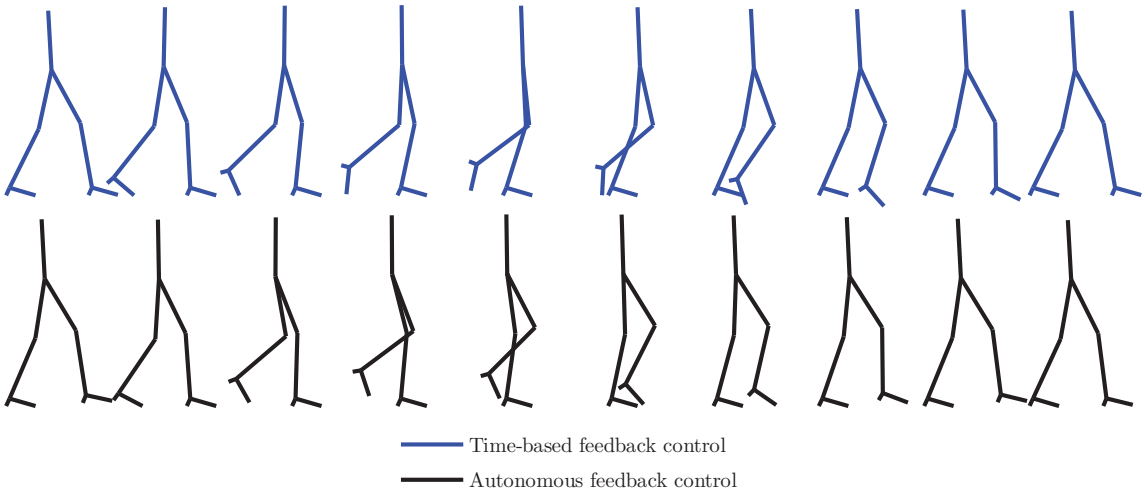

Figure 5.10: Comparison of simulated walking gaits. Time-based feedback control and autonomous feedback control.

available online.[2]

5.3 Autonomous Feedback Controller Design

In general, autonomous control is preferred over non-autonomous, time-based control as autonomous controllers tend to be more robust. In this subsection, a method is given which shows how to remove the time-dependence from the "canonical" functions described in the previous subsection. A common trick in the literature [171] for converting time-based trajectories into state-based trajectories is to parameterize time by a state-dependent function; this results in an autonomous feedback control strategy.

5.3.1 State-Based Trajectory Parameterization

Recall that the functions discussed in the previous subsection are directly dependent on time, i.e., they can be written $y_v^d(t)$. Furthermore, these functions are all defined on some interval $[t^- = 0, t^+ = P] = \mathcal{I} \subset \mathbb{R}_0^+$ with P the period of the gait (that is, one step with one leg); in other words, a given tracking function can be

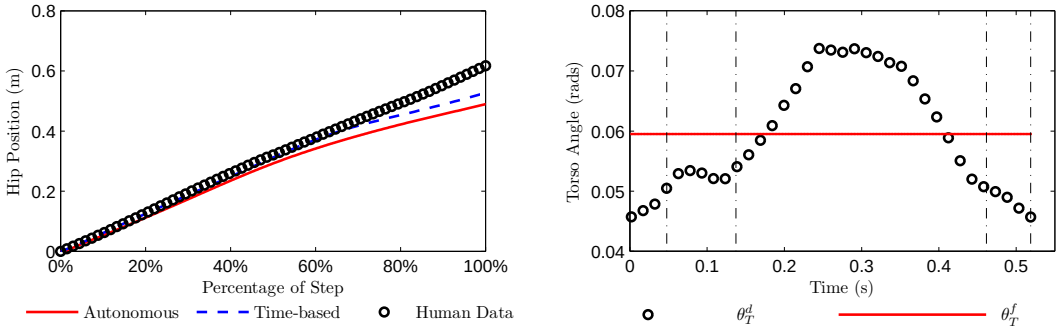

(a) Comparison of hip movement

(b) Angular motion of torso

Figure 5.11: Trajectories for the hip (a) and torso (b).

written as a map $y_v^d : \mathcal{I} \to \mathbb{R}$. Autonomous state feedback can be achieved by simply choosing a state-based parameterization $\varsigma : \mathcal{Q} \to \mathcal{I}$ and substituting for time, i.e., $y_v^d(\varsigma(q))$.

When choosing a parameterization, $\varsigma(q)$, it is important to consider its role in the system. Since $\varsigma(q)$ is a parameterization for time t, the relationship between $\varsigma(q)$ and t should be as linear as possible. Examination of the human hip data, as shown in Figure 5.11(a), reveals that the hip velocity v_{hip}^x is constant throughout the gait; as a result, the hip position approximately satisfies $p_{hip}^x(q(t)) = v_{hip}^x t + p_{hip}^x(q^-)$, with q^- the state at the beginning of a step. Here, the assumption can be made, without loss of generality, that time starts at zero at the beginning of any given step. The linearity of the hip position, $p_{hip}^x(q(t))$, with respect to time, makes it a good candidate for time parameterization; substituting $\varsigma(q) \to t$ and solving for $\varsigma(q)$ gives the parameterization

$$\varsigma(q) = \frac{p_{hip}^x(q) - p_{hip}^x(q^-)}{v_{hip}^x}. \tag{5.11}$$

The parameters $p^x_{hip}(q^-)$ and v^x_{hip} should be chosen based on the quantities they represent (i.e., v^x_{hip} should be the average velocity of the hip and $p^x_{hip}(q^-)$ should be the x-position of the hip at the beginning of a step). In this work, these values were found by examining the simulation of the time-based controller from the previous subsection. Specifically, a good choice for v^x_{hip} is the parameter for the hip velocity constraint, $A_{3,1}$ (found in Table 5.3). Using the parameterization (5.11), the desired trajectories can be expressed by substituting the parameterization $\varsigma(q)$ for time t; that is, the desired trajectories will be given by $y^d_v(\varsigma(q))$.

5.3.1.1 Control Design Modification

Implementation of state feedback allows for the removal of time from the virtual outputs, that is, the control law is no longer time-dependent. Therefore, the virtual output of (5.4) becomes

$$y_v(q, \dot{q}) = y^a_v(q, \dot{q}) - y^d_v(\varsigma(q))$$

with $\varsigma(q)$ the parameterization given in (5.11). Following the derivation of the time-based controller, the outputs are grouped based on relative degree:

$$y_v(q, \dot{q}) = (y_{v,1}(q, \dot{q}), y_{v,2}(q)).$$

The control law which drives $y_v(q, \dot{q}) \to 0$ is then given by

$$u(q, \dot{q}) = -\mathcal{A}_v^{-1}(q, \dot{q}) \left(\begin{bmatrix} 0 \\ L_{f_v} L_{f_v} y_{v,2}(q) \end{bmatrix} + \begin{bmatrix} L_{f_v} y_{v,1}(q, \dot{q}) \\ 2\varepsilon L_{f_v} y_{v,2}(q) \end{bmatrix} + \begin{bmatrix} \varepsilon y_{v,1}(q, \dot{q}) \\ \varepsilon^2 y_{v,2}(q) \end{bmatrix} \right),$$

with $A_v(q)$ the decoupling matrix given by

$$\mathcal{A}_v(q, \dot{q}) = \begin{bmatrix} L_{g_v} y_{v,1}(q, \dot{q}) \\ L_{g_v} L_{f_v} y_{v,2}(q) \end{bmatrix} \tag{5.12}$$

and $(f_v,\, g_v)$ the control system given in (3.15). Application of this control law to the control system yields the closed-loop system:

$$f_{cl,v} = f_v(q, \dot{q}) + g_v(q)\, u(q, \dot{q}). \tag{5.13}$$

The virtual outputs are chosen to be the same as those in the time-based controller, specified in Table 5.2. The end result is an autonomous hybrid system specified by

$$\Sigma_a = (\Gamma,\, D,\, S,\, \Delta,\, \mathcal{F}_a). \tag{5.14}$$

with $\mathcal{F}_a$ the set of vector fields $\{f_{cl,v}\}_{v \in V}$.

5.3.2 Simulation of Autonomous Feedback Controller

The analysis of the stability of the autonomous system is analogous to that shown in Section 5.2.3. The control gain is again chosen to be $\varepsilon = 15$. The parameters are tweaked, as before, by multiplying row six by 1.25. This simulation results in the fixed point:

$$q^*_{s,t} = \begin{pmatrix} -\ .404 & .245 & .208 & -\ .488 & .388 & .088 \end{pmatrix}$$
$$\dot{q}^*_{s,t} = \begin{pmatrix} -1.287 & .282 & 1.078 & 0.711 & -2.452 & -.076 \end{pmatrix}$$

on the guard of domain hl. Only the shape coordinates are shown, as in the analysis of the time-based feedback controller. The Jacobian matrix of a linearization of

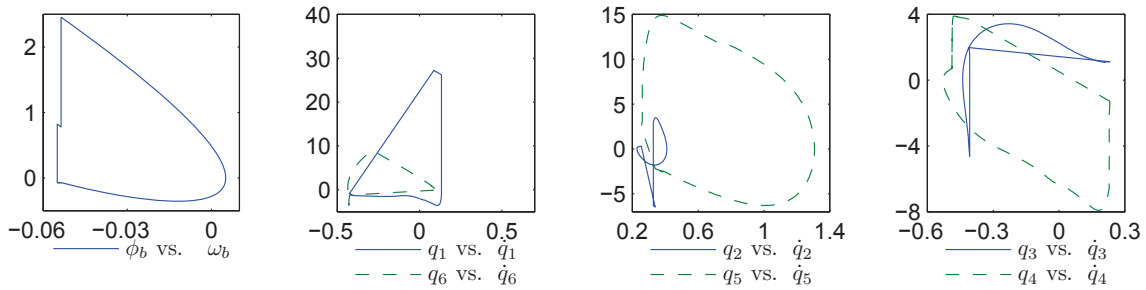

(a) Body frame angle (b) Ankle angles (c) Knee angles (d) Hip angles

Figure 5.12: Phase portraits of simulation of autonomous system Σ_a.

the Poincaré map about the fixed point $(q_s^*, \dot{q}_s^*)$ yields eigenvalues of the following magnitudes:

$$|\lambda_a| \in \{0.1902,\, 0.0680,\, 0.0680,\, 0.504,\, 0.0058,\, \ldots\},$$

where, again, only the five eigenvalues with the largest magnitudes are shown. The phase portraits are shown in Figure 5.12.

6. SIMULATION RESULTS*

This section provides example systems to help provide intuition into energy shaping procedures and to demonstrate the outcome of applying energy shaping to these example systems. Four examples are covered and they are arranged by complexity. The first example covered is the cart–spring system, which is a single–degree-of-freedom system. This example is, perhaps, the most informative due its simplicity: with one degree-of-freedom, it is possible to provide figures demonstrating the domain of attraction and to plot a proper phase portrait. The next example is the compass-gait biped walking down a shallow slope. This system which is motivated largely by McGeer's work [97] has two degrees-of-freedom and exhibits conservation of energy in the continuous dynamics. The third system is a three-link biped with a torso walking on flat ground under the influence of controlled symmetries[148] and additional non-conservative forcing. The fourth and final system is a seven-link, multi-domain biped which uses a number of controllers to achieve walking. This model is rather complex in comparison to the other examples and is provided primarily to demonstrate energy shaping on multi-domain hybrid systems.

In addition to verifying the formal results guaranteed by Theorem 1, this section will also attempt to provide some substance to the claims made about the benefits of energy shaping. It was loosely mentioned that energy shaping can be used to improve robustness of systems with respect to perturbations in initial conditions. Although it may be possible to demonstrate the domain of attraction for some models, doing so requires the explicit construction of a Lyapunov function. And though Theorem 1

*A portion of this section is reprinted from J. W. Grizzle, Christine Chevallereau, R. W. Sinnet and A .D. Ames, "Models, feedback control, and open problems of 3D bipedal robotic walking," *Automatica*, vol. 50, no. 8, pp. 1955–1988, 2014, with permission from Elsevier.

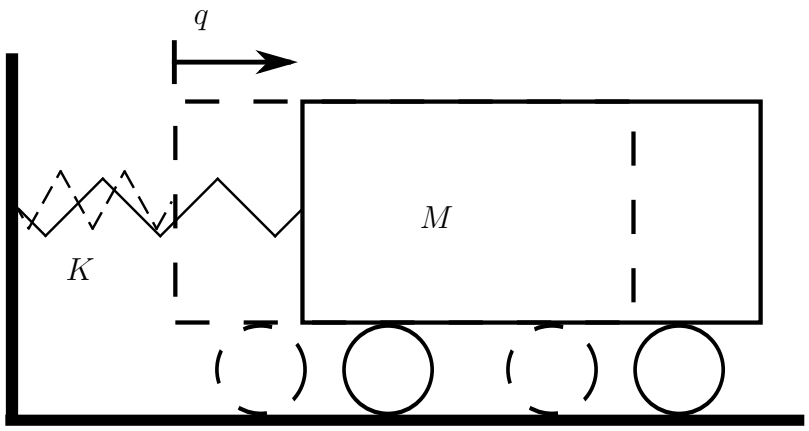

Figure 6.1: Configuration of the cart–spring system. Values used in simulation shown in Table 6.1.

Table 6.1: Physical parameters for the cart–spring simulation.

$$M = 1 \text{ kg}, \quad K = 1 \text{ N/m}, \quad \gamma = .2 \text{ kg/m}^2/\text{s}$$

guarantees the implicit existence of a valid Lyapunov function by fulfilling the necessary conditions for Lyapunov's direct method (converse Lyapunov theorem), it does not provide the explicit function in much the same way as the definition of time-to-impact as an implicit function does not provide any clue as to its explicit form. As a result and because of the difficulty of guessing a Lyapunov function,

6.1 Cart–Spring System

The simplest example system to which energy shaping can be applied is a system with a one-dimensional configuration space. The cart–spring system shown in Figure 6.1 (with simulation parameters given in Table 6.1) is just such a system and can be used to build intuition into the methods presented.

6.1.1 Setup

This well-known example is highly idealized and assumes rolling without slipping and no damping. As shown in Figure 6.1, the cart has mass M and is acted on by an idealized spring with stiffness K. It is assumed that (by turning the wheels) a force can be applied directly along the x-axis in the same way in which the spring acts.

Parameterizing the motion of the system by the horizontal displacement, q, with associated velocity $\dot{q}$, leads to the configuration space $\mathcal{Q} = \mathbb{R}$ with tangent bundle $T\mathcal{Q} = \mathbb{R}^2$ which has coordinates $x = (q, \dot{q}) \in \mathbb{T}\mathcal{Q}$. Disregarding physical restrictions on spring length leads to the domain of admissibility for the system being entire, i.e.,

$$D = \mathbb{R}^2.$$

The dynamics of the system obeys the differential equation

$$M\ddot{q} + Kq = u$$

where M is the mass of the cart, K is the spring constant, and u is the control force in newtons.

This system is not intrinsically a hybrid system and, as a result, energy shaping cannot be directly applied. However, this system can be made amenable to energy shaping by embedding it in a hybrid system. Consider that the motion of the cart–spring system involves oscillation about the origin. Thus all non-trivial trajectories pass through the origin repeatedly, so a natural choice for the switching surface (Poincaré section) is the set

$$S = \{(q, \dot{q}) \in T\mathcal{Q} : q = 0 \text{ and } \dot{q} < 0\}. \tag{6.1}$$

Using this switching surface with the domain of admissibility specified above permits reformulation of the cart–spring system as a hybrid system:

$$\Sigma^c = \begin{cases} \dot{x} \;\; = f(q,\dot{q}) + g\,u, & (q^-,\dot{q}^-) \in D \setminus S, \\ x^+ = (q^-,\dot{q}^-), & (q^-,\dot{q}^-) \in S, \end{cases} \tag{6.2}$$

where

$$f(q,\dot{q}) = \begin{pmatrix} \dot{q} \\ -\frac{K}{M}q \end{pmatrix}, \qquad g = \begin{pmatrix} 0 \\ \frac{1}{M}. \end{pmatrix}.$$

For the constructed hybrid system, the discrete dynamics do not have any effect on the configuration and velocity; in other words, the discrete dynamics is the identity map. Moreover, with no control input, the system is conservative and does not exhibit asymptotic stability. In order to demonstrate the application of energy shaping, a limit cycle can be induced in the system using, for example, the same dissipation present in the Van der Pol oscillator (see [71, pp. 13]). As described in Section 4, the state of the system can be augmented to include a storage function for energy flow due to non-conservative forcing, i.e.,

$$x = (q, \dot{q}, W)$$

where W is an energy storage function as in (4.2). Applying the feedback control law

$$u = v(q,\dot{q}) = \gamma(1-q^2)\,\dot{q} + w \tag{6.3}$$

with $\gamma \in \mathbb{R}_{\geq 0}$ leads to the hybrid control system

$$\overline{\Sigma}_c = \begin{cases} \dot{x} \;\; = \bar{f}(q,\dot{q}) + \bar{g}\, w, & (q^-,\dot{q}^-) \in D \setminus S, \\ x^+ = \Delta(q^-,\dot{q}^-), & (q^-,\dot{q}^-) \in S, \end{cases} \tag{6.4}$$

where the nominal controller is subsumed under the system dynamics and energy flow is tracked in the W coordinate, viz.

$$\bar{f}(q,\dot{q}) = \begin{pmatrix} \dot{q} \\ -\frac{K}{M} q + \frac{1}{M}\gamma(1-q^2)\,\dot{q} \\ \gamma(1-q^2)\,\dot{q}^2 \end{pmatrix}, \qquad \bar{g}(\dot{q}) = \begin{pmatrix} 0 \\ \frac{1}{M} \\ 0 \end{pmatrix}, \tag{6.5}$$

and the reset map acts to reset the stored energy, i.e.,

$$\Delta(q,\dot{q}) = (q,\dot{q},0).$$

The hybrid control system (6.4) is of the same form as (4.4) but is written in a more compact way.

6.1.2 Simulation of Nominal System

Beginning from the (post-reset) initial condition

$$(q,\dot{q},W) = (0,-.1,0),$$

a simulation was conducted to illustrate the nominal behavior of cart–spring system governed by (6.4) and (6.5) under influence of the Van der Pol controller defined in

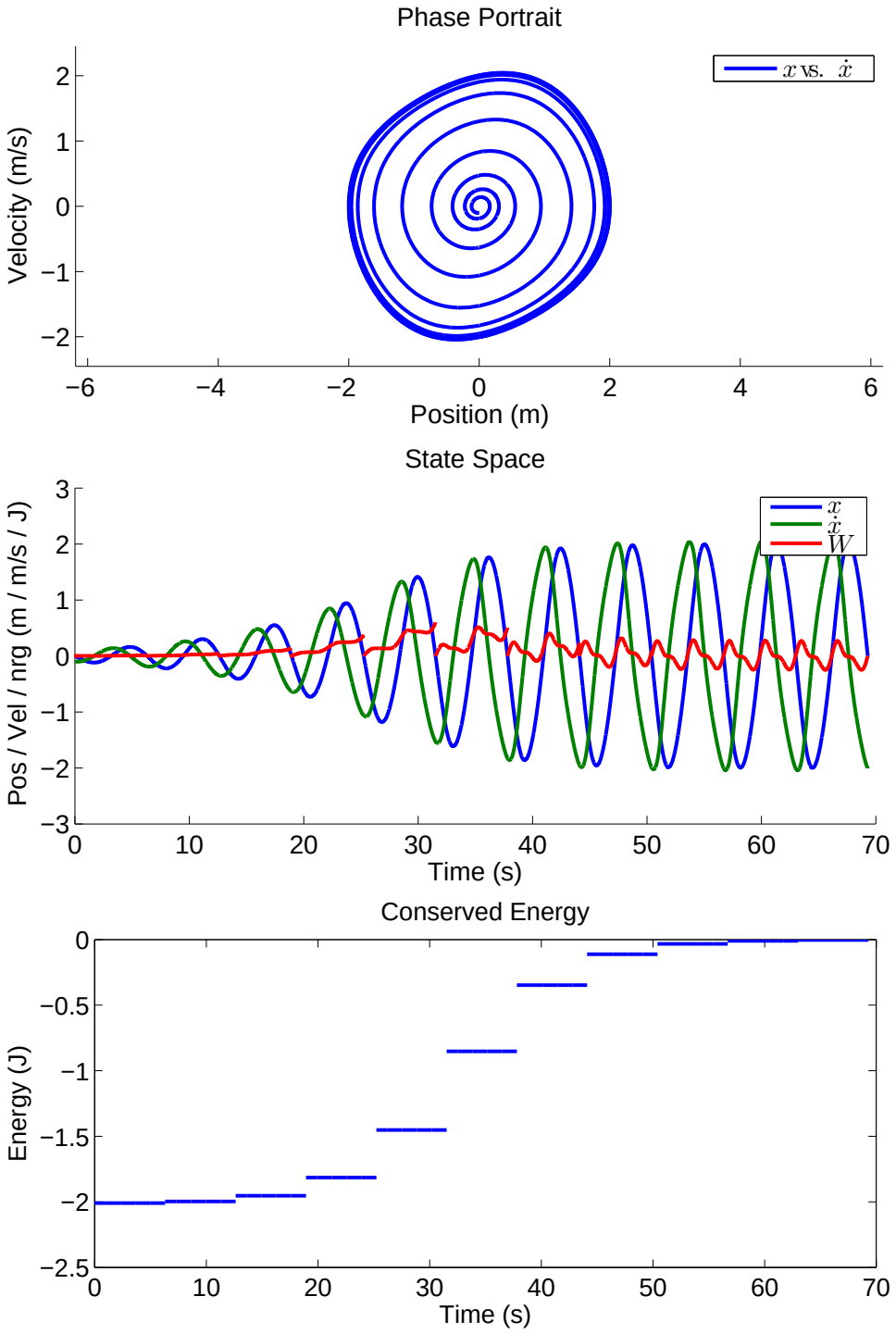

Figure 6.2: Simulation of the nominal cart–spring system. A force from the nominal control law (6.3) acts on the cart. Top: phase portrait demonstrating the existence of a limit cycle; middle: evolution of the state coordinates; bottom: the conserved energy jumps when the storage function is reset at the switching surface.

(6.3) with $w = 0$; that is, the closed-loop hybrid system

$$\overline{\Sigma} = \begin{cases} \dot{x} &= \bar{f}(q, \dot{q}), \qquad (q^-, \dot{q}^-) \in D \setminus S, \\ x^+ &= \Delta(q^-, \dot{q}^-), \quad (q^-, \dot{q}^-) \in S, \end{cases} \tag{6.6}$$

The parameters used are given in Table 6.1; two of the parameters refer to the mass and spring constant as shown in Figure 6.1. The simulation was designed to terminate when the distance between successive crossings of the Poincaré section (6.1) dropped below a threshold—in this case, 10^{-3}—thus serving as the convergence criterion. Mathematically, this convergence criterion can be expressed as

$$\|P_{T_I(x)}(x) - x\| < 10^{-3}, \quad x \in S. \tag{6.7}$$

In this case, the distance metric is the standard Euclidean one and involves only the velocity coordinate due to the definition of the Poincaré section (6.1).

From Figure 6.2, it is apparent that the simulation lasted just under 70 seconds. The phase portrait in Figure 6.2 shows that the system eventually converges to a limit cycle over relatively large number of steps (i.e., iterations of the Poincaré first return map). By counting the jumps in the plot of conserved energy in Figure 6.2, one can see that convergence based on the aforementioned criterion requires 11 "steps"; in other words, the cart passes through the origin from the positive side 11 times.

From the evolution of the coordinates shown in Figure 6.2, it is apparent that the oscillations grow until the system reaches the limit cycle. The conserved energy of the limit cycle (as defined in (4.1) and (4.2)) can be seen to change between iterations in Figure 6.2. This jump is a result of the resetting of the storage function, W, which occurs when the cart passes through the switching surface (6.1).

6.1.3 Simulation of Shaped System

To demonstrate the effect of energy shaping, a simulation was conducted on the cart–spring system described in the previous subsection. The relevant hybrid control system for the application of energy shaping is given in (6.4) and (6.5). In contrast to the nominal simulation, this simulation was conducted with w given by the min-norm control law (4.10) designed to satisfy the conditions of energy shaping (4.8), which results in the hybrid system

$$\overline{\Sigma} = \begin{cases} \dot{x} \;\; = \bar{f}(q,\dot{q}) + \bar{g}\,\mu_\varepsilon(q,\dot{q},W), & (q^-,\dot{q}^-) \in D \setminus S, \\ x^+ = \Delta(q^-,\dot{q}^-), & (q^-,\dot{q}^-) \in S, \end{cases} \tag{6.8}$$

with $\bar{f}$ and $\bar{g}$ as given in (6.5).

The results of the simulation of (6.8) are shown in Figure 6.3. Like the simulation of the nominal system, this simulation of the shaped system (6.8) was designed to terminate upon convergence using the same criterion as specified in (6.7). From this figure, it is immediately obvious that convergence occurs in fewer steps than for the nominal simulation; for this shaped simulation, convergence requires three steps (count the zero-crossings of q in the middle plot of Figure 6.3) and the simulation lasted under 20 seconds. In addition, it is apparent from the phase portrait that the convergence happens very rapidly. The speed of convergence can be affected by varying the gain ε of the energy shaping controller (4.8).

These numerical simulations show that energy shaping can provide improved convergence properties for stable systems. However, because the Van der Pol controller is globally stable, it is not possible to demonstrate an increase in domain of attraction; this benefit of energy shaping will be shown in the next example.

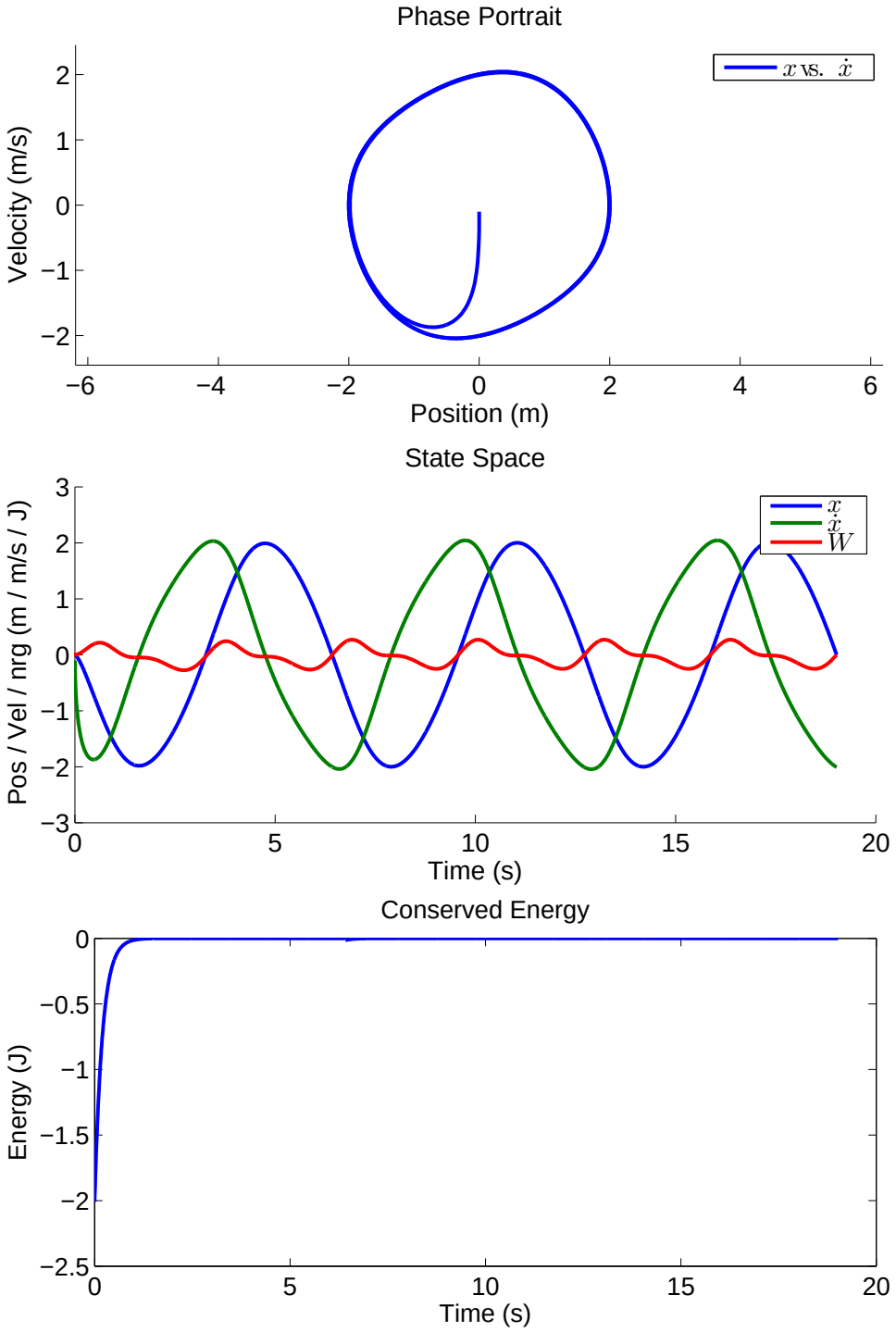

Figure 6.3: Simulation of the shaped cart–spring system. A force from the nominal control law (6.3) acts on the cart along with a force from energy shaping. Top: phase portrait demonstrating the existence of a limit cycle and rapid stabilization; middle: evolution of the state coordinates; bottom: the conserved energy stabilizes to the desired value at an exponential rate.

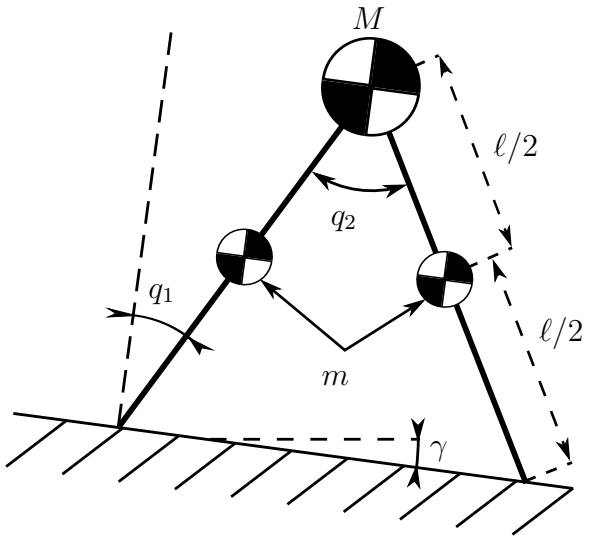

Figure 6.4: Compass-gait biped with walking down a slope.

Table 6.2: Physical parameters for the simulation model.

$M = 20$ kg, $\quad m = 5$ kg, $\quad \ell = 1$ m, $\quad \gamma = .05$ rads

6.2 Compass-Gait Biped

With slightly greater complexity than the cart–spring system described in Section 6.1, the compass-gait biped is a two-link rigid kinematic chain with periodic impacts (foot-strike) which cause instantaneous jumps in the velocity coordinates.

Using the compass-gait biped model shown in Figure 6.4 with parameters as shown in Table 6.2, simulations were conducted to demonstrate the effectiveness of the energy shaping procedure. The limit cycle of the passive system is shown in Figure 6.5 with the dotted lines representing discrete jumps from foot-strike (and coordinate relabeling). This gait has a fixed point

$$(q^*,\ \dot{q}^*) = (-0.2891,\ 0.5781,\ -1.4006,\ -0.2802) \tag{6.9}$$

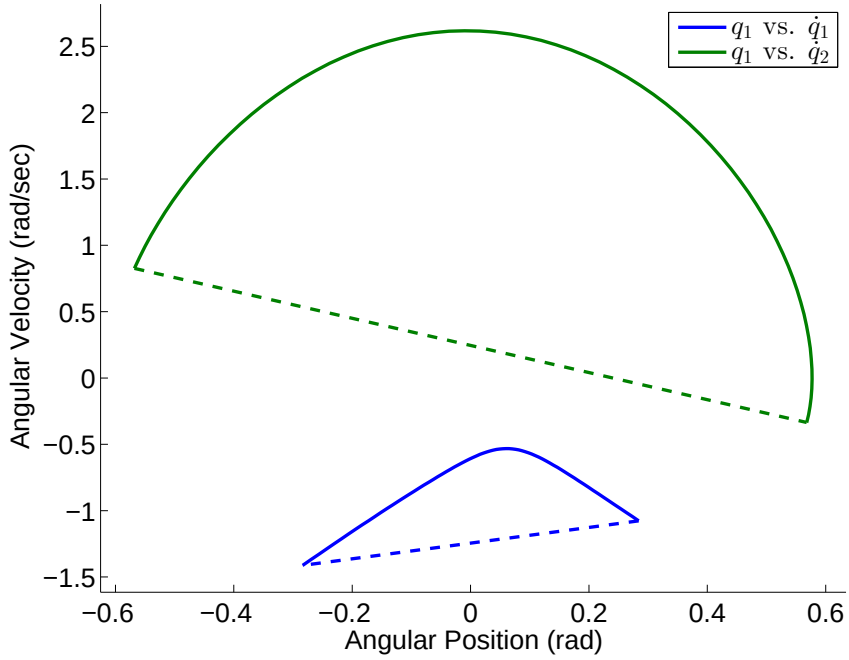

Figure 6.5: Limit cycle of the passive compass gait biped.

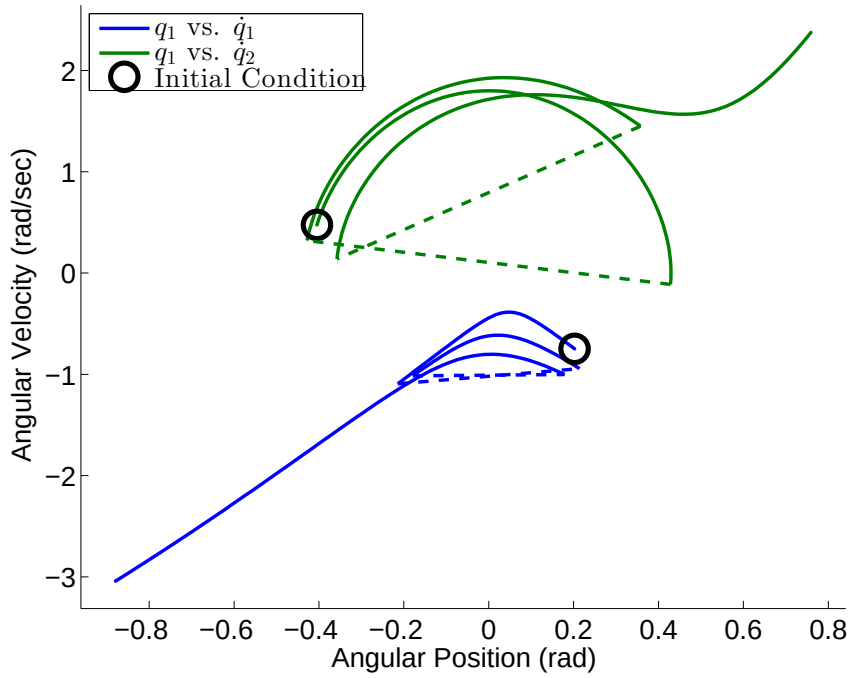

Figure 6.6: The passive system cannot recover from distant states.

on the guard with eigenvalues

$$|\lambda| = (0.5147,\ 0.5147,\ 0.0980) \tag{6.10}$$

corresponding to a linearization of the Poincaré map restricted to the guard. Due to the restriction to the guard, the Poincaré section is a codimension-one hyperplane and is thus characterized with fewer coordinates (one fewer). Because these eigenvalues have magnitude below unity, the corresponding hybrid periodic orbit is locally exponentially stable. The impact map can be applied to the fixed point (6.9) to compute the post-impact coordinates

$$\Delta(q^*,\ \dot{q}^*) = (0.2891,\ -0.5781,\ -1.0681,\ 0.6797). \tag{6.11}$$

To see the benefit of energy shaping, consider two simulations conducted from a perturbed post-impact initial condition,

$$(q_0,\ \dot{q}_0) = (0.2023,\ -0.4047,\ -0.7477,\ 0.4758), \tag{6.12}$$

which was naively obtained by multiplying the post-impact fixed point (6.11) by 0.7 resulting in a relatively large perturbation. For the passive walker, one can see from Figure 6.6 that the biped falls on the third step. When energy shapping is added by choosing $\frac{c_3}{\epsilon} = 1$ as in Figure 6.7, the biped is able to recover from the same initial condition and quickly converges to the limit cycle.

In addition to the ostensible increase in robustness, energy shaping also seems to improve convergence properties. To see this, a simulation was conducted from the

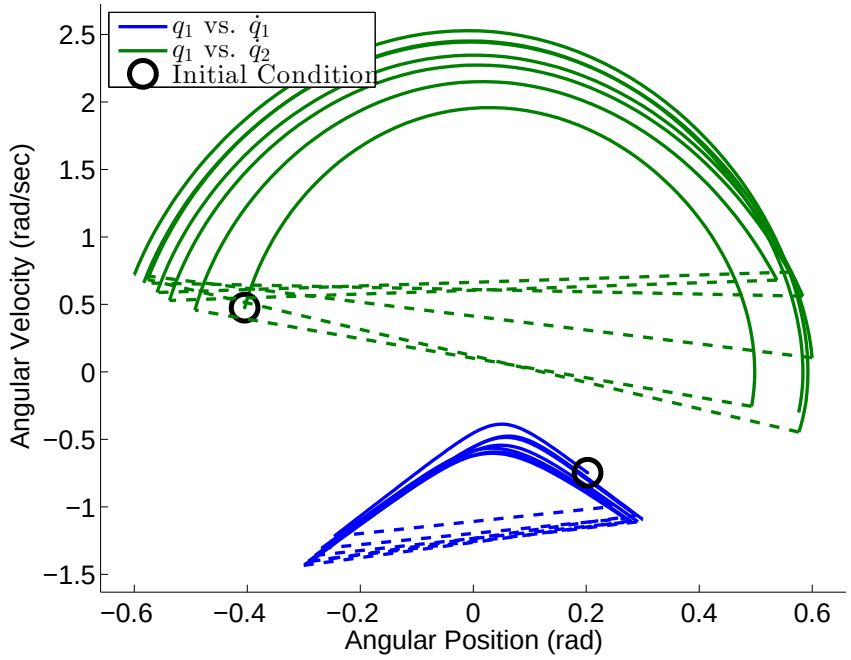

Figure 6.7: Energy shaping allows recovery from more distant states.

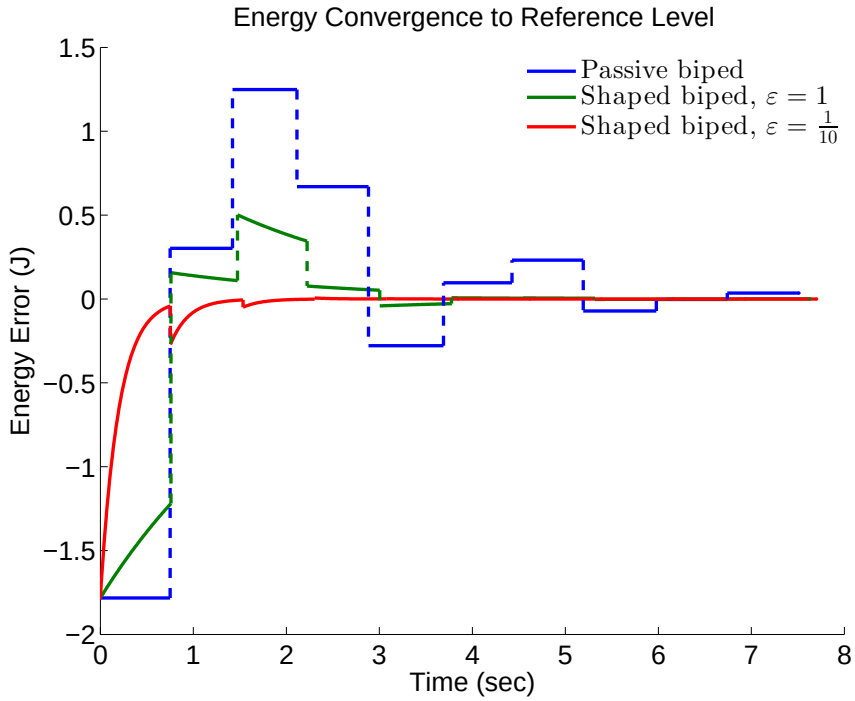

Figure 6.8: Convergence has more desirable behavior with energy shaping. Smaller values of ε offer better convergence.

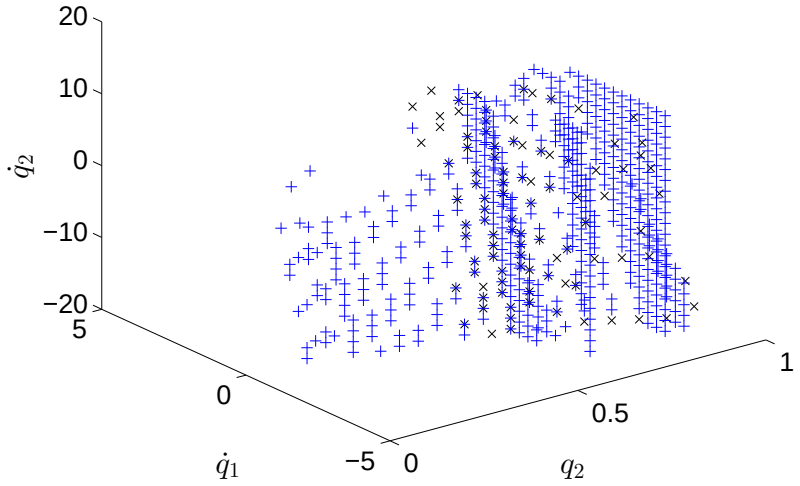

Figure 6.9: The domain of attraction restricted to the guard. The DOA can be viewed in three dimensions with careful scrutiny. The blue "+" symbols represent stable points of the shaped system and the black "x" symbols represents stable points of the passive system.

starting point

$$(q_0,\ \dot{q}_0) = (0.2457,\ -0.4914,\ -0.9079,\ 0.5777), \tag{6.13}$$

which, in similarity to the previous simulation, was obtained by multiplying (6.11) by 0.85. This point had to be closer than (6.12) in order to fall within the domain of attraction (DOA) of the passive biped. The difference in convergence for the energy levels of the passive and shaped systems is shown in Figure 6.8. One can see that the shaped system converges more quickly than the passive system. Whereas the passive system changes energy only through impact, the shaped system also converges during the continuous dynamics. Finally, it seems, stability is mainted for large values of ε, smaller values will result in better convergence so a trade-off naturally arises.

Table 6.3: Physical model parameters of the seven-link biped. Masses and lengths are given in kilograms and meters, respectively.

M	m_t	m_c	m_f	w_f	w
20	5	1	.1	.08	.10

ℓ	ℓ_t	ℓ_c	r_a	r_f	r_h	r_t	r_T
1	.175	.375	.1	.139	.0625	.25	.075

More comprehensive evidence for the expansion of the domain of attraction can be seen in Figure 6.9 which provides a comparison of the stable region on the guard for both the passive and shaped systems. It is interesting to note that the domain of attraction expands most readily into the region of low energy (small steps, small angular velocities) for which states the passive biped would simply lack the energy necessary to fall into a gait.

6.3 Seven-Link Biped

This section describes simulations of the seven-link biped shown in Figure 6.10 with parameters in Table 6.3.

6.3.1 Domain Structure

This gait has a graph $\Gamma = (V, E)$, with vertices and edges

$$V = \{ts,\ tl,\ kl,\ hs\}, \quad E = \{\{ts,\ tl\},\ \{tl, kl\},\ \{kl, hs\},\ \{hs,\ ts\}\}.$$

By convention, the phases are numbered such that the transition from the last domain to the first domain (i.e., $4 \to 1$) corresponds to heel strike as this event signifies that the stance and swing legs should be swapped. For the proper choice of gains, the walking controllers applied in this example can generate a gait for which the hybrid dynamics $h_1(q) = p^z_{stt}(q)$, where $p^z_{stt}(q)$ is height of the stance toe above the ground,

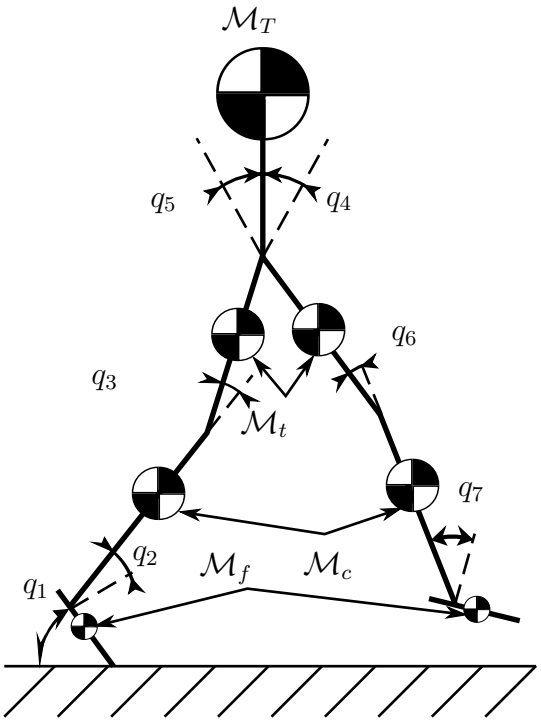

Figure 6.10: Seven-link biped configuration.

can be combined to construct the constraint vector $H_1(q, \dot{q}, u)$. After impact, it is desired that the stance knee be locked, that the stance foot be flat on the ground, and that the swing toe remain fixed to the ground. These requirements dictate an apropos choice of kinematic constraints for constructing a Jacobian for the impact map (3.17). Using toe strike as the transition leads to the switching surface $S^{1\to 2}$ given in (3.2).

6.3.1.1 Phase 1 – Toe Strike (ts)

For simplicity, let the first phase of the gait be *ts*. This phase starts right after the non-stance heel impacts the ground. After the impact, the weight shifts mostly to the impacting leg as the robot moves forward.

6.3.1.2 Phase 2 – Toe Lift (tl).

As the stance foot experiences heel roll from the previous phase and the toe rolls into the ground causing an impact, the stance foot enters a state of flat foot contact while the swing toe remains on the ground. The system continues under these conditions until the vertical constraining force on the back (swing) toe reaches zero, at which point, the ground is no longer undergoing a force interaction with the toe. This force thus represents a non-holonomic constraint on the system which can be used to define both the switching surface and domain of admissibility (which must always be checked). As the force reaches zero, the toe leaves the ground and, as there is no impact, there is no impulsive change in momentum and thus the reset map simplifies to the identity map, as previously mentioned.

6.3.1.3 Phase 3 – Knee Lock (kl).

After the swing toe lifts, the biped continues to locomote with flat foot contact between the stance foot and the ground until the swing knee reaches full extension, resulting in an impact which locks the knee. The locking and unlocking of knees could be accomplished by solenoid actuators. Unlike Phases 1 and 2, which are comparatively short, the biped spends a major part of the gait in Phase 3. This ends up being useful as one could say the biped has full actuation in this phase. The constraints imposed on the system in this domain actually reduce the available degrees of freedom in the mechanical configuration to the same as the number of actuators. Thus the robot can be made to move anywhere within the domain of admissibility providing the appropriate constraints aren't violated.

6.3.1.4 Phase 4 – Heel Strike (hs).

The locking of the stance knee which represents the transition to this domain means that both knees are locked in this domain, but the system still has full actuation. This phase ends when the swing heel strikes the ground, resulting in a transition back to the first phase. A coordinate transformation can be constructed to "swap" the angles of the stance leg and swing leg. For the model presented, the new joint angles are given by the following map:

$$\begin{aligned}\mathcal{T}_q : (q_8, q_7, q_6, q_5, q_4, q_3, q_2, q_1) \\ \mapsto (q_1, q_2, q_3, q_4, q_5, q_6, q_7, q_8).\end{aligned}$$

By choosing the reference frame to be on the torso, the transformation for the base coordinates is simply the identity map. The transformation can then be written as a linear map, $\mathcal{T} = \text{blk diag}(I_6, \mathcal{T}_q)$ which induces pushforward $\mathcal{T}^*$. The post-impact state is thus given, as in (3.17), by $\text{blk diag}(\mathcal{T}, \mathcal{T}^*) \cdot \Delta^{4\to 1}$. Finally, it should be noted that there are certain choices of control which could result in a bi-periodic orbits due to poor control design.

6.3.2 Control Design

The gait considered in this simulation requires the use of several different control laws. For the sake of obtaining a passivity-based feel, controlled symmetries was taken as the basis for sagittal control design. When combined with a spring–damper (PD) controller to stabilize the torso, controlled symmetries can produce stable walking gaits on point foot models under the assumption of full actuation. This is essentially equivalent to a model with trivial foot behavior, i.e., either flat ground contact or no contact. In order to get nontrivial foot action, additional PD

controllers can be added at the ankles and at the non-stance knee. Finally, in order to avoid scuffing, which occurs when the swing toe strikes the ground before desired, a controller is designed to rotate the toe away from the ground with a torque that fades exponentially with the toe's distance from the ground.

6.3.2.1 CS

Controlled symmetries, introduced in [148], works by shaping the potential energy a robot to that of a passive biped walking down a slope. A group action effectively "rotates the world" by operating on the potential energy allowing for walking on flat ground given passive walking down a slope. The goal is to combine controlled symmetries with other control laws to achieve stable walking in the 2D sagittally-restricted kneed biped with feet.

To rotate gravity, consider the group action

$$\Psi_\gamma(q) : (p^x_{st}, p^z_{st}, \phi^y_{st}, q^1_s - \gamma, q_{s,2}, \ldots, q_{s,6}) \longmapsto (p^x_{st}, p^z_{st}, \phi^y_{st}, q_{s,1} \ldots, q_{s,6})$$

for slope angle $\gamma \in \S$ and define the feedback control law

$$K^\gamma(q) := G_{q_s}(q) - G_{q_s}(\Psi_\gamma(q))$$

with $G_{q_s}(q) = \frac{\partial U}{\partial q_s}(q)$ which in the vector fields

$$f_i^\gamma(q, \dot{q}) = f_i(q, \dot{q}) + g_i(q, \dot{q})\, K_i^\gamma(q), \tag{6.14}$$

for $i \in \{1, \ldots, 4\}$.

6.3.2.2 Spring–Damper Controllers

Motivated by the elasticity the human ankle and by human ankle torque (see [11]), PD controllers are considered as a means of meeting specific control objectives. For a given joint j with angle $q_{s,j}$ and angular velocity $\dot{q}_{s,j}$, a typical PD controller takes the form

$$u_{\mathrm{PD},j}(q,\dot{q}) = -k_j(q_{s,j} - q_{s,j,0}) - c_j\,\dot{q}_{s,j}. \tag{6.15}$$

In order to stabilize the torso, (6.15) requires modification:

$$u_{\mathrm{PD},q_{s,4}}(q,\dot{q}) = -k_T(\phi^y_{st} - \vartheta_{T,0}) - c_T\,\omega^y_{st},$$

where ϕ^y_{st} is an Euler angle for the torso and ω^y_{st} is the body-fixed angular velocity of the torso in the sagittal plane for the model described earlier. The controller is applied at the swing hip, $q_{s,4}$. To have the swing foot land in a desirable configuration, and motivated by measurements of human ankle torque during walking, the PD controller (6.15) is applied at $q_{s,6}$. Heuristics has shown that a PD controller at the stance ankle may often contribute to stability and thus (6.15) is used at $q_{s,1}$. In order to get the swing knee moving forward after heel strike, it was necessary to impose (6.15) on $q_{s,5}$.

For simplicity take these controllers to be a set on each domain i such that

$$U^i_\Theta = \begin{cases} \{1,4,5,6\}, & i = 1, \\ \{1,4,6\}, & i = 2,3,4. \end{cases}$$

One can observe that the controllers are continuous through a single step with the exception of the controller designed for the swing knee. In a continuous time system,

Table 6.4: Gains for seven-link biped simulation.

k_1	c_1	$q_{s,1,0}$	k_T	c_T	$q_{T,0}$	β_1	γ
30	0.1	-0.5	100	5	0	10	0.05
k_5	c_5	$q_{s,5,0}$	k_6	c_6	$q_{s,6,0}$	β_2	g
70	1	0.5	30	1	0	20	9.81

this would mean the torques for smooth control laws would be smooth, but in a hybrid system with impulse-like forces due to impacts, discontinuities will occur in the velocities causing jumps in those control laws which depend on these variables. The keen observer might notice that if equivalent controller parameters were found for $q_{s,1}$ and $q_{s,6}$, these controllers could be replaced by actual spring–damper mechanisms. These controllers can be combined to construct

$$K_i^{\Theta}(q, \dot{q}) := \sum_{j \in U_{\Theta}^i} u_{PD,j}(q, \dot{q}) \cdot b_{q_s,j},$$

where $b_{q_s,j}$ is the j^{th} basis vector for the coordinates q_s. Applying these controllers to (6.14) gives

$$f_i^{\gamma,\Theta}(q, \dot{q}) = f_i^{\gamma}(q, \dot{q}) + g_i(q)\, K_i^{\Theta}(q), \tag{6.16}$$

where gains (Table 6.4) are lumped into superscripts.

6.3.2.3 Scuffing Prevention Controller

In order to avoid the scuffing phenomenon, a controller can be designed which repels the swing toe from the ground. To minimize interference with the rest of the system's control, the scuffing prevention controller imposes exponential spatial disipation that and thus only makes a significant contribution when the swing toe

passes near the floor. This control law thus takes the form

$$K^{\beta}(q) = -\beta_1 e^{\beta_2 \cdot p^z_{swt}(q)} \cdot b_6,$$

where $\beta_1, \beta_2 \in \mathbb{R}$ are positive constants and represent the strength of repulsion and spatial dissipation rate, respectively, $b_{q_s,6}$ is the 6^{th} basis vector in q_s, and $p^z_{swt} : \mathcal{Q} \to \mathbb{R}$ is the height of the swing toe above the ground. This control law is only desirable when the swing toe is in the air, so appropriate application leads to the following vector fields:

$$f_i^{\gamma,\Theta,\beta}(q,\dot{q}) = f_i^{\gamma,\Theta}(q,\dot{q}) + \begin{cases} \mathbf{0}, & \text{i} = 1,\, 2, \\ g_i(q)\, K_i^{\beta}(q), & \text{i} = 3,\, 4. \end{cases}$$

6.3.3 Simulation of Nominal System

Applying the feedback control laws as shown above to the hybrid control system Σ^c gives the hybrid system

$$\Sigma^{\gamma,\Theta,\beta} = (\Gamma,\, D,\, S,\, \Delta,\, \mathcal{F}^{\gamma,\Theta,\beta}),$$

where $\mathcal{F}^{\gamma,\Theta,\beta} = \{f_i^{\gamma,\Theta,\beta}\}_{i=1}^4$. This hybrid system was simulated with model parameters given in Table 6.3 and control parameters given in Table 6.4. The joint angles and torques resulting from this walking simulation are shown in Figure 6.11. The stability of the gait can be examined by considering the codimension-one Poincaré section S_4^1, which is the guard of domain 4 (i.e., heel strike) and involves switching legs. To minimize the perturbations necessary to examine the Poincaré map, one can perturb along a minimal set of bases that span the Poincaré map locally.

Non-holonomic constraints represent restrictions on the degrees of freedom of

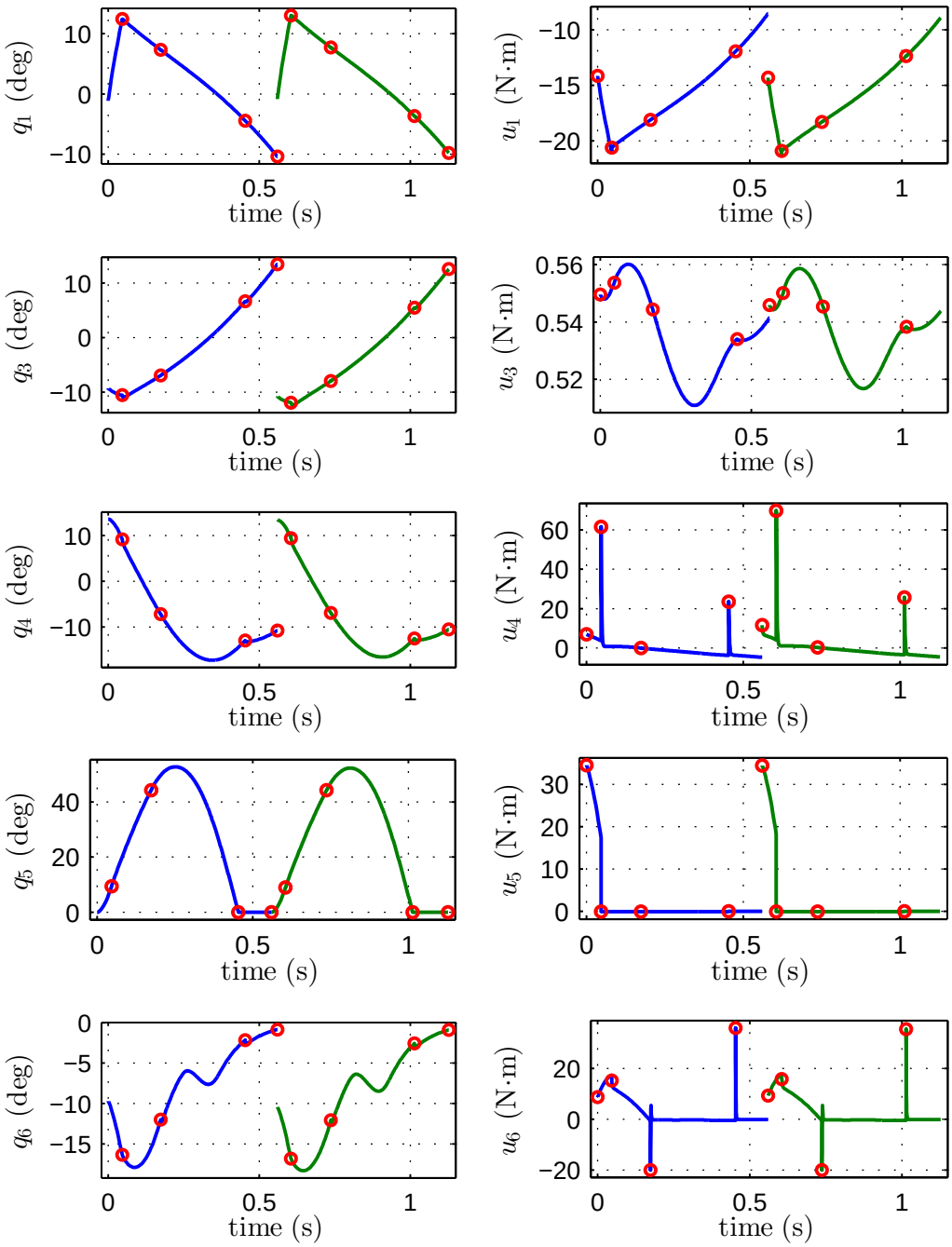

Figure 6.11: Joint and torque profiles for the seven-link biped gait over two steps. The small circles represent the points where the discrete transitions occur.

a system and this shows up in a dropping of rank in the Poincaré map. For this particular model, these minimal bases can be found by moving the fixed frame to the fixed stance foot, then perturbing along angles $q_{s,3}$, $q_{s,4}$, $q_{s,6}$ and angular velocities $\dot{q}_{s,1}$, $\dot{q}_{s,3}$, $\dot{q}_{s,4}$, $\dot{q}_{s,6}$. Because the knees are locked, $q_{s,2} = \dot{q}_{s,2} = q_{s,5} = \dot{q}_{s,5} = 0$ and one can solve for $q_{s,1}$ such that the swing heel is on the ground. Thus the Poincaré map for the orbit drops rank to seven. Through optimization, the fixed point

$$q_s^* = (-.163, 0, .245, -.139, 0, -.003),$$
$$\dot{q}_s^* = (-.987, 0, 1.090, 1.068, 0, .067),$$

is found. A numerical approximation of a linearization of the Jacobian of the Poincaré map in the seven minimnal bases yields eigenvalues with magnitudes 0.613, 0.169, 0.056, ... In general, eigenvalues with magnitudes below unity for discrete-time systems indicate stability. The Poincaré map for the simulated system is indeed stable thus implying $(q^*, \dot{q}^*)$ is a fixed point of a stable periodic orbit which represents the stable walking gait.

One could perform a similar analysis taking a different Poincaré section such as the guard for knee lock. This map has two bases more than the guard for heel strike as used above; one may no longer solve for $q_{s,1}$ and $\dot{q}_{s,5}$ becomes arbitrary. By taking this Poincaré section and performing analysis, one would find seven non-zero eigenvalues for the reasons alluded to above.

The main purpose of this subsection is to demonstrate the application of energy shaping to a multi-domain hybrid system. This four-phase gait has a different energy level at each phase of the walking; that is, the conserved energy of the system, E_c, has a different value of E_{ref} depending on the phase of walking. For a phase v which is a vertex in the domain graph Γ, the E_{ref}^v value is selected to be the energy level of

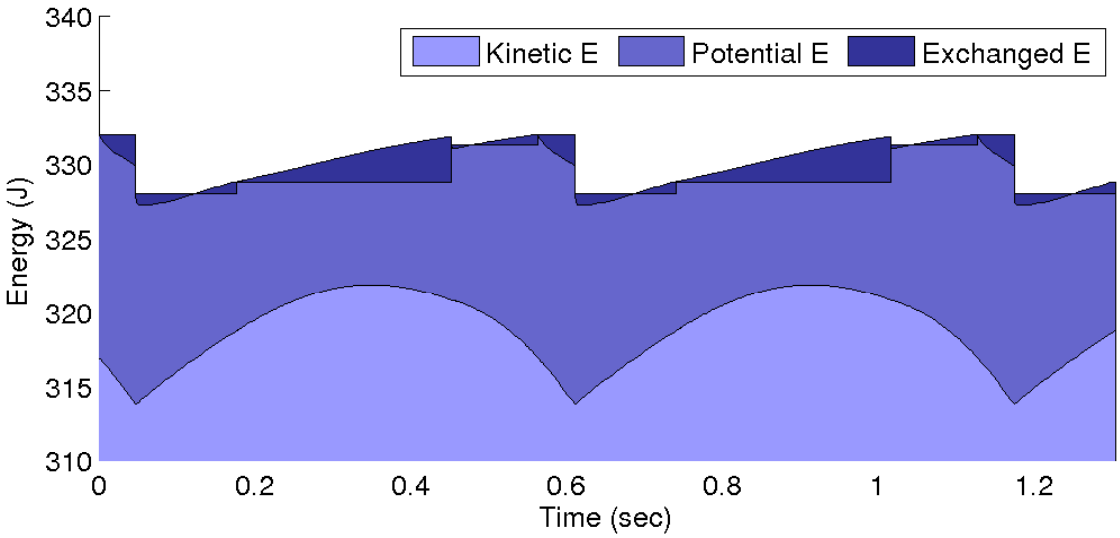

Figure 6.12: Energy exchange in seven-link biped simulation.

the system at the beginning of the domain:

$$E_{\text{ref}}^{ts} = 331.91, \quad E_{\text{ref}}^{tl} = 327.96, \quad E_{\text{ref}}^{kl} = 328.78, \quad E_{\text{ref}}^{hs} = 331.22.$$

The interplay between kinetic, potential, and exchanged energy can be seen in Figure 6.12. This figure shows that these three components sum to a constant reference level for each given phase of walking.

6.3.4 Simulation of Shaped System

In order to demonstrate the effect of energy shaping, two simulations were conducted from the starting point

$$q = (0, -0.0859,\ 0,\ 0.1106,\ -0.0916,\ 0,\ -0.0073),$$
$$\dot{q} = (0, -0.5339,\ 0,\ 0.6401,\quad 0.3758,\ 0,\quad 0.0886).$$

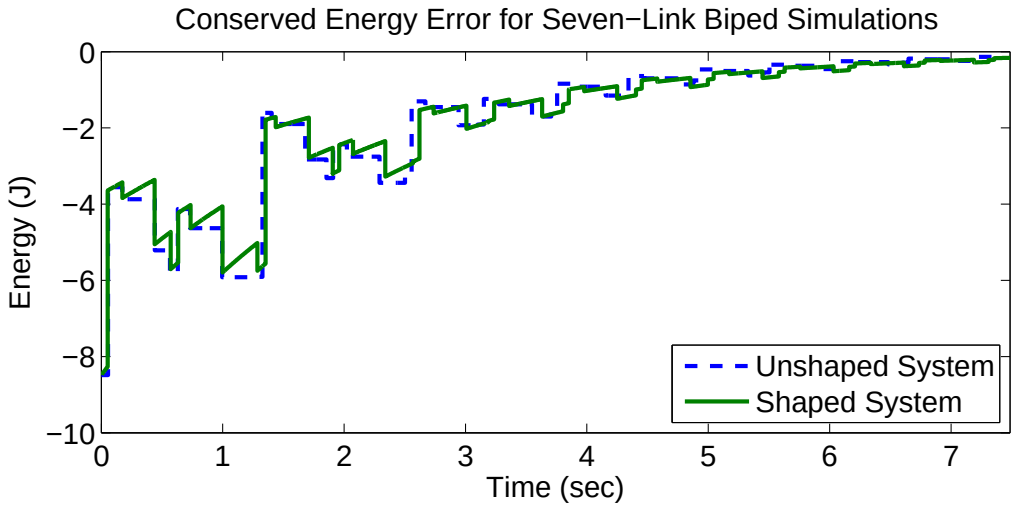

Figure 6.13: Comparison of unshaped and shaped seven-link biped simulations. Shown is the distance of the conserved quantity from the reference, i.e., $E_c - E_{\text{ref}}$.

These coordinates correspond to those shown as q_1 through q_7 in Figure 6.10. It is clear that both knees are straight on the switching surface. The effect of energy shaping can be clearly seen in Figure 6.13 where the error in conserved energy is plotted for both the unshaped and shaped simulations. In comparison to the previous examples, this system admits a much lesser degree of energy shaping. This is due to the nature of the gait and in particular the foot behavior: Large energy shaping can cause the feet to behavior undesirably resulting in falling. However, this also demonstrates the limitations of energy shaping as the theorem only guarantees that energy shaping works for ε above a certain threshold. Moreover, this comparison highlights the stabilizing effect that the discrete dynamics can provide to a biped.

7. CONCLUSION

This dissertation presented formal results for the method of energy shaping in mechanical systems. By taking advantage of conservation of energy, energy shaping seeks to improve the performance characteristics of existing periodic behaviors. Through the use of control Lyapunov functions, energy shaping acts on a non-conservative system while guaranteeing that the periodic behaviors are not destabilized. This formal guarantee is a novel contribution that provides a significant improvement over existing results which lacked this consideration.

As demonstrated, the methods, in some cases, may increase the domain of attraction thereby increasing robust with respect to perturbations in initial condition. Simulation results also demonstrated that energy shaping appears to drive systems to faster convergence. The method was demonstrated on simple models to provide intuition and then on more complex models to show versatility. Simulations results and modeling for a multi-phase human gait for a biped with feet were also provided to demonstrate energy shaping on a multi-domain hybrid system.

When proving energy shaping, it was shown that a Lyapunov function exists locally in the Poincaré map. The exact form of this Lyapunov function is not known, but this begs the question: is it possible to explicitly construct a Lyapunov function, perhaps by guessing, that could be used to analytically examine the domain of attraction? In doing so, one would likely obtain a more complete understanding of robustness properties. Despite the lack of formal claims with respect to global properties, the local stability properties are practically useful when using energy shaping as a stabilizing controller in operating regions around the desired behavior.

In addition, this dissertation does not make any claims about robustness with

respect to model uncertainties and measurement uncertainties. It would be worthwhile to investigate model and measurement robustness in the context of energy shaping and control Lyapunov functions in a wider context. Such discussions are spread throughout the literature; see, e.g., [35]. Open questions about the domain of attraction and robustness are pervasive and are not unique to energy shaping; however, their answers are left as the subject of future exploration.

When it comes to implementing formal algorithms on cyber-physical systems, there is a number of pertinent considerations which determine the viability and efficacy of a given controller. A control algorithm which updates its commands too slowly will cause shaky motion which in itself is indicative of imprecise control. In addition, a slow loop rate means the system is slow to react to external disturbances which makes it more difficult to reject them, thereby decreasing the robustness of the system. With bipeds this concern is of the utmost importance as the stability of a biped depends on balancing the dynamic moment to keep the robot from toppling over. Because feet tend to be narrow, stability in the coronal plane is a challenge that frequently plagues roboticists.

In order to achieve smooth behavior in dynamic robots, it is therefore necessary to have a relatively fast control loop and thus researchers seek to design controllers which are computationally tractable. Nonlinear controllers often give superior behavior in simulation but their complexity renders them impractical for real-time implementation. Oftentimes, controllers for robots are formulated as optimization problems which use internal models to determine the appropriate control values. The idea is to constrain the optimization problem to achieve the desired behavior; typical formulations might take into consideration control of the zero moment point to guarantee the system remains standing.

Considerations such as these generally lead to nonlinear optimization problems

which are problematic for a variety of reasons. While a complex nonlinear formulation may represent a rigorous model of known physical phenomena and may therefore match up very well with reality, the computation cost may be prohibitive rendering such a formulation useful only in simulation. To overcome this problem, some researchers are turning quadratic programs for which there exist efficient algorithms to quickly find solutions. If one can formulate the constraints as a convex set, the solution can be found easily and one can guarantee optimality whereas with nonlinear optimizations, there is no guarantee on optimality over a given region.

The formulation presented in this paper is in the form of a quadratic program whose optimization variables are joint torques and ground reaction wrenches. This has great value because one can approximate friction cones with friction pyramids (see [46]) which are convex sets rendering friction constraints amenable to the optimization problem. Since the zero-moment point has a linear dependence on joint torques and ground reaction wrench, this can also be factored into a quadratic program. In addition, it is straightforward to impose bounds on torque. Any of the above constraints or their combination may destroy the feasibility of the optimization posed in (4.8). This potential issue with feasibility, however, can be addressed by relaxing the constraints of the control Lyapunov function although this mitigates the formal guarantee on stability. Yet this leads to an interesting question: is it possible to relax the constraints of a control Lyapunov function given in Definition 11 and still guarantee stability?

A recent trend has found researchers formulating model predictive controllers which attempt to determine control values by predicting their effect on the behavior of the system over a future time window. Energy shaping fits right into model predictive control (MPC) and could be used to provide controllers which exhibit the benefits of energy shaping. With MPC in particular, it is extremely important to have

tractable controllers as such controllers require multiple evaluations as the algorithm must integrate forward to solve the relevant optimization problem. The growth of computers is changing this paradigm but effective and robust bipeds generally have fast control loops and this trend will likely continue for some time.

Another area of interest which is seeing recent growth is precision control of series elastic actuators (SEA), particularly in systems such as bipeds which experience a wide range of dynamic forces. While control of SEA is more challenging than control of traditional actuators, the potential benefits make it an important phenomenon to understand. The addition of series compliance not only allows for force sensing at joints but also for energy storage which can be utilized through design methods like energy shaping. Force sensing leads to additional possibilities such as online system identification which can provide vital information about the mass distribution of a robot. By improving the internal model, model-based methods such as energy shaping see improved robustness; this is particularly helpful for MPC.

The models studied in this paper involve traditional actuation schemes rather than SEA. This decision choice was instrumental in achieving formal results but it is important to recognize that SEA is seeing increasing use in robot design and this trend is likely to continue. In order to handle SEA formally, new control schemes have to be formulated which take the compliance into account. This naturally begs the question: Can energy shaping be formulated in a tractable way on systems with SEA? The answer to this question is not likely be straightforward as SEA requires the addition of double integrators in the model which would change the nature of an optimization problem like (4.8).

One clear benefit provided by control Lyapunov functions is the guarantee of exponential stability. And this guarantee holds provided given an ideal system model and ideal actuator response. Though these assumptions are often violated in prac-

tice, the deviation from ideality is not so severe as to render effective stabilization impractical. As a rule of thumb, the more accurate the model, the better the control. At a certain level of accuracy, these controllers become highly effective and thus the development of these methods is intertwined with the development of methods in system identification.

REFERENCES

[1] M. Ackermann, "Dynamics and energetics of walking with prostheses," Ph.D. dissertation, University of Stuttgart, Stuttgart, Germany, 2007.

[2] M. Ahmadi and M. Buehler, "Controlled passive dynamic running experiments with the ARL-Monopod II," *IEEE T. Robot.*, vol. 22, no. 5, pp. 974–986, 2006.

[3] A. D. Ames, "First steps toward automatically generating bipedal robotic walking from human data," in *Robot Motion and Control 2011*, ser. Lecture Notes in Control and Information Sciences, vol. 422. London, U. K.: Springer, 2012, pp. 89–116.

[4] A. D. Ames, K. Galloway, K. Sreenath, and J. W. Grizzle, "Rapidly exponentially stabilizing control Lyapunov functions and hybrid zero dynamics," *IEEE T. Automat. Contr.*, vol. 59, no. 4, pp. 876–891, 2014.

[5] A. D. Ames, R. Vasudevan, and R. Bajcsy, "Human-data based cost of bipedal robotic walking," in *Proc. 14th Int. Conf. Hybrid Systems Computation Control*, Chicago, IL, Apr. 2011, pp. 153–162.

[6] ——, "Human-data based cost of bipedal robotic walking," in *Proc. 14th Int. Conf. Hybrid Syst.: Comp. Control*, Chicago, Apr. 2011, pp. 153–162.

[7] S. O. Anderson, M. Wisse, C. G. Atkeson, J. K. Hodgins, G. J. Zeglin, and B. Moyer, "Powered bipeds based on passive dynamic principles," in *Proc. 5th IEEE–RAS Int. Conf. Humanoid Robots*, Tsukuba, Japan, Dec. 2005, pp. 110–116.

[8] H. A. Antosiewicz, "A survey of Liapunov's second method," *Ann. Math. Stud.*, vol. 4, no. 41, pp. 141–166, 1958.

[9] P. J. Antsaklis, J. A. Stiver, and M. Lemmon, "Hybrid system modeling and autonomous control systems," in *Hybrid Systems*, ser. Lecture Notes in Computer Science, vol. 736. Berlin, Germany: Springer, 1993, pp. 366–392.

[10] Z. Artstein, "Stabilization with relaxed controls," *Nonlinear Analysis: Theory, Methods & Applications*, vol. 7, no. 11, pp. 1163–1173, 1983.

[11] S. K. Au, J. Weber, and H. Herr, "Powered ankle–foot prosthesis improves walking metabolic economy," *IEEE T. Robot.*, vol. 25, no. 1, pp. 51–66, 2009.

[12] E. A. Barbashin and N. N. Krasovskiĭ, "On the existence of a function of Lyapunov in the case of asymptotic stability in the large," *Prikl. Mat. Meh.*, vol. 18, pp. 345–350, 1954.

[13] H. Baruh, *Analytical Dynamics*. Boston, MA: McGraw–Hillhol, 1998.

[14] A. Benveniste, M. Borgne, and P. Guernic, "Hybrid systems: the SIGNAL approach," in *Hybrid Systems*, ser. Lecture Notes in Computer Science, vol. 736. Berlin, Germany: Springer, 1993, pp. 230–254.

[15] R. Blickhan, "The spring–mass model for running and hopping," *J. Biomech.*, vol. 22, no. 11–12, pp. 1217–1227, 1989.

[16] A. M. Bloch, D. E. Chang, N. E. Leonard, and J. E. Marsden, "Controlled Lagrangians and the stabilization of mechanical systems II: Potential shaping," *IEEE T. Automat. Contr.*, vol. 46, no. 10, pp. 1556–1571, 2001.

[17] A. M. Bloch, N. E. Leonard, and J. E. Marsden, "Controlled Lagrangians and the stabilization of mechanical systems I: The first matching theorem," *IEEE T. Automat. Contr.*, vol. 45, no. 12, pp. 2253–2270, 2000.

[18] E. Borzova and Y. Hurmuzlu, "Passively walking five-link robot," *Automatica*, vol. 40, no. 4, pp. 621–629, 2004.

[19] M. S. Branicky, V. S. Borkar, and S. K. Mitter, "A unified framework for hybrid control: model and optimal control theory," *IEEE T. Automat. Contr.*, vol. 43, no. 1, pp. 31–45, 1998.

[20] R. W. Brockett, "Essays on control," in *Hybrid Models for Motion Control Systems*, ser. Progress in Systems and Control Theory, vol. 14. Boston: Birkhuser, 1993, pp. 29–53.

[21] B. Brogliato, *Nonsmooth Impact Mechanics*, ser. Lecture Notes in Control and Information Sciences. Berlin, Germany: Springer, 1996.

[22] R. A. Brooks, "A robust layered control system for a mobile robot," *IEEE J. Robot. Autom.*, vol. RA-2, no. 1, pp. 14–23, 1986.

[23] L. Cesari, *Asymptotic Behavior and Stability Problems in Ordinary Differential Equations*, 3rd ed., ser. Ergebnisse der Mathematik und ihrer Grenzgebiete. New York: Springer–Verlag, 1971, vol. 16.

[24] B. V. Chapnik, G. R. Heppler, and J. D. Aplevich, "Modeling impact on a one-link flexible robotic arm," *IEEE T. Robot. Autom.*, vol. 7, no. 4, pp. 479–488, 1991.

[25] G. Chesi, *Domain of Attraction: Analysis and Control via SOS Programming*, ser. Lecture Notes in Control and Information Sciences. London: Springer, 2011, vol. 415.

[26] C. Chevallereau, G. Bessonnet, G. Abba, and Y. Aoustin, *Bipedal Robots: Modeling, Design and Walking Synthesis*. Hoboken, NJ: John Wiley & Sons, 2009.

[27] J. Choi and J. W. Grizzle, "Planar bipedal walking with foot rotation," in *Proc. 2005 Am. Control Conf.*, vol. 7, Portland, OR, Jun. 2005, pp. 4909–4916.

[28] S. Collins, A. Ruina, R. Tedrake, and M. Wisse, "Efficient bipedal robots based on passive-dynamic walkers," *Science*, vol. 307, no. 5712, pp. 1082–1085, 2005.

[29] J. H. Conway, R. T. Curtis, S. P. Norton, R. A. Parker, and R. A. Wilson, *Atlas of Finite Groups: Maximal Subgroups and Ordinary Characters for Simple Groups*. New York: Oxford University Press, 1985.

[30] M. H. Dickinson, C. T. Farley, R. J. Full, M. A. R. Koehl, R. Kram, and S. Lehman, "How animals move: An integrative view," *Science*, vol. 288, no. 5463, pp. 100–106, 2000.

[31] B. Espiau and A. Goswami, "Compass gait revisited," in *Proc. IFAC Symp. Robot Control*, Capri, Italy, Sep. 1994, pp. 839–846.

[32] C. T. Farley, J. Glasheen, and T. A. McMahon, "Running springs: Speed and animal size," *J. Exp. Biol.*, vol. 185, pp. 71–86, 1993.

[33] R. P. Feynman, R. B. Leighton, and M. Sands, *The Feynman Lectures on Physics, Vol. 1: Mainly Mechanics, Radiation and Heat*. Reading, MA: Addison–Wesley, 1964.

[34] A. F. Filippov, *Differential Equations with Discontinuous Righthand Sides*, ser. Mathematics and Its Applications. Dordrecht, The Netherlands: Springer, 1988, vol. 18.

[35] R. A. Freeman and P. Kokotović, *Robust Nonlinear Control Design*. Boston, MA: Birkhäuser, 1996.

[36] R. J. Full and C. T. Farley, "Biomechanics and neural control of posture and movement," in *Musculoskeletal Dynamics in Rhythmic Systems: A Comparative Approach to Legged Locomotion*. New York: Springer, 2000, pp. 192–205.

[37] R. J. Full and D. E. Koditschek, "Templates and anchors: neuromechanical hypotheses of legged locomotion on land," *J. Exp. Biol.*, vol. 202, pp. 3325–3332, 1999.

[38] M. Garcia, A. Chatterjee, A. Ruina, and M. Coleman, "The simple walking model: Stability, complexity, and scaling," *ASME J. Biomech. Eng.*, vol. 120, no. 2, pp. 281–288, 1998.

[39] J. Geursen, D. Altena, and C. Massen, "A model of the standing man for the description of his dynamic behaviour," *Agressologie*, vol. 17, no. B, pp. 63–69, 1976.

[40] R. Goebel, R. G. Sanfelice, and A. R. Teel, "Hybrid dynamical systems," *IEEE Control Syst. Mag.*, vol. 29, no. 2, pp. 28–93, 2009.

[41] A. Göllü and P. Varaiya, "Hybrid dynamical systems," in *Proc. 28th IEEE Conf. Decision Control*, vol. 3, Tampa, FL, Dec. 1989, pp. 2708–2712.

[42] D. Gorinevsky, A. Formalsky, and A. Schneider, *Force Control of Robotics Systems*. Boca Raton, FL: CRC Press, 1997.

[43] A. Goswami, "Postural stability of biped robots and the foot-rotation indicator (FRI) point," *Int. J. Robot. Research*, vol. 18, no. 6, pp. 523–533, 1999.

[44] J. W. Grizzle, G. Abba, and F. Plestan, "Asymptotically stable walking for biped robots: analysis via systems with impulse effects," *IEEE T. Automat.*

Contr., vol. 46, no. 1, pp. 51–64, 2001.

[45] J. W. Grizzle, C. Chevallereau, A. D. Ames, and R. W. Sinnet, "3D bipedal robotic walking: Models, feedback control, and open problems," in *Proc. 8th IFAC Symp. Nonlinear Control Syst.*, Bologna, Sep. 2010, pp. 505–532.

[46] J. W. Grizzle, C. Chevallereau, R. W. Sinnet, and A. D. Ames, "Models, feedback control, and open problems of 3D bipedal robotic walking," *Automatica*, vol. 50, no. 8, pp. 1955–1988, 2014.

[47] J. Guckenheimer and P. Holmes, *Nonlinear Oscillations, Dynamical Systems, and Bifurcations of Vector Fields*, ser. Applied Mathematical Sciences. New York: Springer, 1983, vol. 42.

[48] W. M. Haddad, V. Chellaboina, and N. A. Kablar, "Non-linear impulsive dynamical systems. part i: Stability and dissipativity," *Int. J. Control*, vol. 74, no. 17, p. 16311658, Jan. 2001.

[49] W. Hahn, *Stability of Motion*, ser. Die Grundlehren der mathematischen Wissenschaften. New York: Springer, 1967, vol. 138.

[50] D. Harel, "Statecharts: a visual formalism for complex systems," *Sci. Comput. Prog.*, vol. 8, no. 3, pp. 231–274, 1987.

[51] A. Herdt, H. Diedam, P. Wieber, D. Dimitrov, K. Mombaur, and M. Diehl, "Online walking motion generation with automatic footstep placement," *Adv. Robot.*, vol. 24, no. 5–6, pp. 719–737, 2010.

[52] J. K. Hodgins and M. H. Raibert, "Adjusting step length for rough terrain locomotion," *IEEE T. Robot. Autom.*, vol. 7, no. 3, pp. 289–298, 1991.

[53] A. L. Hof, M. G. J. Gazendam, and W. E. Sinke, "The condition for dynamic stability," *J. Biomech.*, vol. 38, no. 1, pp. 1–8, 2005.

[54] J. M. Hollerbach, "A recursive Lagrangian formulation of maniputator dynamics and a comparative study of dynamics formulation complexity," *IEEE T. Syst. Man Cy.*, vol. 10, no. 11, pp. 730–736, 1980.

[55] J. M. Hollerbach, I. W. Hunter, and J. Ballantyne, "The robotics review 2," in *A comparative analysis of actuator technologies for robotics*. Cambridge, MA: MIT Press, 1992, pp. 299–342.

[56] P. Holmes, R. J. Full, D. E. Koditschek, and J. Guckenheimer, "The dynamics of legged locomotion: Models, analyses, and challenges," *SIAM Rev.*, vol. 48, no. 2, pp. 207–304, 2006.

[57] J. Hooman, "Hybrid systems," in *A compositional approach to the design of hybrid systems*, ser. Lecture Notes in Computer Science, vol. 736. Berlin, Germany: Springer, 1993, pp. 121–148.

[58] F. C. Hoppensteadt, "Singular perturbations on the infinite interval," *Trans. Amer. Math. Soc.*, vol. 123, no. 2, pp. 521–535, 1966.

[59] Y. Hu, G. Yan, and Z. Lin, "Gait generation and control for biped robots with underactuation degree one," *Automatica*, vol. 47, no. 8, pp. 1605–1616, 2011.

[60] Y. Hurmuzlu, F. Génot, and B. Brogliato, "Modeling, stability and control of biped robots—a general framework," *Automatica*, vol. 40, no. 10, pp. 1647–1664, 2004.

[61] Y. Hurmuzlu and D. B. Marghitu, "Rigid body collisions of planar kinematic chains with multiple contact points," *Int. J. Robot. Research*, vol. 13, no. 1, pp. 82–92, 1994.

[62] A. Hurwitz, "Über die bedingungen unter welchen eine gleichung nur wurzeln mit negativen reellen teilen besitzt," *Math. Ann.*, vol. 46, pp. 273–284, 1895.

[63] S. Hyon, J. G. Hale, and G. Cheng, "Full-body compliant human–humanoid interaction: Balancing in the presence of unknown external forces," *IEEE T. Robot.*, vol. 23, no. 5, pp. 884–898, 2007.

[64] S. Kajita, F. Kanehiro, K. Kaneko, K. Yokoi, and H. Hirukawa, "The 3D linear inverted pendulum mode: a simple modeling for a biped walking pattern generation," in *Proc. 2001 IEEE/RSJ Int. Conf. Intel. Robots Syst.*, vol. 1, Maui, HI, Oct. 2001, pp. 239–246.

[65] S. Kajita, M. Morisawa, K. Miura, S. Nakaoka, K. Harada, K. Kaneko, F. Kanehiro, and K. Yokoi, "Biped walking stabilization based on linear inverted pendulum tracking," in *Proc. 2010 IEEE/RSJ Int. Conf. Intel. Robots Syst.*, Taipei, Taiwan, Oct. 2010, pp. 4489–4496.

[66] S. Kajita and K. Tani, "Study of dynamic biped locomotion on rugged terrain-theory and basic experiment," in *5th Int. Conf. Adv. Robot.*, vol. 1. IEEE, Jun. 1991, pp. 741–746.

[67] S. Kajita, T. Yamaura, and A. Kobayashi, "Dynamic walking control of a biped robot along a potential energy conserving orbit," *IEEE T. Robotic. Autom.*, vol. 8, no. 4, pp. 431–438, 1992.

[68] K. Kaneko, F. Kanehiro, M. Morisawa, K. Akachi, G. Miyamori, A. Hayashi, and N. Kanehira, "Humanoid robot HRP-4 – humanoid robotics platform with lightweight and slim body," in *2011 IEEE/RSJ Int. Conf. Intel. Robots Syst.*, San Francisco, CA, Sep. 2011, pp. 4400–4407.

[69] I. Kato, S. Ohteru, H. Kobayashi, K. Shirai, and A. Uchiyama, "On theory and practice of robots and manipulators: Volume i," in *Information-Power Machine with Senses and Limbs*, ser. International Centre for Mechanical Sciences, vol. 201. Vienna, Austria: Springer, 1974, pp. 11–24.

[70] N. S. Khalikoff, "On the stability "in the large" of the solutions of differential equations," *Bull. Soc. Phys.-Math., Kazan*, vol. 3, no. 9, pp. 31–57, 1937.

[71] H. K. Khalil, *Nonlinear Systems*, 3rd ed. Upper Saddle River, NJ: Prentice Hall, 2002.

[72] T. Komura, A. Nagano, H. Leung, and Y. Shinagawa, "Simulating pathological gait using the enhanced linear inverted pendulum model," *IEEE T. Biomed. Eng.*, vol. 52, no. 9, pp. 1502–1513, Sep. 2005.

[73] T. Koolen, T. de Boer, J. Rebula, A. Goswami, and J. E. Pratt, "Capturability-based analysis and control of legged locomotion, part 1: Theory and application to three simple gait models," *Int. J. Robot. Research*, vol. 31, no. 9, pp. 1094–1113, 2012.

[74] V. V. Kozlov and D. V. Treshchev, *Billiards: A Genetic Introduction to the Dynamics of Systems with Impacts*, ser. Translations of Mathematical Monographs. Providence, RI: American Mathematical Society, 1991, vol. 89.

[75] N. N. Krasovskiĭ, *Stability of Motion Applications of Lyapunov's Second Method to Differential Systems and Equations*. Stanford, CA: Stanford University Press, 1963.

[76] S. Kudoh, T. Komura, and K. Ikeuchi, "The dynamic postural adjustment with the quadratic programming method," in *Proc. 2002 IEEE/RSJ Int. Conf. Intel. Robots Syst.*, vol. 3, Lausanne, Switzerland, Sep. 2002, pp. 2563–2568.

[77] A. D. Kuo, "Stabilization of lateral motion in passive dynamic walking," *Int. J. Robot. Research*, vol. 18, no. 9, pp. 917–930, 1999.

[78] ——, "Energetics of actively powered locomotion using the simplest walking model," *ASME J. Biomech. Eng.*, vol. 124, no. 1, pp. 113–120, 2002.

[79] ——, "Choosing your steps carefully," *IEEE Robot. Autom. Mag.*, vol. 14, no. 2, pp. 18–29, 2007.

[80] R. Kurazume, T. Hasegawa, and K. Yoneda, "The sway compensation trajectory for a biped robot," in *Proc. 2003 Int. Conf. Robot. Autom.*, vol. 1, Taipei, Taiwan, Sep. 2003, pp. 925–931.

[81] J. Kurzweil, "On the inversion of Liapunovs second theorem on stability of motion," *Amer. Math. Soc. Transl. Ser. 2*, vol. 24, pp. 19–77, 1956.

[82] A. Lamperski and A. D. Ames, "Lyapunov theory for zeno stability," *IEEE T. Automat. Contr.*, vol. 58, no. 1, pp. 100–112, 2013.

[83] J. P. LaSalle, "Recent advances in Liapunov stability theory," *SIAM Review*, vol. 6, no. 1, pp. 1–11, 1964.

[84] J. P. LaSalle and S. Lefschetz, *Stability by Liapunov's direct method: with applications*. New York: Academic Press, 1961, vol. 4.

[85] Z. Li, N. G. Tsagarakis, and D. G. Caldwell, "Walking pattern generation for a humanoid robot with compliant joints," *Autonomous Robots*, vol. 35, no. 1, pp. 1–14, 2013.

[86] H. Lim, Y. Kaneshima, and A. Takanishi, "Online walking pattern generation for biped humanoid robot with trunk," in *Proc. 2002 Intl. Conf. Robotics Autom.*, Washington, DC, May 2002, pp. 3111–3116.

[87] A. M. Lyapunov, "The general problem of the stability of motion," *Int. J. Control*, vol. 55, no. 3, pp. 531–773, 1992.

[88] J. Lygeros, K. H. Johansson, S. N. Simić, J. Zhang, and S. S. Sastry, "Dynamical properties of hybrid automata," *IEEE T. Automat. Contr.*, vol. 48, no. 1, pp. 2–17, 2003.

[89] A. Majumdar, A. A. Ahmadi, and R. Tedrake, "Control design along trajectories with sums of squares programming," in *Proc. 2013 IEEE Int. Conf. Robot. Autom.*, Karlsruhe, Germany, May 2013, pp. 4054–4061.

[90] I. G. Malkin, "Verallgemeinerung des fundamentalsatzes von Liapounoff," *Doklady Akademii Nauk SSSR*, vol. 18, pp. 162–164, 1938.

[91] ——, "On the question of the reciprocal of Lyapunov's theorem on asymptotic stability," *Prikl. Mat. Meh.*, vol. 18, pp. 129–138, 1954, in Russian.

[92] Z. Manna and A. Pnueli, "Verifying hybrid systems," in *Hybrid Systems*, ser. Lecture Notes in Computer Science, vol. 736. Berlin, Germany: Springer, 1993, p. 435.

[93] M. Marachkoff, "On a theorem of stability," *Bull. Soc. Phys.-Math., Kazan*, vol. 3, no. 12, pp. 171–174, 1940.

[94] J. L. Massera, "On Liapounoff's conditions of stability," *Ann. Math.*, vol. 50, no. 3, pp. 705–721, 1949.

[95] ——, "Contributions to stability theory," *Ann. Math.*, vol. 64, no. 1, pp. 182–206, 1956.

[96] V. M. Matorosov, "On the stability of motion," *J. Appl. Math. Mech.*, vol. 26, pp. 1337–1353, 1962.

[97] T. McGeer, "Passive dynamic walking," *Int. J. Robot. Research*, vol. 9, no. 2, pp. 62–82, 1990.

[98] ——, "Passive walking with knees," in *Proc. 1990 IEEE. Int. Conf. Robot. Autom.*, vol. 3, Cincinnati, May 1990, pp. 1640–1645.

[99] T. A. McMahon and G. C. Cheng, "The mechanics of running: How does stiffness couple with speed?" *J. Biomech.*, vol. 23, pp. 65–78, 1990.

[100] A. N. Michel, L. Hou, and D. Liu, *Stability of Dynamical Systems: Continuous, Discontinuous, and Discrete Systems*, ser. Systems & Control: Foundations & Applications. Boston, MA: Birkhaüser, 2007.

[101] H. Miura and I. Shimoyama, "Dynamic walk of a biped," *Int. J. Robot. Research*, vol. 3, no. 2, pp. 60–74, 1984.

[102] S. Mochon and T. A. McMahon, "Ballistic walking," *J. Biomech.*, vol. 13, no. 1, pp. 49–57, 1980.

[103] B. Morris and J. W. Grizzle, "A restricted Poincaré map for determining exponentially stable periodic orbits in systems with impulse effects: Application to bipedal robots," in *Proc. 44th IEEE Conf. Decision Control*, Seville, Dec. 2005, pp. 4199–4206.

[104] ——, "Hybrid invariant manifolds in systems with impulse effects with application to periodic locomotion in bipedal robots," *IEEE T. Automat. Contr.*, vol. 54, no. 8, pp. 1751–1764, Aug. 2009.

[105] K. Murakami and M. Yamamoto, "On the asymptotic property of the ordinary differential equation," *Proc. Japan Acad, Ser. A, Math. Sci.*, vol. 64, no. 10, pp. 373–376, 1988.

[106] R. M. Murray, Z. Li, and S. S. Sastry, *A Mathematical Introduction to Robotic Manipulation*. Boca Raton, FL: CRC Press, 1994.

[107] K. Nagasaka, H. Inoue, and M. Inaba, "Dynamic walking pattern generation for a humanoid robot based on optimal gradient method," in *IEEE Int. Conf. Syst. Man Cy.*, vol. 6, Tokyo, Japan, Oct. 1999, pp. 908–913.

[108] K. Nishiwaki, S. Kagami, Y. Kuniyoshi, M. Inaba, and H. Inoue, "Online generation of humanoid walking motion based on a fast generation method of motion pattern that follows desired ZMP," in *IEEE/RSJ Int. Conf. Intel. Robots Syst.*, vol. 3, Lausanne, Switzerland, Sep. 2002, pp. 2684–2689.

[109] Y. Ogura, H. Aikawa, K. Shimomura, H. Kondo, A. Morishima, H. Lim, and A. Takanishi, "Development of a new humanoid robot WABIAN-2," in *Proc. 2006 IEEE Int. Conf. Robot. Autom.*, Orlando, FL, May 2006, pp. 76–81.

[110] Y. Or and A. D. Ames, "Stability and completion of Zeno equilibria in Lagrangian hybrid systems," *IEEE T. Automat. Contr.*, vol. 56, no. 6, pp. 1322–1336, 2011.

[111] I. Park, J. Kim, J. Lee, and J. Oh, "Mechanical design of humanoid robot platform KHR-3 (KAIST Humanoid Robot 3: HUBO)," in *Proc. 5th IEEE–RAS Int. Conf. Humanoid Robots*, Tsukuba, Japan, Dec. 2005, pp. 321–326.

[112] J. H. Park and K. D. Kim, "Biped robot walking using gravity-compensated inverted pendulum mode and computed torque control," in *Prof. 1998 Int. Conf. Robot. Autom.*, vol. 4, Leuven, Belgium, May 1998, pp. 3528–3533.

[113] T. S. Parker and L. O. Chua, *Practical Numerical Algorithms for Chaotic Systems*. New York: Springer, 1989.

[114] J. L. Patton, Y. Pai, and W. A. Lee, "Evaluation of a model that determines the stability limits of dynamic balance," *Gait Posture*, vol. 9, no. 1, pp. 38–49,

1999.

[115] L. Perko, *Differential Equations and Dynamical Systems*, ser. Texts in Applied Mathematics. New York: Springer, 2001, vol. 7.

[116] F. Pfeiffer, K. Loffler, and M. Gienger, "The concept of Jogging JOHNNIE," in *Proc. 2002 Intl. Conf. Robot. Autom.*, vol. 3, Washington, DC, May 2002, pp. 3129–3135.

[117] M. B. Popovic, A. Goswami, and H. Herr, "Ground reference points in legged locomotion: Definitions, biological trajectories and control implications," *Int. J. Robot. Research*, vol. 24, no. 12, pp. 1013–1032, 2005.

[118] G. A. Pratt, "Legged robots at MIT: what's new since Raibert?" *IEEE Robot. Autom. Mag.*, vol. 7, no. 3, pp. 15–19, 2000.

[119] J. Pratt, J. Carff, S. Drakunov, and A. Goswami, "Capture point: A step toward humanoid push recovery," in *6th IEEE–RAS Int. Conf. Humanoid Robots*, Genova, Italy, Dec. 2006, pp. 200–207.

[120] J. Pratt, C. Chew, A. Torres, P. Dilworth, and G. Pratt, "Virtual model control: An intuitive approach for bipedal locomotion," *Int. J. Robot. Research*, vol. 20, no. 2, pp. 129–143, 2001.

[121] J. Pratt, T. Koolen, T. de Boer, J. Rebula, S. Cotton, J. Carff, M. Johnson, and P. Neuhaus, "Capturability-based analysis and control of legged locomotion, part 2: Application to M2V2, a lower-body humanoid," *Int. J. Robot. Research*, vol. 31, no. 10, pp. 1117–1133, 2012.

[122] J. E. Pratt and S. V. Drakunov, "Derivation and application of a conserved orbital energy for the inverted pendulum bipedal walking model," in *Proc. 2007 IEEE Int. Conf. Robot. Autom.*, Rome, Italy, Apr. 2007, pp. 4653–4660.

[123] J. E. Pratt and G. A. Pratt, "2nd international conference on climbing and walking robots and the support technologies for mobile machines: Clawar 99," in *Exploiting natural dynamics in the control of 3D bipedal walking simulation.* Hoboken, NJ: John Wiley & Sons, 1999, pp. 797–807.

[124] J. E. Pratt and R. Tedrake, "Fast motions in biomechanics and robotics," in *Velocity-Based Stability Margins for Fast Bipedal Walking*, ser. Lecture Notes in Control and Information Sciences, vol. 340. Berlin, Germany: Springer, 2006, pp. 299–324.

[125] M. H. Raibert, "Hopping in legged systems – modeling and simulation for the two-dimensional one-legged case," *IEEE T. Syst. Man Cy.*, vol. SMC-14, no. 3, pp. 451–463, 1984.

[126] ——, *Legged Robots That Balance*, ser. Artificial Intelligence Series. Cambridge, MA: MIT Press, 1986, vol. 15.

[127] ——, "Trotting, pacing and bounding by a quadruped robot," *J. Biomech.*, vol. 23, pp. 79–98, 1990.

[128] M. H. Raibert and H. B. Brown, Jr., "Experiments in balance with a 2D one-legged hopping machine," *J. Dynamic Syst. Meas. Control*, vol. 106, no. 1, p. 75, 1984.

[129] M. H. Raibert, M. Chepponis, and H. B. Brown, Jr., "Running on four legs as though they were one," *IEEE J. Robot. Autom.*, vol. RA-2, no. 2, pp. 70–82, 1986.

[130] J. Rebula, F. Cañas, J. Pratt, and A. Goswami, "Learning capture points for humanoid push recovery," in *7th IEEE–RAS Int. Conf. Humanoid Robots*, Pittsburgh, PA, Nov. 2007, pp. 65–72.

[131] E. J. Routh, *A Treatise on the Stability of a Given State of Motion, Particularly Steady Motion*. London, U. K.: Macmillan and co., 1877.

[132] N. Sadati, G. A. Dumont, K. A. Hamed, and W. A. Gruver, *Hybrid Control and Motion Planning of Dynamical Legged Locomotion*. Hoboken, NJ: John Wiley & Sons, Sep. 2012.

[133] Y. Sakagami, R. Watanabe, C. Aoyama, S. Matsunaga, N. Higaki, and K. Fujimura, "The intelligent ASIMO: system overview and integration," in *2002 IEEE/RSJ Int. Conf. Intel. Robots Syst.*, vol. 3, Lausanne, Switzerland, Sep. 2002, pp. 2478–2483.

[134] S. S. Sastry, *Nonlinear Systems*, ser. Interdisciplinary Applied Mathematics. New York: Springer, 1999.

[135] A. Seyfarth, H. Geyer, M. Günther, and R. Blickhan, "A movement criterion for running," *J. Biomech.*, vol. 35, no. 5, pp. 649–655, 2002.

[136] B. Siciliano and O. Khatib, *Springer Handbook of Robotics*. Berlin, Germany: Springer, 2008.

[137] B. Siciliano and L. Villani, *Robot Force Control*, ser. The Springer International Series in Engineering and Computer Science. New York: Springer, 1999, vol. 540.

[138] R. W. Sinnet and A. D. Ames, "2D bipedal walking with knees and feet: A hybrid control approach," in *Proc. 48th IEEE Conf. Decision Contr./28th Chinese Contr. Conf.*, Shanghai, China, Dec. 2009, pp. 3200–3207.

[139] ——, "3D bipedal walking with knees and feet: A hybrid geometric approach," in *Proc. 48th IEEE Conf. Decision Contr./28th Chinese Contr. Conf.*, Shanghai, China, Dec. 2009, pp. 3208–3213.

[140] ——, "Bio-inspired feedback control of three-dimensional humanlike bipedal robots," *J. Robot. Mech.*, vol. 24, no. 4, pp. 595–601, 2012.

[141] ——, "Extending two-dimensional human-inspired bipedal robotic walking to three dimensions through geometric reduction," in *Proc. 2012 Am. Control Conf.*, Montreal, Canada, Jun. 2012, pp. 4831–4836.

[142] R. W. Sinnet, S. Jiang, and A. D. Ames, "A human-inspired framework for bipedal robotic walking design," *Int. J. Biomech. Biomed. Robot.*, vol. 3, no. 1, p. 20, 2014.

[143] R. W. Sinnet, M. J. Powell, S. Jiang, and A. D. Ames, "Compass gait revisited: A human data perspective with extensions to three dimensions," in *Proc. 50th IEEE Conf. Decision Control/European Control Conf.*, Orlando, FL, Dec. 2011, pp. 682–689.

[144] R. W. Sinnet, M. J. Powell, R. P. Shah, and A. D. Ames, "A human-inspired hybrid control approach to bipedal robotic walking," in *Proc. 18th IFAC World Cong.*, Milan, Italy, Sep. 2011, pp. 6904–6911.

[145] R. W. Sinnet, H. Zhao, and A. D. Ames, "Simulating prosthetic devices with human-inspired hybrid control," in *Proc. 2011 IEEE/RSJ Int. Conf. Intel. Robots Syst.*, San Francisco, CA, Sep. 2011, pp. 1723–1730.

[146] M. W. Spong, "Passivity based control of the compass gait biped," in *Proc. 14th IFAC World Congress*, Beijing, China, Jul. 1999, pp. 19–24.

[147] M. W. Spong and G. Bhatia, "Further results on control of the compass gait biped," in *Proc. 2003 IEEE/RSJ Int. Conf. Intel. Robots Syst.*, vol. 2, Las Vegas, Oct. 2003, pp. 1933–1938.

[148] M. W. Spong and F. Bullo, "Controlled symmetries and passive walking," *IEEE T. Automat. Contr.*, vol. 50, no. 7, pp. 1025–1031, Jul. 2005.

[149] M. W. Spong, J. K. Holm, and D. Lee, "Passivity-based control of bipedal locomotion," *IEEE T. Robotic. Autom.*, vol. 14, no. 2, pp. 30–40, 2007.

[150] B. Stephens, "Humanoid push recovery," in *7th IEEE–RAS International Conference on Humanoid Robots*, Pittsburgh, PA, Nov. 2007, pp. 589–595.

[151] ——, "Push recovery control for force-controlled humanoid robots," Ph.D. dissertation, Carnegie Mellon University, Pittsburgh, PA, 2011.

[152] B. J. Stephens and C. G. Atkeson, "Push recovery by stepping for humanoid robots with force controlled joints," in *Proc. 10th IEEE–RAS Int. Conf. Humanoid Robots*, Nashville, TN, Dec. 2010, pp. 52–59.

[153] A. Strauss, "Liapunov functions and L^p solutions of differential equations," *Trans. Amer. Math. Soc.*, vol. 119, p. 3737, 1965.

[154] D. Sun, "A further result on an implicit function theorem for locally Lipschitz functions," *Oper. Res. Lett.*, vol. 28, no. 4, pp. 193–198, 2001.

[155] A. Takanishi, M. Ishida, Y. Yamazaki, and I. Kato, "The realization of dynamic walking by the biped walking robot WL-10 RD," *J. Robot. Soc. Japan*, vol. 3, no. 4, pp. 325–336, 1985.

[156] A. Takanishi, T. Takeya, H. Karaki, and I. Kato, "A control method for dynamic biped walking under unknown external force," in *IEEE Int. Workshop Intel. Robots Syst.*, vol. 2. Ibaraki, Japan: IEEE, 1990, pp. 795–801.

[157] T. Takenaka, T. Matsumoto, and T. Yoshiike, "Real time motion generation and control for biped robot: 3$^{\text{rd}}$ report: Dynamics error compensation," in

2009 IEEE/RSJ Int. Conf. Intel. Robots Syst., St. Louis, MO, Oct. 2009, pp. 1594–1600.

[158] R. Tedrake, I. R. Manchester, M. Tobenkin, and J. W. Roberts, "LQR-trees: Feedback motion planning via sums-of-squares verification," *Int. J. Robot. Research*, vol. 29, no. 8, pp. 1038–1052, 2010.

[159] A. R. Teel and L. Praly, "Results on converse Lyapunov functions from class-$\mathcal{KL}$ estimates," in *Proc. 38th IEEE Conf. Decision Control*, vol. 3, Phoenix, 1999, pp. 2545–2550.

[160] G. Teschl, *Ordinary Differential Equations and Dynamical Systems*, ser. Graduate Studies in Mathematics. Providence, RI: American Mathematical Society, 2012, vol. 140.

[161] C. Tomlin, G. J. Pappas, and S. Sastry, "Conflict resolution for air traffic management: a study in multiagent hybrid systems," *IEEE T. Automat. Contr.*, vol. 43, no. 4, pp. 509–521, 1998.

[162] A. van der Schaft and H. Schumacher, *An Introduction to Hybrid Dynamical Systems*, ser. Lecture Notes in Control and Information Sciences. London, U. K.: Springer, 2000, vol. 251.

[163] P. Varaiya, "Smart cars on smart roads: problems of control," *IEEE T. Automat. Contr.*, vol. 38, no. 2, pp. 195–207, 1993.

[164] R. Vasudevan, A. D. Ames, and R. Bajcsy, "Persistent homology for automatic determination of human-data based cost of bipedal walking," *Nonlinear An. Hybr. Syst.*, vol. 7, no. 1, pp. 101–115, 2013.

[165] M. Vidyasagar, *Nonlinear Systems Analysis*. Englewood Cliffs, NJ: Prentice Hall, 1993.

[166] M. Vukobratović and B. Borovac, "Zero-moment point – thirty five years of its life," *Int. J. Human. Robot.*, vol. 01, no. 01, pp. 157–173, 2004.

[167] M. Vukobratović, B. Borovac, and V. Potkonjak, "ZMP: A review of some basic misunderstandings," *Int. J. Human. Robot.*, vol. 03, no. 02, pp. 153–175, 2006.

[168] M. Vukobratović, B. Borovac, D. Surla, and D. Stokić, *Biped Locomotion: Dynamics, Stability, Control and Application*, ser. Communications and Control Engineering Series. Berlin, Germany: Springer, 1990, vol. 7.

[169] Q. F. Wei, P. S. Krishnaprasad, and W. P. Dayawansa, "Modeling of impact on a flexible beam," in *Proc. 32nd IEEE Conf. Decision Control*, vol. 2, San Antonio, TX, Dec. 1993, pp. 1377–1382.

[170] E. D. B. Wendel and A. D. Ames, "Rank properties of Poincaré maps for hybrid systems with applications to bipedal walking," in *Proc. 13th Int. Conf. Hybrid Syst.: Comp. Control*, Stockholm, Sweden, Apr. 2010, pp. 151–160.

[171] E. R. Westervelt, J. W. Grizzle, C. Chevallereau, J. Choi, and B. J. Morris, *Feedback Control of Dynamic Bipedal Robot Locomotion.* Boca Raton, FL: CRC Press, 2007.

[172] F. W. Wilson, "Smoothing derivatives of functions and applications," *Trans. Amer. Math. Soc.*, vol. 139, pp. 413–428, 1969.

[173] D. A. Winter, "Human balance and posture control during standing and walking," *Gait Posture*, vol. 3, no. 4, pp. 193–214, 1995.

[174] ——, *Biomechanics and Motor Control of Human Movement*, 4th ed. Hoboken, NJ: John Wiley & Sons, 2009.

[175] M. Wisse and R. Q. van der Linde, *Delft Pneumatic Bipeds*, ser. Springer Tracts in Advanced Robotics. Berlin, Germany: Springer, 2007, vol. 34.

[176] J. Yamaguchi, E. Soga, S. Inoue, and A. Takanishi, "Development of a bipedal humanoid robot-control method of whole body cooperative dynamic biped walking," in *Proc. 1999 IEEE Int. Conf. Robot. and Autom.*, vol. 1, Detroit, MI, May 1999, pp. 368–374.

[177] H. Ye, A. N. Michel, and L. Hou, "Stability theory for hybrid dynamical systems," *IEEE T. Automat. Contr.*, vol. 43, no. 4, pp. 461–474, 1998.

[178] T. Yoshizawa, *Stability Theory and the Existence of Periodic Solutions and Almost Periodic Solutions*, ser. Applied Mathematical Sciences. New York: Springer, 1975, vol. 14.

[179] G. Zeglin and B. Brown, "Control of a bow leg hopping robot," in *Proc. 1998 IEEE Int. Conf. Robot. Autom.*, vol. 1, Leuven, Belgium, May 1998, pp. 793–798.

[180] F. Zhang, *The Schur Complement and Its Applications*, ser. Numerical Methods and Algorithms. New York: Springer, 2005, vol. 4.